CRANFIELD UNIVERSITY

WASIU AJIBOLA AYOOLA

Study of Fundamental Laser Material Interaction Parameters in Solid and Powder Melting

School of Aerospace, Transportation and Manufacturing
(Welding Engineering)

PhD Thesis
Academic Year: 2015 - 2016

Supervisors: Professor Stewart Williams and Dr. Wojciech Suder
May, 2016

CRANFIELD UNIVERSITY

School of Aerospace, Transportation and Manufacturing

(Welding Engineering)

PhD

Academic Year 2015 - 2016

Wasiu Ajibola Ayoola

Study of Fundamental Laser Material Interaction Parameters in Solid and Powder Melting

Supervisor: Professor Stewart Williams and Dr. Wojciech Suder
May, 2016

This thesis is submitted in partial fulfilment of the requirements for the degree of
Doctorate of Philosophy

ABSTRACT

This study attempts to develop a set of parameters controlling the bead profile of deposits in powder melting, based on the spatial energy distribution of laser. Four parameters, identified as the laser material interaction parameters were used to study the bead profile formation in powder melting. The focus is put on control of the dimensional accuracy of powder deposits independently of the optical set-up and laser system.

In the initial stage to understand the effect of welding parameters on the development of the fusion zone, a solid metal with homogenous and known thermal properties was used. The results indicate that for large beam diameters, typically used in cladding, power density and interaction time control the depth of penetration and beam diameter and interaction time controls the weld width. However, for small beam diameters, typically used in powder bed additive manufacturing, it was found that it is more difficult to achieve steady state conduction welds due to high conduction losses to the bulk material and rapid transition to keyhole regime. Therefore, with small beam diameters it is challenging to achieve pure conduction welds, which should guarantee good quality of deposits and low spatter.

In the second part, the melting behaviour of solid material and powder for the same material type was compared. The build height in powder melting depends on layer thickness of the deposited powder and energy density, which needs to be provided to fuse the powder to the workpiece, which is equivalent to penetration in laser welding of solids. Similar to solid melting, the build width in powder melting is controlled by beam diameter and the interaction time. It was also found that with small beam diameters and large particle sizes it is more difficult to generate keyhole in the base plate, as compared to solid material. Therefore, despite the presence of spatter in the process, a full keyhole is often not generated.

A set of parameters to describe the conduction welding process based on spatial distribution of laser energy has been developed. This enables

achievement of a particular weld profile with various optical set-ups and potentially transfers of results between machines. However, more complex melting characteristics of powder requires some additional factors to be included to develop a similar model for powders.

ACKNOWLEDGEMENTS

Every opportunity in this life is a privilege. Thanks to the Executive Secretary and Staff of Petroleum Technology Development Fund (PTDF) for given me this opportunity to study in one of the world prestigious Universities – Cranfield University.

My sincere appreciation goes to my supervisors Professor Stewart Williams and Dr. Wojciech Suder for their kind guardian and provision of directions during this research. Thank you for given me opportunity to carry out my research in the area of laser welding and making my stay at Cranfield University a memorable event. It is a great opportunity that I appreciate.

I also thank the academic staff how has contributed positively to my study in Cranfield. I appreciate the effort of Dr. Ganguly Supriyo. He has been my subject advisor over the last three years. I appreciate the help and contribution of colleagues and friends.

I also thank the technical staff of the Welding Engineering and Laser Processing Centre and Metallography Laboratory, Cranfield University. Most important are Brain Brook, Flemming Nielsen and Andrew Dyer for their support. They made my activities in laboratory easier and interesting.

My kind gesture and respect go to my lovely wife and children. I thank them for their understanding and support.

TABLE OF CONTENTS

LIST OF FIGURES

LIST OF TABLES

NOMENCLATURES

A	Absorptivity
AM	Additive manufacturing
FLMIP	Fundamental laser material interaction parameters
(P_d)	Power density (W/m^2)
(t_i)	Interaction time (s)
(E_{SP})	Specific point energy (J)
(E_d)	Energy density (J/m^2)
(A_s)	Cross sectional area of laser beam (m^2)
(t_s)	Travel speed (ms^{-1})
ρ	Density (kgm^{-3})
α	Thermal diffusivity (m^2s^{-1})
P	Laser power (W)
D_B	Beam diameter (m)
(PF)	Power factor (W/m)
T_v	Boiling temperature (K)
(T_m)	Melting point (K)
k	Thermal conductivity $(W/(mK))$
$Meff$	Melting efficiency
Pe	Peclet number

d	Depth of penetration (m)
ww	Weld width (m)
W_a	Weld area (m^2)
BH	Build height (m)
BW	Build width (m)
(B_a)	Build area (m^2)

1 INTRODUCTION

Powder-bed additive manufacturing (AM) utilises a laser beam to fuse precisely powder, in a layer-by-layer principle, to build three-dimensional (3-D) parts directly from a computer model. This is because of unique advantages of a laser beam, which include directionality, non-contact operation and flexibility. The purpose of the laser in this application is to provide the heat source that can be controlled and used to melt the powder. Depending on the diameter of the laser beam and its power density, heating, melting or vapourisation of material is possible. It is also possible to focus such beam to a narrow region on a powder surface, resulting in high precision. Since the laser can be tailored to a particular application, this provides design freedom (Gusarov et al., 2007; Yasa, Deckers and Kruth, 2011).

The current approach of characterising the build profile in powder bed additive manufacturing is difficult and transferring data between two or more machines is complex. The complexity arises from variations in the optical set-up (e.g. beam diameter) and system parameters (laser power and scanning speed) are usually used to develop a build procedure on an individual basis. Therefore, it is not clear how to achieve similar build height or width in powder bed additive manufacturing when using different machines. In the majority of cases reported in the literature, the system parameters (beam diameter, laser power and scanning speed) approach was used. This evidenced by papers stating that build profile in additive manufacturing is controlled by either laser power or scanning speed (El Cheikh et al., 2012; Kobryn et al., 2000; Sun and Hao, 2012). In reality, the same laser power and scanning speed do not produce the same build profile when the beam diameter changes. Also galvo-scanners are used to manipulate the laser beam across the working envelope to achieve fast scanning process (Romero et al., 2011). However, one of the downsides of galvo-scanners is the distortion of the projected laser spot, which varies continuously during the processing. Thus, the build profile changes with beam diameter due to the process, which depends on the spatial and temporal energy

distribution and material properties. A similar problem reported in welding indicated that the fundamental material laser interaction parameters (FLMIP) of absorbed power density, interaction time and specific point energy control the weld profile. In general, the beam diameter acts in two ways; a decrease of beam diameter for a given laser power and travel speed results in an increase in power density and a decrease of interaction time and specific point energy at the same time. Alternatively, an increase of beam diameter for a given laser power results in a decrease in power density and an increase of interaction time and specific point energy. A change in beam diameter, therefore, means that it is unclear what the result will be unless the effects of the FLMIP on the weld profile are understood. It is anticipated that such changes in beam diameter occur during operation of powder machine without the knowledge of the laser user due to the variation of the spot size when a galvo-scanner is used to translate the beam. Furthermore, there is a significant variation in beam characteristics between different machines leading to variations in build properties for the same system parameters (except spot diameter). This beam diameter can change with time as well.

There are two main regimes of laser welding: keyhole and conduction (Assuncao, E. et al., 2012; Chelladurai, A.M. et al., 2014). In powder bed additive manufacturing the situation is further complicated as it is not clear whether the melting of the powder is happening in the keyhole or conduction regimes. For best quality of melting, it is desirable to operate in the conduction regime so it was assumed that the designers of powder systems tried to achieve this.

It may be possible to overcome the difficulties identified in the current approach of characterising the build profile in powder bed additive manufacturing by the application of fundamental laser material interaction parameters (FLMIP). The interaction parameters that uniquely characterised weld bead profile independently of a laser system have been identified for keyhole regime with relatively large beam diameters (compared to those used in powder bed systems) and solid materials (Suder, W.J. and Williams, S.W., 2012). It was

found that power density and specific point energy control the depth of penetration and interaction time controls the weld width. To achieve a constant depth of penetration in this regime, the system parameters of beam diameter and laser power were combined into a phenomenological model called power factor (Suder, W.J. and Williams, S., 2014). Thus, to obtain a weld with a particular depth an appropriate combination of power factor and interaction time is selected depending on the weld quality required. The depending on the beam diameter used the appropriate system parameters of power and travel speed could be identified. If a system with a different beam diameter was used appropriately could be identified through the power factor and interaction time required to give an identical weld. Furthermore, if the beam varied for some reason the required system parameters to achieve the same weld could be readily calculated.

2 Research Aim, objectives and approach

The principle research question is can a phenomenological model similar to that developed for laser keyhole welding be developed for the welding regime used in commercial laser powder systems, so that variations in build profile in a single machine are avoided. This is to enable the simple transfer of parameters between different powder bed machines with different beam qualities. Therefore, the aim of this study is characterisation of the conduction welding process in terms of FLMIP and a comparison of solid material and powder melting over various welding regimes. To achieve this aim, several specific objectives were defined.

- What fundamental laser material interaction parameters control weld bead profile in conduction welding?
- Is there an equivalent parameter to power factor in conduction welding?
- How does powder melting compare to the melting of solid?
- What welding regime is prevalent in powder melting?

2.1 Research approach

The research approach can be understood from Figure 1.1, which shows the hierarchical structure for investigation of laser welding regimes in solid and powder materials.

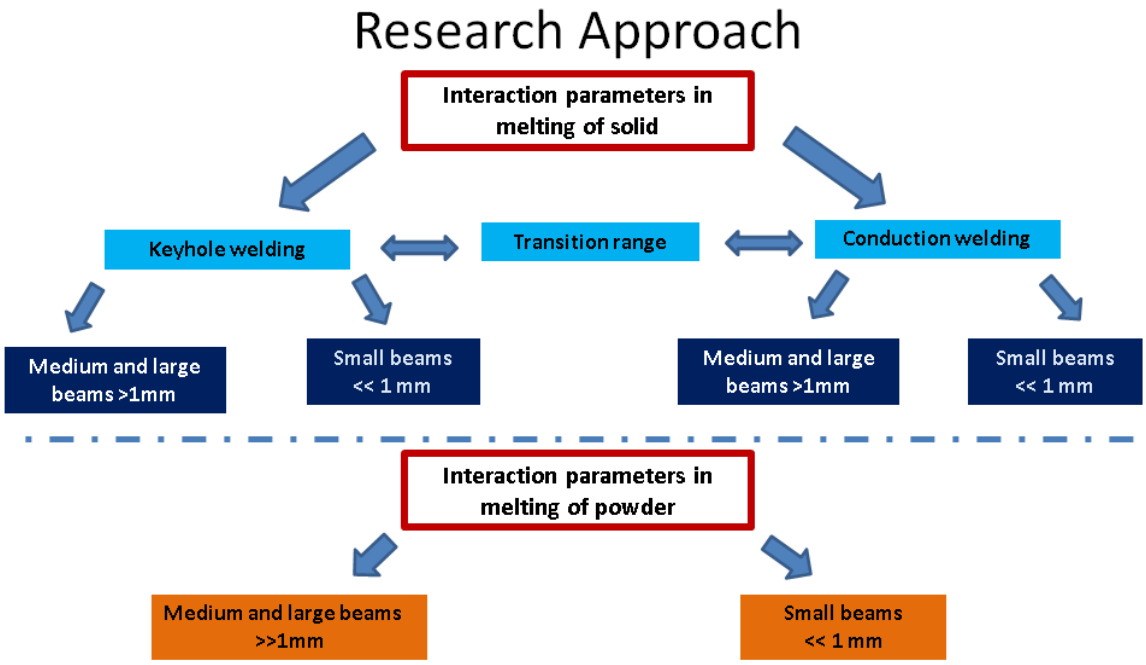

Figure 2-1: Hierarchical structure for investigation of laser welding regimes in solid and powder materials.

It was decided to begin the study of the FLMIP in conduction welding in solid material to avoid any complications due to powder material properties, variations in absorption behaviour and quality issues. This was firstly done with medium and large beams to simplify the analysis make sample preparation easier and minimise experimental errors. Following this, the conduction welding study was extended to small beams more characteristic of commercial laser powder bed systems. For these small beams, close attention was paid to the behaviour of the conduction/keyhole transition. The next stage was to carry out direct comparisons between powder and solid melting. Again, attention was paid to conduction/keyhole transition. Finally, an assessment was made of the potential application of a phenomenological to the welding regime found in commercial laser powder bed machines.

2.2 Thesis structure

This thesis consists of nine chapters. Chapter 1 contains the introduction and Chapter 2 consists of the research aim and objectives. In Chapter 3, the science of weld bead shape and powder bed additive manufacturing are reviewed from literature. The previous studies were reviewed for both conduction welding and powder bed additive manufacturing. In Chapter 4, details of the experiment procedures and materials used are given. Chapter 5 describes experimental results on the effect of fundamental laser material interaction parameters on the weld bead geometry for different optical set-ups with medium to large beam diameters. In Chapter 6, the fundamental laser material interaction parameters were also studied but for beam diameters commonly used in powder bed machines. In Chapter 7, the effect of power density distribution profile and beam shape on weld bead profle is studied. In Chapter 8, processing conditions used in solid melting (Chapters 5 and 6) were replicated in powder melting to understand the melting behaviour of powder and the effect of the beam diameter, power density, interaction time and powder layer thickness. The results obtained in this section were compared to the solid melting. In Chapter 9 consists of the critical discussion of Chapter 5 to Chapter 8. Finally, Chapter 10 provides the conclusions from this study and the recommendations for future work.

3 **LITERATURE REVIEW**

This chapter gives the overview of previous studies carried out in laser welding and powder melting processes. The core areas reviewed are the processing regimes in solid melting, bead profile formation and state-of-the-art of the technology. Also discussed is the effect of material properties on solid and powder materials. These topics are importance in understanding the formation of bead profile in solid and powder melting.

3.1 Solid melting and bead formation with application of laser

Every fusion melting process requires a heat source for the weld bead formation. In solid melting with a laser, the laser beam provides the energy that is focused on the workpiece, which allows wide or deep seams to be achieved at variable welding speeds. The laser beam generates a liquid melt pool, which grows to the desirable size and then propagates through the solid interface eliminating the original seam between the components to be joined. Thus, a weld bead profile is formed (Duley, 1999; Steen, W.M., 2010).

Solid melting by the application of a laser allows better control compared to other welding processes due to better control of applied energy and accuracy. The two main regimes of solid melting in laser welding are conduction and keyhole. These can be distinguished based on power density, interaction time and weld bead characteristic i.e. shape and quality (Assuncao, E. et al., 2012). Conduction welding requires a low power density to avoid material vaporisation (Bardin et al., 2005; Chelladurai, A.M. et al., 2014). Depending on the beam diameter, the process usually involves longer interaction times than keyhole to enable the heat to conduct inside of the material (Assuncao, E., Ganguly, S., Yapp D. and Williams, 2010, 2010b; Assuncao, E. et al., 2012). The seam has a relatively shallow depth of penetration and good surface finish, as shown in Figure 3.1a. The conduction welding surface finish is similar to that of laser forming (Knupfer and Moore, 2010). Thus, a conduction weld has a better

quality than a keyhole weld. Conduction welding relies on the thermal conduction of the heat in the base materials (Huang and Zeng, 2010). In the keyhole regime, the incident power density delivered to the workpiece surface is high enough to initiate local vaporisation of the metal. The recoil pressure from the escaping vapour causes a depression in the molten metal. As the power density is increased further, the cavity becomes deeper and a keyhole is formed. The keyhole formed in the molten metal enable deep penetration of laser beam into the material, resulting in a weld profile with a high depth to width ratio, as shown in Figure 3.1b.

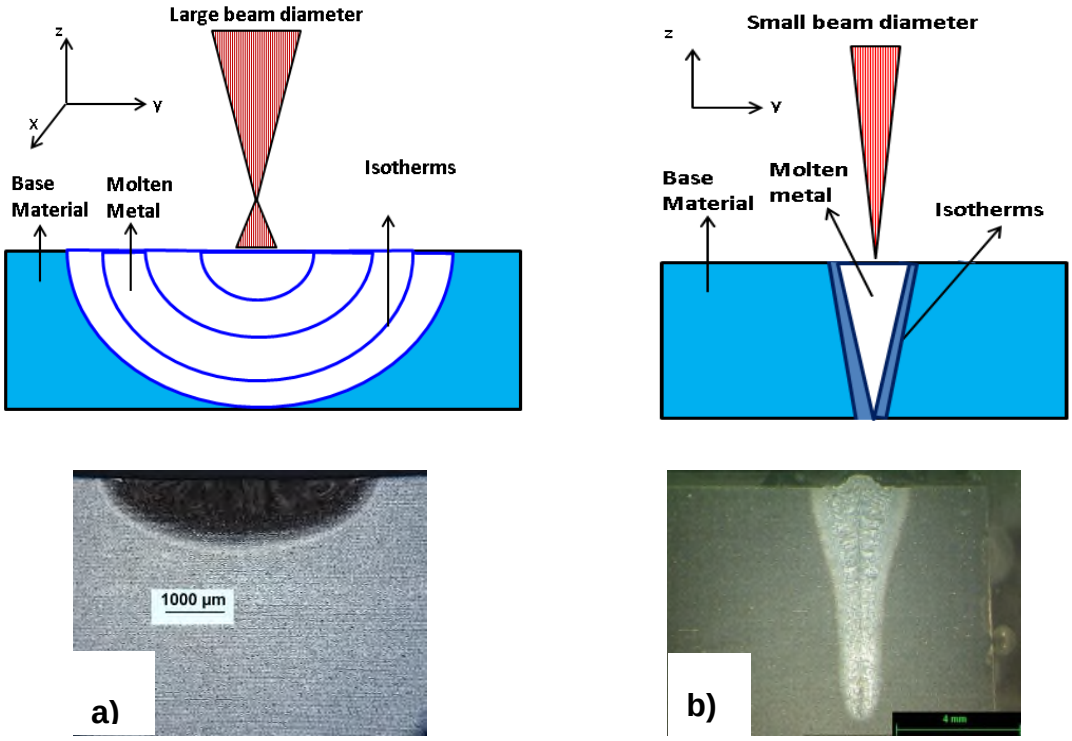

Figure 3-1: Classification of laser welding regimes a) conduction regime and b) keyhole regimes

The ratio of the depth of penetration to the weld width (the aspect ratio) is a basic factor that helps distinguish conduction welds from keyhole welds. Shown

in Figure 3-2 is the dependence of aspect ratio on power density (Assuncao, E. et al., 2012) and energy density (Chelladurai, A.M. et al., 2014). In Figure 3-1, three regimes can be identified – conduction, transition and keyhole. In conduction and keyhole regimes, the aspect ratio increases significantly with increasing power density and energy density. The transition regime shows a gradual increment of aspect ratio with increasing power density and energy density. The maximum aspect ratio for conduction regime is 0.40, for transition regime is between 0.40 and 0.60 while welds with aspect ratio above 0.60 are in keyhole regime. This implies that when the power density exceeds the 0.5 $MWcm^{-2}$, keyhole commences for the beam diameter investigated, as shown in Figure 3.2a. Thus, both applied power density, energy and the aspect ratio is important for the regime identification.

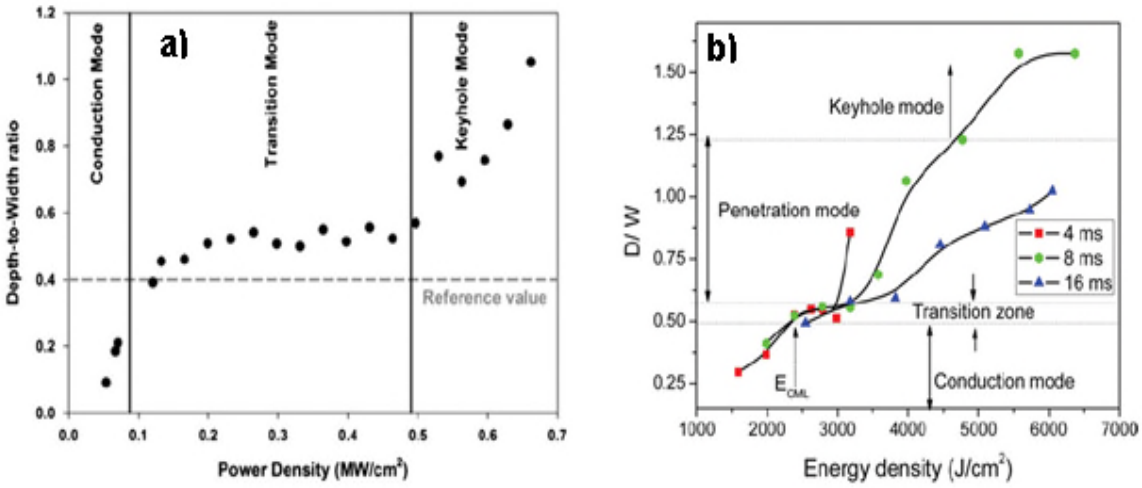

Figure 3-2: Aspect ratio as a function of a) power density and b) energy density (Assuncao, E. et al., 2012; Chelladurai, A.M. et al., 2014)

3.2 Powder melting and state of the art

Powder melting (additive manufacturing) is a fusion process. Powder bed melting has two main groups of Selective Laser Melting (SLM) and Selective

Laser Sintering (SLS). SLS consists of two or more structural materials that are in solid state and a binder material, which is in molten state during the process. Subsequently, a post-processing is required to improve the densification of the part. SLM is a complete melting of powder process. A almost full dense component that requires little or no post-processing is often achieved (Kruth et al., 2007; Olakanmi, 2013). In both processes, the ultimate aim is to deposit tracks by pre-placing powder on a build platform and then consolidating it by laser, on a layer by layer basis to produce functional products or cladded layers against corrosion or wear (Liu et al., 2015; Ye et al., 2011). There are many commercially available machines for powder melting. However, each of the machines is designed with a specific focus, for instance, either enhancing productivity (Schleifenbaum et al., 2010) or improving parts resolution (Lewis and Schlienger, 2000). The machines are designed with different optical set-ups (beam diameters) for a different range of processing parameters.

Figures 3-3 shows the schematic illustration of a powder bed machine. A cylindrical container housed the powder, which is deposited on the platform. The automated levelling system then sweeps the powder across the platform. The laser provides the energy for melting. The beam is scanned in a pattern to produce the desired shape. For fast movement of the laser energy, a galvo scanner is used. The bed is then lowered and another layer of powder is added. The process is repeated until a complete part is built. The layer thickness of the machines may range between 20 μm and 2.00 mm (Hanzl et al., 2015; Osakada and Shiomi, 2006; Schleifenbaum et al., 2010; Toyserkani, E. et al., 2005; Yadroitsev, I. et al., 2010). The particle sizes of the powder affect the layer thickness spread on the platform. Therefore, it is generally recommended that the layer thickness should be higher than powder or particle size. This reduces likelihood of defects significantly (Bertrand et al., 2007; Louvis et al., 2011).

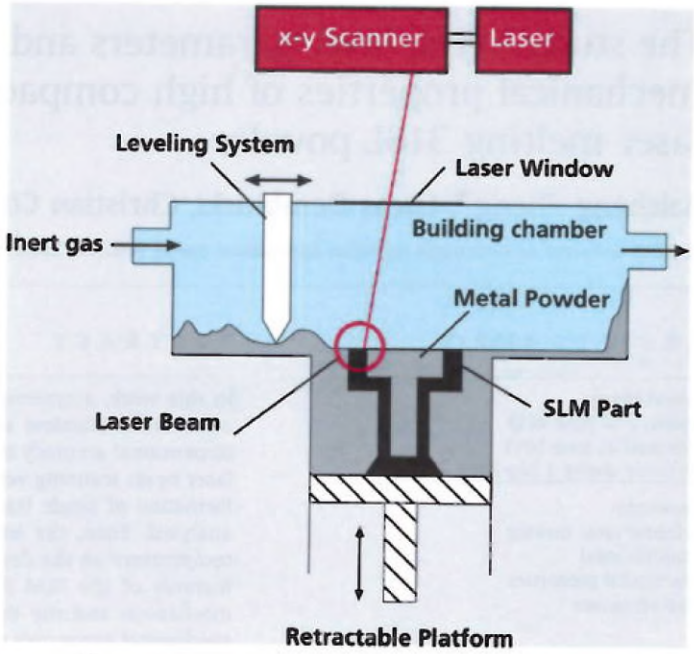

Figure 3-3: Schematic diagram of the powder bed additive manufacturing machine (Zhang, Dembinski and Coddet, 2013)

The main research effort in the field of powder melting (additive manufacturing and cladding) has been focused on the reduction of the lead time of production and increase of buy-to-fly ratio (Kong et al., 2010). The main advantages of powder melting are saving of resources, reduction in the emission of the toxic substance in leisure industries and eco-design optimisation. This is because there is a significant reduction of the raw materials used in the process, which also reduces the energy used for the production compared to other convection (Buchbinder et al., 2011; Ye et al., 2011). Apart from improving the productivity and lead-time of production, there is a positive impact on the environment. Furthermore, the parts produced are comparable to the existing products made by other manufacturing techniques, such as casting and extrusion, provided that there is fully densification of parts made. The fine grain structures of the built layers significantly enhanced the parts made due to the heat conduction in the melt zone is more rapid compared to casting. Thus, the solidification of the process is faster, which leads to the formation of the unbalanced crystal phase,

which enhances the mechanical properties (Hanzl et al., 2015; Verwimp et al., 2011).

In recent times, the focus has been on the improvement of microstructural and mechanical properties of the fabricated parts. However, the main challenge of the process is the achievement of 100% density without additional treatment, such as baking or heat treatment (Jia and Gu, 2014; Simonelli et al., 2014; Song et al., 2014). There is a strong relationship between the relative density and mechanical properties of materials. They also reported that the built parts of highest levels of ultimate tensile strength, hardness and low surface roughness corresponded to highest relative density, which has similar mechanical properties with other products produced by conventional methods. The mechanical properties of the parts produced were improved because of increasing energy density that resulted in a parabolic pattern of solidification and thus each layer of the tracks overlapped one another and led to a reduction of surface roughness (Casalino et al., 2015). In a similar study carried by (Liu et al., 2011), martensitic microstructure was achieved in high carbon steel as the effect of high cooling rate. To mitigate undesirable effects of hard microstructures, such as warpage, cracking, residual stresses and thermal shock, the base material was preheated. Thus, both aspects of microstructure and part integrity are related to the welding conditions used and melting characteristics. To further make powder bed additive manufacturing viable the quality of deposits and production rate need to be improved.

There are up to 140 processing parameters affecting bead profiles (Steen and Mazumder J, 1999). Some of these processing parameters are not related to the applied energy but may affect the bead profile of additive manufacturing (Kruth et al., 2004; Yang et al., 2002). Such parameters can be classified has secondary processing parameters. These include operator experience, scan strategy, substrate thickness etc. The primary processing parameters are those related to the energy and material properties. The primary processing parameters include beam diameter, laser power, scanning speed, scanning spacing, layer thickness, substrate temperature, quality of the powder.

Therefore, the focus of this work relates to laser spot parameters and applied energy.

This has been the main interest of many research institutions. There has been a lot of effort to increase deposition rate without compromising mechanical properties. Authors made different recommendations. Kong et al. showed that optimum conditions of deposition rate and quality were achieved for a beam diameter of 1.50 mm and laser power of 1.5 kW (Kong et al., 2010). Adequate heat input was responsible for the low porosity and lack of defects. A certain heat input is required to fuse the powder completely and avoid defects, depending on the beam diameter. According to the research by Hanzl et al., a fully consistent melted surface was achieved when laser power of 300 W and scanning speed and 50 mm/s were used (Hanzl et al., 2015). Song et al. reported different conditions for the most optimum deposits (Song et al., 2012). Capello and Previtali investigated the importance of the operator skills on the quality of fabricated parts and showed no correlation. However, some of these processing variables are yet to be probably addressed, for instance the beam diameter. This could be the reason why different processing variables achieve different build profile and build quality.

What seems unknown is about how the beam diameter affects the processes, particularly in powder melting. At a certain point adjusting laser power and scanning speed to improve bead quality will be ineffective and adjusting the beam diameter is the only option (Buchbinder et al., 2011; Schleifenbaum et al., 2010). Some authors claim that high-quality deposition is mainly possible by increasing the laser power and scanning speed (Averyanova et al., 2012; Zhang et al., 2012). However, quality deposits are not possible only by increasing the laser power and scanning speed. For a given beam diameter, high laser power initiates metal evaporation, which causes stability issues during processing. Similarly, fast scanning speed together with high laser power may lead to erratic melt flow and inconsistent weld profiles evident as balling. Potentially the only way of adding more energy to the system without inducing evaporation is by enlarging the beam diameter of the laser. Thus, to improve the build-up rate and

achieve good quality beads, larger beam diameters should be used than currently. However, to facilitate the relationship between bead profile and quality, beam diameter need to be understood. This will enable a significant increase in deposition rate and improvement of data transferability between different machines. Furthermore, the laser beam has different power density distributions, such as Gaussian or top-hat. The advantage of top-hat beams is a homogeneous distribution of laser energy (Toyserkani, E. et al., 2005). A Gaussian beam exhibits higher peak power density. Thus, it is important to investigate how the change in beam diameter and shapes affect the build profile. Also, challenges are exacerbated by the use of galvo-scanners, which change the shape of the projected beam on the surface as the beam is translated across the workspace, as shown in Figure 3-4. This means that the beam diameter of the laser is continuously changing during the processing and this change will be dependent on the size of the powder bed, type of optics, laser source and optical set-up. If the process is developed based on system parameters then in certain cases, the melting characteristics will be continuously changing leading to anisotropy between parts built in different zones of the powder bed. This is due to the change of spatial distribution of energy during processing.

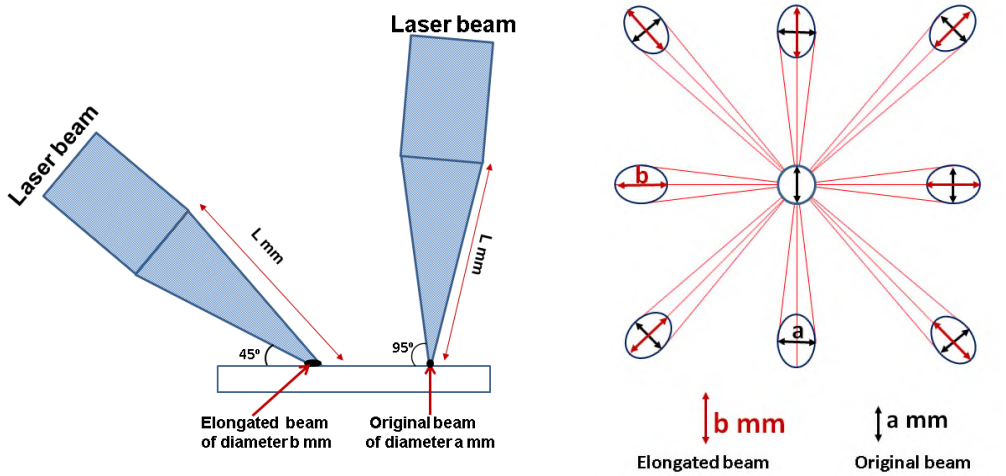

Figure 3-4: Change in beam shape due to the beam distortion

The future of powder bed machines depends on the ability to transfer data between machines and understanding real parameters that control melting of powder needed to improve the quality of built parts. The ability to develop processing conditions on one machine and transfer them onto a parallel system would be the ultimate goal for powder melting processes. However, up to date, there is no study on the transfering of data between machines reported. The problem is very complex. The complexity arises from the melting characteristics and interaction between powder and laser that are dependent on many factors.

In laser welding with solid melting, a similar issue has been addressed with the fundamental laser material interaction parameters for keyhole welding. In their study, the system parameters of beam diameter and laser power and travel speed were combined into a phenomenological model called power factor (Suder, W.J. and Williams, S., 2014). To achieve similar weld profile on different machines, the same power factor and interaction time have to be selected depending on the required quality of welds. High quality beads correspond to a longer interaction time. It is anticipated that such approach may apply to powder melting (detail in Section 3.4). Furthermore, the welding regime can also have a great effect on the quality of deposits. There are three welding regimes in laser welding; conduction, transition and keyhole. Conduction welding occurs at low powder densities. This regime can be characterised by smooth weld profile and low level of defects such porosity, gas entrapment or blow holes. Therefore, to avoid such defects in powder melting, low power density should be used. In powder melting, due to the process characteristics and a wide range of the beam diameters used for different applications, the processing regime of powder of powder melting is unclear. There have been studies suggesting that laser cladding with different beam diameters is a conduction welding. This was identified based on the processing parameters, which corresponded to energy levels commonly used in conduction welding of solid materials. One way of reducing power density below vaporisation and increasing productivity is to

increase beam diameter. However, this compromises the process resolution, as the smallest feature that can be fused is dependent on the beam size.

3.3 Application of fundamental laser material interaction parameters (FLMIPs)

Fundamental laser material interaction parameters (FLMIPs) enable a better understanding of weld profile behaviour in solid melting. This is because it specifies the process uniquely in terms of spatial energy distribution (Suder, W.J. and Williams, S.W., 2012). (Ion, J.C., 2005) and (Steen and Mazumder J, 1999) discussed material processing with interaction parameters and then developed process map, as shown in Figure 3-5. The figure is used to map different laser processes and understand differences in energy requirement between them. The range of energy density required for heating, melting or vaporisation are represented. Note that these are approximate values and energy density does not account for the heat source area. Thus, the actual energy for melting and vaporisation may vary significantly, depending on aspects, such as beam diameter, welding environment and material properties.

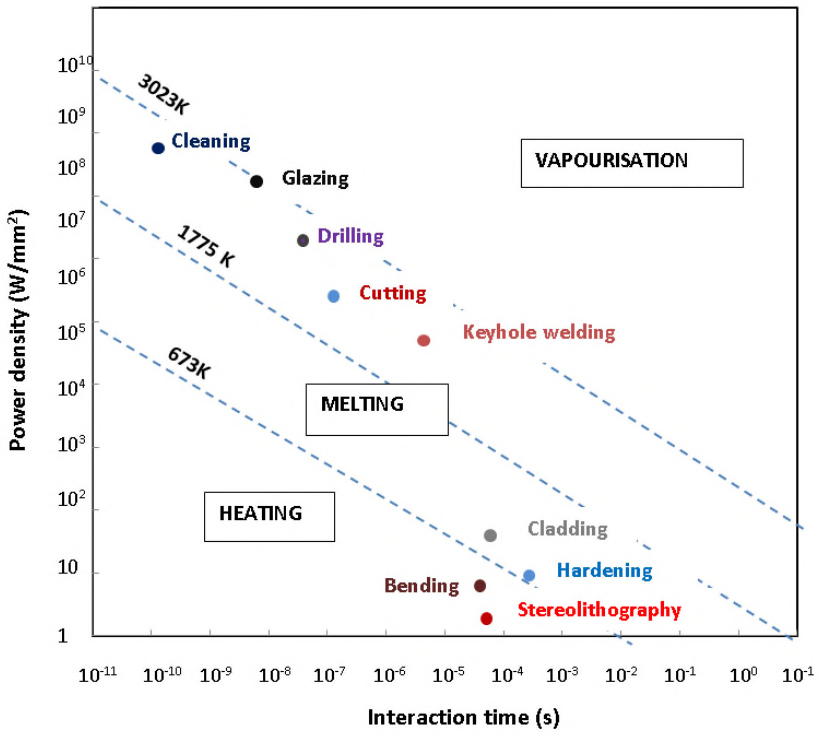

Figure 3-5: Laser material processing map based on power density and interaction time (Ion, J.C., 2005; Steen and Mazumder J, 1999)

In reality, primarily two groups of variables determine the formation of weld bead in solid melting. The first is material thermal properties, among them are thermal diffusivity and conductivity, melting and vaporisation temperatures. The second group of variables is parameters characterising heat source, which includes power density, interaction time and specific point energy. The first group of researchers to highlight the important of power density and interaction time relation to the material properties are (Ion, J.C., 2005; Steen, W.M., 2010). Only the energy density (product of power density and interaction time) does not account for effect of the heat source. Due to the characteristics of the heat source (beam diameter) that affects the process, specific point energy was also formulated (Suder, W.J. and Williams, S.W., 2012). During laser processing of materials, the laser user has no direct influence on the material properties but only on the system parameters. Therefore, laser power and travel speed are often adjusted based on engineering approach. However, in such an approach

there is no clear correlation between welding parameters and response in the material, as described for interaction parameters, as shown in Figure 3-6 (Suder, W.J. and Williams, S.W., 2012). The welding regime in laser welding is also dependent on the temperature in the laser interaction point if vaporisation point is exceeded then keyhole regime is present, otherwise, conduction welding occurs below the vaporisation threshold. In reality, this is controlled by the amount of absorbed energy and its distribution on the workpiece surface (Elsen M.V. et al., 2008). In a given material with given thermal properties, this will result in a particular thermal cycle, which will determine the response in the material, as shown in Figure 3-6 (Suder, W.J. and Williams, S.W., 2012).

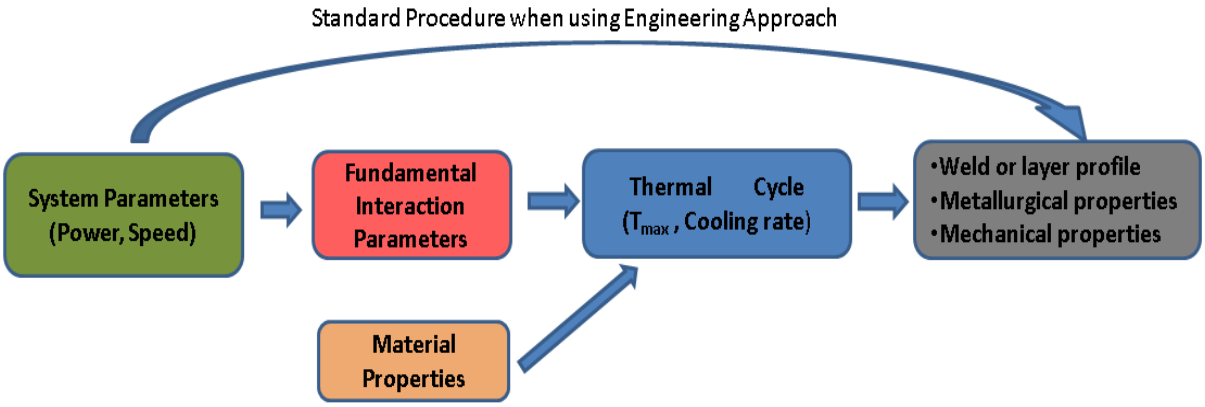

Figure 3-6: Relationship between system parameters and material responses (Suder, 2012)

It would be useful to develop such an approach to powder melting to control the melting characteristics and realise regular build tracks. Such method could help in improving the quality of the build profile and understand data transfer between machines. The parameters used to control the weld bead profile in laser welding are the following:

Power density

The power density refers to the spatial distribution of power across the beam. The average power density (P_d) is the ratio of laser power (P) to the cross sectional area of laser spot (A_s) projected on the workpiece surface, given as

$$P_d = \frac{4P}{\pi D_B^2}[Wm^{-2}] \quad (1)$$

Interaction time

When a laser of a known beam diameter is moving at a constant travel speed over a workpiece surface, the time over which a particular point of the workpiece is exposed to the laser energy is referred to as interaction time (Ion, J.C., 2005; Steen and Mazumder J, 1999). Interaction time is the ratio of beam length (D_B) in the welding direction to the travel speed (t_s). It represents the time of irradiation between the workpiece and laser beam, represented as given in Equation 2.

$$t_i = \frac{D_B}{t_s}[s] \quad (2)$$

Specific point energy (SPE)

Recently, to uniquely characterise the laser processing, a third interaction parameter called specific point energy was introduced. The specific point energy (E_{SP}) accounts for the effect of energy contained within the laser spot, which corresponds to a discrete version of energy applied. The definition of SPE assumes laser welding to be a periodic process, in which the interaction time is the period. It represents the integral of intensity and interaction time over

the diameter of the laser spot as in Equation 3 (Suder, W.J. and Williams, S.W., 2012).

$$E_{SP} = \iint P_d(xy).t_i.dxdy[J]$$

$$E_{SP} = P_d t_i A_s \quad (3)$$

Energy density

Energy density describes the spatial distribution of energy applied on the surface of a given material. Energy density is the product of power density and interaction time as shown in Equation 4 (Ion, J.C., 2005).

$$E_d = P_d.t_i[Jm^{-2}] \quad (4)$$

Figure 3-6 shows the standard approach of characterising weld bead profile based on system parameters. Figure 3-7 shows the experimentally determined threshold power density and interaction time for different beam diameters for conduction welding (Assuncao, E. et al., 2012). The details of the interaction parameters are given in Table 3-1. Above these threshold values, vaporisation temperature is reached and the welds begin to show characteristics of transition regime, such a small depression in the surface, no significant change in penetration and eventually high ratio of the depth of penetration to weld width. For the range of beam diameters shown in Table 3-1, the threshold power density decreases with increasing beam diameter at constant interaction times. This means that vaporisation required much greater power density with smaller beams. This threshold is also dependent on the interaction time, at constant beam diameter, the threshold power density increases with decreasing interaction time due to the effect of specific point energy. With smaller beams or shorter interaction times, the specific point energy is lower and therefore the vaporisation does not occur as easy as with larger beams or longer interaction times. This implies that that not only power density and interaction time are important but energy as well.

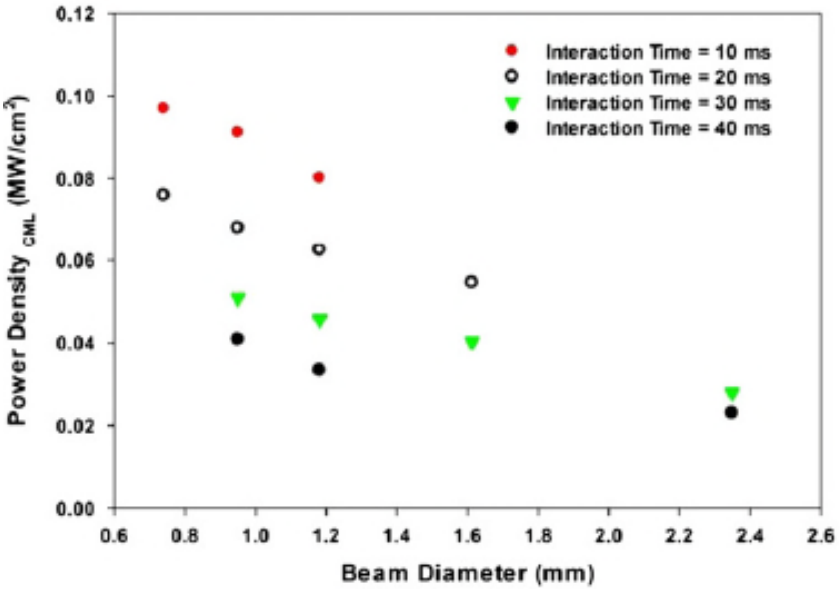

Figure 3-7: Variation of threshold power density with beam diameter for different interaction times (Assuncao, E. et al., 2012)

Table 3-1: Experimentally determined threshold interaction parameters for conduction welding (Assuncao, E. et al., 2012)

System parameters			**Fundamental laser material interaction parameters**	
Laser power (kW)	Beam diameter (mm)	Travel speed (m/min)	Threshold Power density (kW/cm^2)	Interaction time (ms)
0.33	0.74	2.31	77	20
0.64	0.95	5.21	90	10
0.55	1.18	2.40	50	30
1.20	1.61	4.70	58	20
1.30	2.35	4.70	30	30

Table 3-2 shows different sets of welding conditions reported in the literature as optimum for conduction welding. The corresponding interaction parameters were calculated based on Equations 1 and 2 (Ion, J.C., 2005). Despite significant differences in laser power and travel speed used, the interaction

parameters obtained suggest that the welds are likely to be in conduction regime, based on data shown in Figure 3-7. In this case, it is easier to understand the process as compared to the system parameters approach.

Table 3-2: System parameters and calculated interaction parameters used in conduction welding based on literature

System parameters			**Fundamental laser material interaction parameters**			**Ref.**
Laser power (kW)	Beam diameter (mm)	Travel speed (m/min)	Power density (kW/cm^2)	Interaction time (ms)	Specific point energy (J)	
1.5 – 2.75	2.04	1.00 – 4.50	46.00 – 84.00	27-122	7.48-184	1
0.45-0.55	0.50	1.50	229.2-280.10	20	9-11	2
7.00	5.25	0.30	32.40	1050	7350	3
4.00	10.00	0.39	5.10	1500	6153	4
4.00	13.00	0.40	3.00	2000	7800	4
1.50	1.50	6.36	85.00	14	21	5

Note 1.(Sánchez-Amaya et al., 2009); 2.(Stanciu et al., 2012); 3.(Assuncao, E., Ganguly, S., Yapp D. and Williams, 2010a); 4.(Meco et al., 2012); 5.(Zhao and Debroy, 2001)

Table 3-3 and Table 3-4 show the summary of processing parameters commonly used in powder melting. Table 3-3 shows the parameters of laser cladding with large beam diameters. Table 3-4 summarises the interaction parameters of powder bed fusion processes with small beam diameters. The data in Table 3-3 are similar to that of the Table 3-2, which suggests conduction regime in laser cladding. However, the data shown in Table 3-4 are different from those in Table 3-2. From Table 3-4, it can be seen that in certain cases (higher layer thickness and small beam diameter) required a higher power density and energy to achieve melting, which suggests vaporisation threshold for the powder melting in the case of small beam diameters. Therefore, it is anticipated that specifying the process based on fundamental laser material

interaction parameters (FLMIP) and material properties will improve control of the process and the process regime.

From all the work in the literature discussed so far, to identify the welding regimes of powder melting, the applied power density, interaction time and energy used are the primary determinant parameters. The transition between conduction and keyhole is complex phenomenon depending on many conditions, such as energy density, specific point energy, material type, etc. However, there have been some attempts to define the process regime analytically. In one example, a dimensionless number Peclet was used to describe melting and vaporisation thresholds, as given in Equation 5 (Patschger A. et al., 2013a). Equation 5 can be used to calculate the energy needed for melting and vaporisation based on a Gaussian power density distribution. In this equation, the thermal properties of the materials and Peclet number are on the right-hand-side. The ratio of applied laser power to the beam diameter, which is also the power factor is on the left-hand side. The process regime will shift from melting to vaporisation when the Gaussian power density exceeded the material properties according to Equation 5. Such equation gives an approximate value of the threshold for melting and vaporisation and enables a quick evaluation of the process regime based on the processing parameters.

$$\frac{P}{D_B} = \sqrt{\pi} * \frac{M_p}{A} * \sqrt{\frac{P_e + 4.4}{4}} [W/m] \quad (5)$$

. While $P_e = \frac{ww * t_s}{\lambda}$

Where P - laser power; D_B - beam diameter; λ - thermal diffusivity; M_p - melting point; A - absorptivity constant; P_e - Peclet number; t_s - travel speed and ww - the weld width

Table 3-3: System parameters and corresponding interaction parameters commonly used for cladding based on literature

System Parameter		Optic setup	Fundamental Laser Material Interaction Parameters			Ref.
Laser power (kW)	Scan speed (m/min)	Beam Diameter (mm)	Power density (kW/cm^2)	Interaction time (ms)	Specific point energy (J)	
1.40 – 1.80	1.00 1.32	3.50	14.60–18.8	160 – 210	222-378	1
1.40 – 1.80	1.00 1.32	3.50	14.60–18.8	160 – 210	254-432	1
0.70 – 1.15	0.15	4.00	5.60–10.0	1600	1120-1840	2
0.70 – 1.50	0.30 – 1.50	3.00	8.70 – 12.5	300 - 600	84-900	3
No information	0.30 - 0.42	No information	28 – 36	No information		4
1.20	6.00	0.60	353 – 424	6	7.2	5
1.10	0.40	1.40	71.5	210	231	6
0.60	1.00	1.00	76.4	60	36	7
3.00	0.30	6.00	10.6	600	3600	8
3.50	0.55	3.50	36.4	381	1336	9

Note 1.(Ye et al., 2011); 2.(Li et al., 2012); 3.(Cottam and Brandt, 2011); 4.(Shepeleva et al., 2000); 5.(Shon et al., 2015); 6.(Paydas et al., 2015); 7. (Nagaoka et al., 2015); 8.(Qu et al., 2015); 9.(Liu et al., 2015)

Table 3-4: System parameters and corresponding interaction parameters commonly used in powder bed machine based on literature

System Parameter		Layer thickness (mm)	Optic setup	Fundamental Laser Material Interaction Parameters			Ref
Laser (W)	Scan speed (m/min)		Beam Diameter (mm)	Power density (kW/cm^2)	Interaction times (ms)	Specific point energy (mJ)	
95	0.6-1.8	0.07	0.20	303	0.4 – 20	633-1900	1
70 – 200	3.0-24.0	0.25	0.60	24.7 - 70.7	1.5-30	105-2400	2
85 -105	3.0 – 12.0	-	0.20	271 – 3340	1 – 4	85-420	3
85 – 300	3.0-12.0	-	0.05	4329 – 15278	0.25 – 1.0	20-300	3
80 – 160	5.3-10.8	0.05	0.09	1258 - 2515	0.5-1.0	40-160	4
200	15	0.04	0.1	2546	0.4	80	5
50	3.6-14.4	0.05	0.07	1300	0.3-1.2	15-58	6
25	3.6-7.2	0.05	0.07	650	0.6-0.2.3	15-30	6
50	0.6-30	0.10	0.04	796-3979	0.08-4.0	4-200	7
20-250	1.2-15.0	0.25	0.6	14 – 57	2.4-30	48-7500	8
35- 50	3.0-9.0	0.05	0.07	909-1300	0.5-1.4	16-70	9
70 – 225	3.0-36	0.10	0.2	223-716	0.4-4	23-900	10
100 – 130	24 – 36	-	0.07	2598 - 3378	0.12 - 0.18	116-230	11

1.(Rombouts et al., 2006); 2. (Kruth et al., 2004); 3. (Yasa et al., 2011); 4.(Tsopanos et al., 2010); 5. (Guan et al., 2013); 6. (Yadroitsev, I. et al., 2010); 7. (Khan and Dickens, 2012); 8. (Olakanmi, 2013); 9. (Averyanova et al., 2012); 10. (Simchi, A., 2004); 11. (Jia and Gu, 2014)

The parameters that affect the build profiles can be divided into two groups (see Section 3.2). The current process of developing processing parameters is very dependent on the material types and the optical set-up, which means that every case has to be optimised individually. Some authors tried to optimise the optimum condition in the form of processing maps, as summarised in Table 3-5 and Figure 3-8. It can be seen that the welding speed and laser power required for stable processing are different for each case. Some differences are expected because of differences in the material properties and optical set-up. Note that in every example, there are differences in material type and beam diameter, but the energy for melting between powder iron and stainless steel is quite comparable. The effect of beam size can be better understood in terms of fundamental laser material interaction parameters. To get the optimum fusion

Song et al used 100 W and 0.2 mm/s and Yadroitsev et al used 40 W and 0.12 m/s. When these are transferred to interaction parameters, they lead to energy density of 0.75 kJ/cm^2 and 0.61 kJ/cm^2, which are quite similar. This shows that energy density to melt a particular thickness of powder is very similar in these cases. In the other example (Kruth et al and Olakanmi) of iron powder and aluminium were compared, the difference is more significant.

Table 3-5: Selective laser melting with system parameters and layer thickness used by different authors

System parameters	Song et al. 2014	Yadroitsev et al. 2010	Kruth et al. 2004	Olakanmi, 2006
Laser power (W)	90 – 110	12.5 – 50	70 – 200	20 – 240
Scanning speed(mm/s)	100 – 400	40 – 240	20 – 400	20 – 250
Spot size (mm)	0.034	0.07	0.80	0.60
Shielding gas	Argon	Argon	Nitrogen or Argon	Argon
Layer thickness (mm)	0.05	0.05	0.25	0.25
Material	Iron powder	Stainless steel	Iron powder	Al alloys
Laser type	CW	CW	CO_2	CO_2
Substrate type	Steel	Steel	Steel	No indication was given
Power density for smooth bead (kWcm^{-2})	11000	1040	28	43
Interaction time for smooth bead (ms)	0.17	0.58	3.33	7.50
Energy density for smooth bead (kJcm^{-2})	0.75	0.61	0.053	0.31

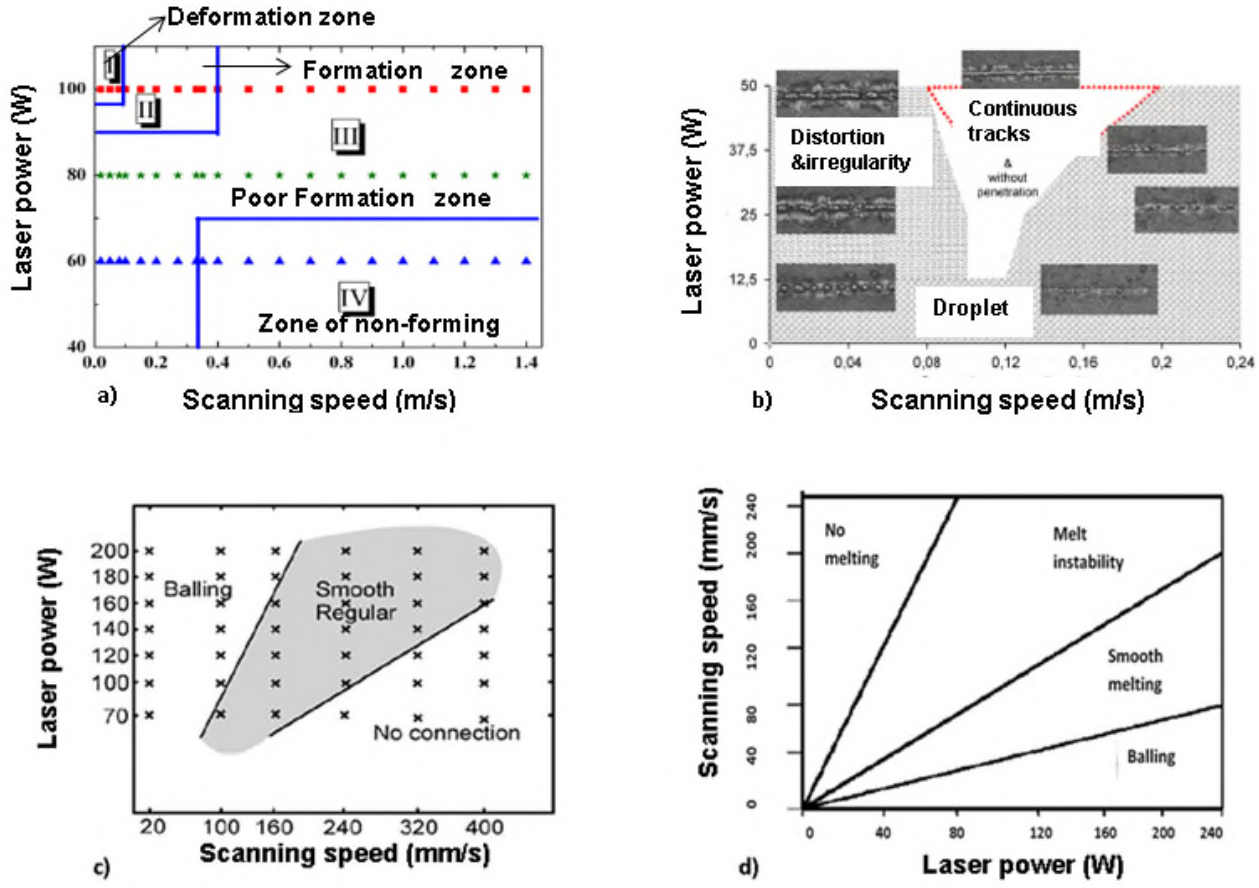

Figure 3-8: Comparison of processing maps between different powder bed systems a) (Song et al., 2014) (b) (Yadroitsev, I. et al., 2010) (c) (Kruth et al., 2004) and (d) (Olakanmi, 2013)

3.4 Power factor model

In laser welding processes, achieving a similar depth of penetration and required weld profile are of interest to the laser users. To attain a similar depth of penetration, it is a common practice to adjust system parameters such as laser power and travel speed to the laser spot on the workpiece surface. In many studies, it has been shown that laser power and travel speed affect the fusion zone geometry (Anawa and Olabi, 2008; Benyounis, K.Y. et al., 2005; El-Batahgy, 1997; Moradi, M. and Ghoreishi, M., 2010; Sánchez-Amaya et al., 2009). However, such optimised process works only with a particular laser

system with a particular optical set-up and beam diameter. To uniquely characterise the weld bead profile, the power factor model was developed (Suder, W.J. and Williams, S., 2014). The study showed that laser welding is a periodic process whose period is the interaction time. Furthermore, for a given interaction time, the depth of penetration was observed to be proportional to the power density and specific point energy, which was combined into one parameter. The product of the power density and specific point energy, which is the ratio of laser power to the beam diameter was defined as power factor, as shown in Equation 6. To achieve a similar depth of penetration in keyhole for different beam diameters, power factor (PF) and interaction time (t_i) have to be selected depending on the weld quality needed. Using beam different diameters, the appropriate system parameters can be then selected for each system, as shown in Figure 3.9. Application of power factor seems to be simple and successfully used for keyhole welding. Development of similar model would be useful in powder melting.

$$t_i = \frac{D_B}{t_s}[s] \tag{2}$$

$$P_F = \frac{P}{D_B}[W/m] \tag{6}$$

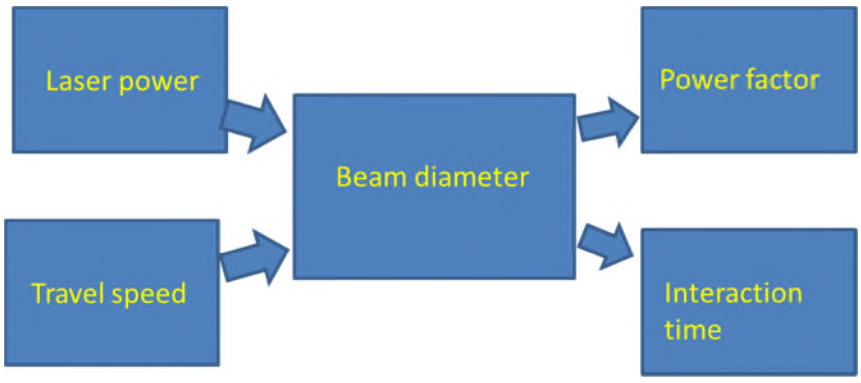

Figure 3-9: Parameters selection for power factor and interaction time to achieve similar weld profile

3.5 Other variables affecting bead formation in solid melting

When laser welding is carried out in conduction or keyhole regime, the weld geometry (depth of penetration and weld width) and the surface weld quality is also influenced by the welding environment (e.g. shielding gas) and laser beam characteristics and material properties. To achieve conduction or keyhole welds with a desirable profile, it is important to evaluate and understand the effect of these variables on bead geometry. Therefore, it is important to maintain the balance between the heat applied by laser radiation, the heat utilised for melting and dissipated for different losses by the workpiece (Anawa and Olabi, 2008; Childs, Hauser and Badrossamay, 2005b; Gusarov et al., 2007; Semak and Matsunawa, 1999).

3.5.1 Welding environment

The welding environment is an important factor that determines the fusion characteristics and the flow of liquid metal. The effect of welding environment, such as the type of shielding gas, gas properties, flow rate and feeding position also affect the fusion characteristics. The properties of shielding gases that are important in this aspect are temperature, ionisation potential, thermal conductivity and type of molecules (Duley, 1999). Also, the laser properties such as wavelength can affect weld profile differently. It has been established that the temperature of shielding gases affects the rate the heat is absorbed. During welding, when the temperature exceeds 6,000 K, the plasma plume is formed (Sayegh, 1998). This plasma or plume if not ionised, affects the quality of the weld bead profile by absorbing the incident laser energy. The ionisation potential of the shielding gas determines the ability of gas to reduce absorption of laser energy in vapour plasma. Particularly when processing with high power density laser beams, part of the material is vaporised when the temperature exceeds the boiling point of the material and this is exhibited as a bright column

suspended above the laser interaction point. This vapour plume can interact with an incoming laser beam (Ming et al., 2007). The propagating beam when passing through this plume is partially absorbed or scattered by the vapour particles. Depending on the wavelength of the laser and the type of material, different mechanisms occur. The long wavelength of the CO_2 laser (10.6 μm) makes laser beam absorption more significant than shorter wavelength Nd:YAG or fibre lasers (10.6 μm), which affect the bead profile differently (Hess et al., 2011; Kaplan and Matti, 2015).

Studies have been carried out to understand how the shielding gases affect the weld pool and the resulting weld bead profile. For instance, it was found that helium and argon influence the depth of penetration and weld width in keyhole regime differently due to their differences in ionisation potential (Wang et al., 2007). In the keyhole regime, a higher penetration was achieved with helium compared to argon. However, in conduction regime, no significant difference in weld bead profile was noticed between these two gases (Quintino et al., 2011). This difference was attributed to plume/plasma formation, which is present in keyhole welding and absent in conduction. It has also been demonstrated that for the same laser energy, it is possible for a weld bead to exhibit different weld profiles depending on the shielding gas composition (Gao, M. et al., 2007; Valiente Bermejo et al., 2014). As shown in Figure 3-10, shielding only with argon induced shallow penetration with a CO_2 laser. However, when the proportion of helium added double the argon, the weld became deeper for the same processing energy. When pure Ar was used for shielding, the discontinuous and scraggy surface was seen. At appropriate combination of shielding gases, there is a continuous and uniform surface, which exhibit stable welding process and full penetration. This was attributed to the right combination of gas shielding parameters that result in a stable process and efficient synergetic effects. Thus, the penetration increased. Furthermore, Figure 3-11 shows the relationship between plasma height and depth of penetration of welds. The smaller the plasma/plume height, the greater the absorbed energy by the workpiece and the more penetration into the substrate

is achieved. This shows that the shielding gas can have a significant effect on the weld bead profile in laser welding.

To avoid the significant effect of shielding gases, it is imperative to ensure that the same conditions and gas are used during the melting processes.

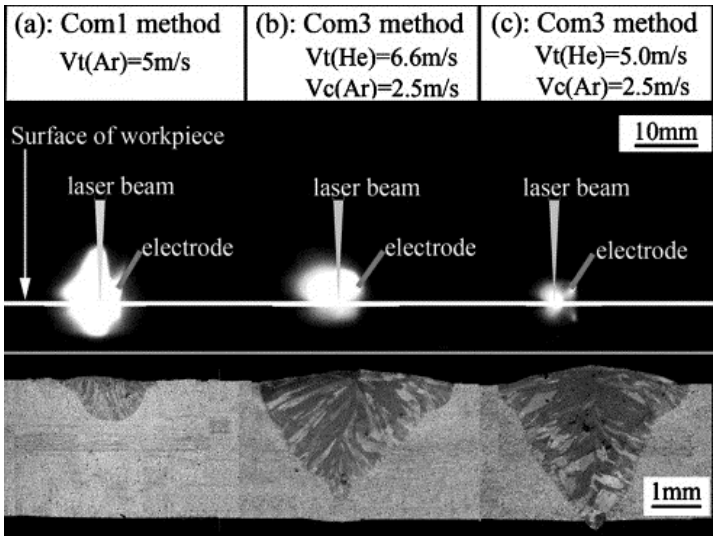

Figure 3-10: Effect of shielding gas on plasma/plume and weld bead profile (Ming et al., 2007)

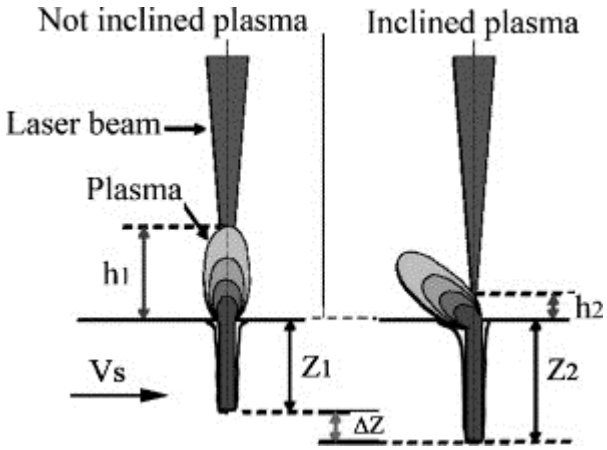

Figure 3-11: Influence of plasma/plume height on depth of penetration in laser welding (Ming et al., 2007)

3.5.2 Fluid flow dynamics and its effect on weld geometry

There have been theories explaining the influence of melt flow direction on the weld profile. Formation of a weld bead profile is the result of melting and solidification of melt pool. The dynamics can be affected by the melt flow, which is influenced by welding conditions. The primary forces affecting the melt flow are the surface tension and buoyancy force. Both of these depend on the chemical composition and thermal gradient of the liquid metal.

3.5.2.1 Surface tension

Surface tension gradient is capable of inducing strong melt flow, which can affect the weld bead or build profile. Surface tension gradient exists between fluids when subjected to a temperature gradient. An interfacial tension between the centre and edge points of the melt pool is consequently induced. Since the temperature also affects the surface tension, the temperature gradient creates a surface tension gradient that will often induce shear stresses leading to a movement of fluid. Depending on the chemical composition of the liquid, the system can have a positive or negative surface tension gradient. When the surface tension gradient is negative, the fluid flow patterns tend to be outward that is, it flows from a colder region to hotter region and positive flow moves inward (Lautrup, 2011; Eriksson and Powell, 2014).

Theories have been proposed to explain how fluid flow changes bead shapes. The change in weld pool is because of convective flow, which is driven by surface tension gradient. The surface tension gradient is caused by the difference in the temperature of the weld pool surface (Burgardt et al., 1986). These theories also suggest that metal chemistry plays a fundamental part. The weld bead shape formed depends on the surface tension magnitude and direction, which is affected by the presence of impurities called surfactants. This is because the elements tend to agglomerate on the fluid surface thereby

altering the flow direction. (Aidun and Martin, 1997) and (Roper et al., 1983) categorised these impurities, which can be divided into three main groups.

a) Surface active elements with non-reactive impurities: pure metals or alloys that have elements that can react with surface active elements to form compounds that have no influence on the surface tension e.g. pure metals or alloys.
b) Surface-active elements: elements that a small presence of which can significantly influence the surface tension and surface tension coefficient e.g. sulphur, oxygen, selenium, bismuth and tellurium
c) Surface active elements with reactive impurities: These impurities prevent the surface active elements presence influencing the surface tension e.g. aluminium, calcium, silicon and manganese.

The weld penetration and width vary with the direction of fluid flow and type of elements present in the molten pool. For most metals in their pure state or alloyed form with low presence of sulphur and oxygen surfactants, the weld geometry is wider and shallower because fluid flow provides substantially greater heat transport in the outward direction and decreasing the ratio of the depth of penetration to weld width. Therefore, the surface tension will exhibit the highest value at the edge away from the heat source (coldest region) and lowest under the heat source (hottest point), as shown in Figure 3-12a (Heiple and Roper, 1981; Zhao et al., 2010).

The presence of some substances referred to as surface active elements reverse the process by changing the entropy of the system. Notable elements in small quantity are oxygen, selenium sulphur and tellurium, which tend to the formation of soluble compounds (e.g. FeS) change the surface tension gradient. Such compounds have lower surface tension than pure iron (Aidun and Martin, 1997). Figure 3-11b shows a typical example of inward movement of fluid when surface active element significantly influences the surface tension. Previous studies demonstrated that presence of sulphur in the molten pool causes inward

fluid flow. The active elements affect the fluid flow provided that the input energy density is below the keyhole threshold. In the keyhole regime, the effect of the active elements is less important. In keyhole regime, the vaporisation pressure is more dominant than surface tension gradient (Heiple and Roper, 1981; Hu et al., 2012; Roper, Stagner and Aden, 1983).

The significant influence of the surface tension and applied energy on the melt pool can be analysed when the same condition is ensured in the melting process. In this way, the effect of reactive elements will be the same during the melting process.

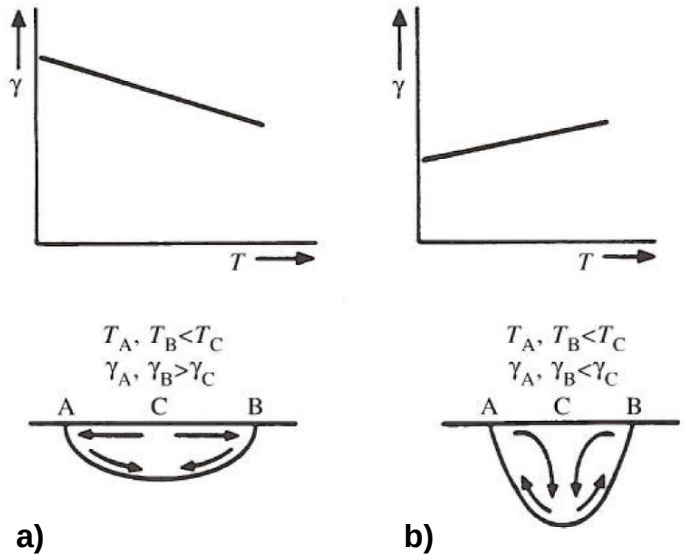

Figure 3-12: Schematic diagram of fluid flow in the weld pool a) surface tension with negative coefficient and b) surface tension with positive coefficient; T – temperature and γ –surface tension (Verhaeghe, G. and Hilton, P., 2005)

3.5.2.2 Buoyancy force

Buoyancy flow is present in any fusion process (laser, arc, oxy-fuel). This force occurs when there is a density gradient within the liquid (Kruth et al., 2007). Depending on the location of the heat source; the liquid flows from region of

high density to a region of low density typically, from hotter area to less hot region. This implies that the molten pool under the influence of buoyancy rises to the surface (Figure 3-13a) and begins to sinks (Figure 3-13b). The circulatory motion of both positive and negative buoyancy motion of the fluid flow defines the weld pool surface (Turner, 1973; Wu, 1988).

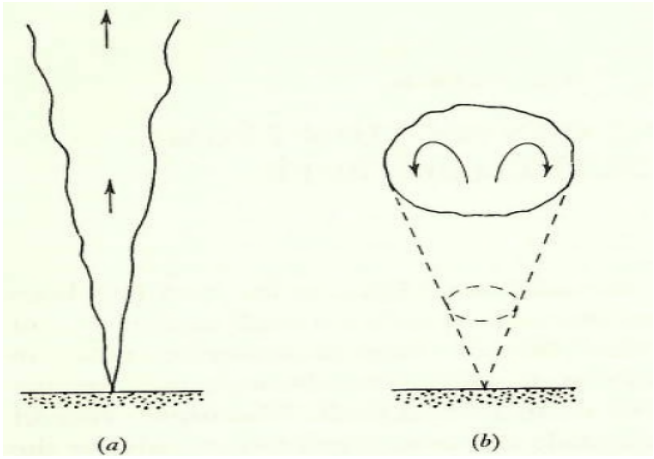

Figure 3-13: Schematic diagram of buoyancy fluid flow a) positive buoyancy flow and b) negative buoyancy flow (Turner, J.S., 1973)

Buoyancy affects the motion of the liquid metal in the weld pool. It strength depends on whether the force can influence the fluid flow magnitude and direction. The stability of keyhole and conduction welds in laser welding depends on various forces such as buoyancy, surface tension, vaporisation and hydrostatic and hydrodynamic pressures. However, surface tension pressure is the most dominant. For instance, the hydrostatics pressure is 75 N/m^2 compared to that of the surface tension of 10^4 N/m^2. Surface tension and vaporisation pressure in keyhole regime are two main forces that determine the bead formation. The vaporisation pressure is the main force required to keep the keyhole in weld profile while the surface tension tries to collapse the keyhole. Keyhole welding involves metal vaporisation and deep penetration. Hence, the vaporisation pressure is greater than the surface tension force. In

conduction welding, surface tension force is the most significant driven force for melt flow (Duley, 1999; Volpp, 2012). Tsao et al. (Tsao K.C. and Wu, C.S., 1988) investigated the significance of buoyancy force on the weld pools. They compared how changes in the magnitude of the fluid velocity and temperature field influenced the weld pools. They mentioned that buoyancy force is less dominant than surface tension driven flow. In addition, since the full welds are done in the same position, buoyancy effects are constant.

3.6 Solidification rate

Factor that affects the microstructural features when materials solidify is the shape of the solid-liquid interface. Thermal and compositional conditions that are present between the adjacent interfaces determine the nature and stability of the solid-liquid interface. In general, the variables that affect the solidification morphology are the growth rate, the temperature gradient in the liquid and alloy composition. The three methods of over which the interface can grow are: planar, cellular and dendritic (Ion, J.C., 2005). They play a dominant role in bead formation in both laser welding and powder melting. Solidification rate in solid melting (laser welding) and powder melting (laser cladding or powder bed fusion) is rapid one due short interaction time and fast cooling. When solidification takes place in the materials, the first form of growth is planar. When the temperature gradient of the planar structure is reduced, the cellular structure is also formed. The structures change strongly dependent on thermal cycle and chemical composition of the liquid. Therefore, different thermal properties of powders should result in different solidification behaviours as compared to solid metals. Thus, different bead profiles can be expected depending on material and laser properties.

3.6.1 Material properties

Material properties such as thermal conductivity, packing density, surface roughness, which determines absorptivity, play a dominant role in the interaction between the laser beam and engineering materials. These properties are inter-related and affect bead profile differently. The absorptivity of material is defined as the ratio of absorbed laser energy to the incident energy. It indicates how the applied laser energy is being transferred to the material. This section reviews how absorptivity and conductivity of the material influence build profiles when exposing to laser radiation (Ion, J.C., 2005; Qi et al., 2006; Toyserkani, E. et al., 2005).

Laser beam interactions in relation to the absorptivity vary with the surface condition of materials. The absorptivity of laser energy improved with surface modifications. The surface area of a material increases with increasing surface roughness. A rough surface has a greater surface area, which when exposed to the laser beam increases the likelihood of multiple reflections on a micro-scale thereby improving the absorptivity. This implies that the build profile in powder melting and weld profile of solid melting of the same chemical composition may vary due to the difference in material absorptivity. When a surface modification is applied to a workpiece, the absorptivity will change. In solid materials, the absorptivity is enhanced with different techniques, which include surface coatings, sandblasting, milling, etc. It has been shown that absorptivity of sandblast surface increased by 50% (Sayegh, 1998; Yasa et al., 2011), graphite coating by 86% (Pantsar et al., 2004) and milled surfaces by 5% (Sayegh, 1998). When a surface is sandblasted or milled, the absorptivity increased due to increasing in surface roughness that promotes multiple reflections and increasing surface area. A coated surface usually reduces the reflection of the laser beam. Thus, the expected melt area of solid materials increases significantly with surface modification.

Powder materials have an advantage when it comes to absorptivity, as compared to solid materials. Table 3-6 shows the absorptivity of solid and powder materials. The absorptivity of the solid material was obtained from the optical properties of the materials based on calculation. In the table, the normal spectral absorptance of powders was measured to determine the absorptivity for different powder materials. In their experiment, the radiation which is reflected by powder particles and arrives at the photo receiver was registered and compared with a specimen of known reflectance (Tolochko, N.K. et al., 1997; Tolochko et al., 2000). Table 3-6 shows the comparison between the measured and calculated absorptivity. The table indicates approximate values of absorptivity for different materials. The higher absorptivity of most powders may suggest different absorptivity between the solid and powder materials.

However, there is not any data of a direct comparison of melting between powders and metal reported in the literature.

Table 3-6: Absorptivity of selected solid and powder metals for a laser wavelength of 1.06 µm (Tolochko, N.K. et al., 1997; Tolochko et al., 2000; Toyserkani, E. et al., 2005)

Materials	Solid metal	Powder metal
	Absorptivity (A)	Absorptivity (A)
Aluminium	0.09	Unavailable
Copper	0.01	0.59
Titanium	0.46	0.77
Iron	0.36	0.64
Nickel	0.26	0.64
Lead	0.16	0.79
Tin	0.39	0.77
Zinc	0.42	Unavailable

The mechanism over which laser beam propagates through powder particles has been studied (McVey, R. W. et al., 2007). When the laser beam irradiates a rough surface of powder particles, some portion of laser energy interacts directly with the powder particles and the remaining portion is reflected off, as shown in Figure 3-14. The depth of penetration of the laser beam within the powder particles varies depends on a geometrical configuration of the powder particles and the wavelength of a laser beam (Khan and Dickens, 2012; McVey, R. W. et al., 2007). Therefore, a significant portion of the reflected beam is re-absorbed via multiple reflection mechanism on the subsequent particles. This enhances absorptivity of the powders compared to the solid material. For a

powder of mixture of coarse and fine aggregates, the absorptivity is higher compared to coarse aggregate. The surface area on the powder particle depends on particle size and distribution. A reduction in the particle size enhances the laser beam absorption with a minimum reduction in amount of energy reflected. However, the increment in the absorbed energy of powder material is temporary. As the particle melt to form liquid pool, the reflection of the beam approaches that of a liquid materials. This could be a similar absorption of laser irradiation by both solid and powder materials (Khan and Dickens, 2012; McVey, R. W. et al., 2007).

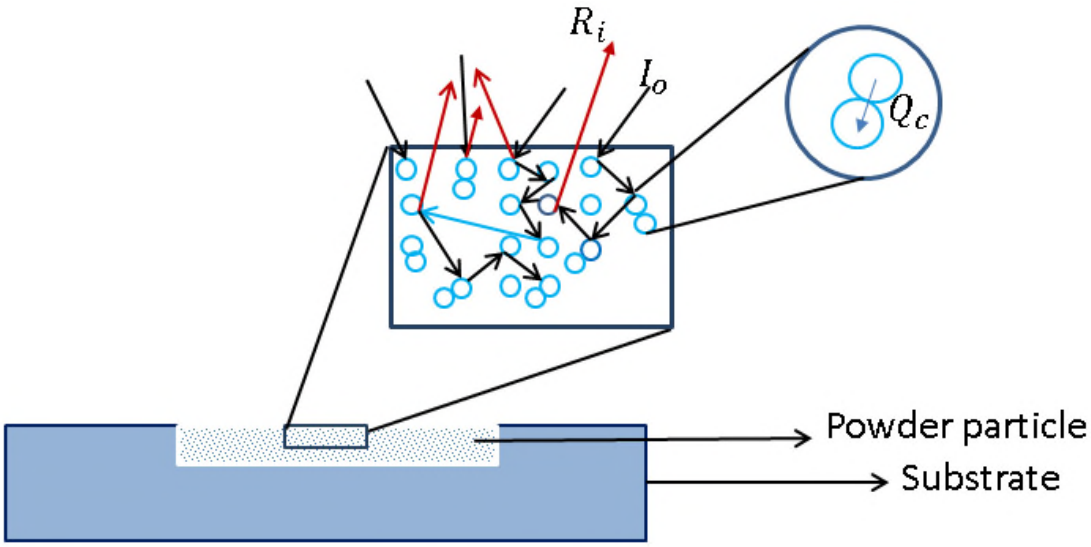

Figure 3-14: Multiple reflections in powder, I_o – incident laser radiation; R_i – reflected laser radiation; Q_c – heat transfer through (Khan and Dickens, 2012)

The laser wavelength is another important aspect in absorptivity. Absorptivity varies with laser wavelength since the optical properties of these materials are fundamentally dependent on wavelength, as shown in Table 3-7. For instance, Table 3-7 indicates that for the same material, absorptivity increases with decreasing wavelength. CO_2 laser has longer wavelength compared to Nd:YAG

laser, which significantly reduces the amount of absorbed laser energy by the workpiece (Kruth, J. P. et al., 2006; Majumdar and Xia, 2007; Sayegh, 1998; Steen and Mazumder J, 1999).

Table 3-7: Comparison of absorptivity of metallic powders for two different wavelength lasers (Kruth, J. P. et al., 2006)

Powder materials (metals)	Nd:YAG (1.06 μm)	CO2 (10.6 μm)
Cu (absorption in solid Cu)	59% (2 – 10%)	26% (1%)
Fe (absorption in solid Fe)	64% (30%)	45% (4%)
Sn	66%	23%
Ti	77%	59%
Pb	79%	
Co-alloy (1%C, 28%Cr & 4%W)	58%	25%
Cu alloy (10%Al)	63%	32%
Ni alloy	72%	51%

Cu – copper, Fe – iron, Sn Tin, Pb – lead, Co - Cobalt, Cr chromium, W – tungsten and Ni - nickel

The role of the interpass temperature and its effect on absorptivity and the build profile was investigated. In their study, the interpass temperature was the temperature of the previous layer before the deposition of the subsequent layer. The role of interpass temperature on the absorptivity was investigated by measuring the mass of built specimens. They observed that changing the temperature between successive tracks influenced the quantity of fused powder, which was due to increased absorptivity, as shown in Figure 3-15. When there was no cooling between successfully deposited tracks, the high

interpass temperature preheated the base material and increased the melt volume of powder (Badrossamay and Childs, 2007).

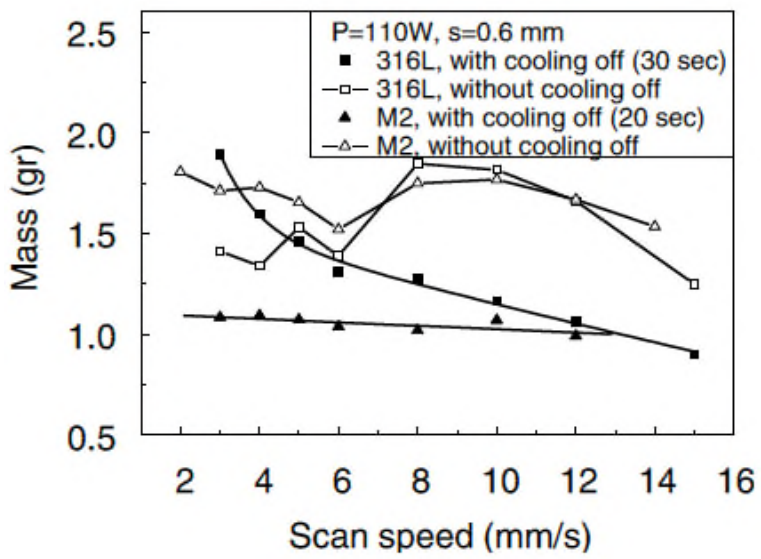

Figure 3-15: Effect of interpass temperature on mass of single track layers in 316L and M2 steels as a function of scan speed at different laser power and scanning spacing (Badrossamay and Childs, 2007)

However, the propagation of the transported heat within the material will also determine weld profile. Since in metallic materials, the main mechanism of heat flow is by conduction, the pores between the particles determine the extent to which the heat propagated inside the material. When there is a poor contact between the particles, the heat cannot be conducted onto surrounding particles, the individual particle will vaporise, and heat is lost. Thermal conductivity determines how fast the heat is transferred from the laser interaction zone to the inner parts of materials. In Section 3.6, it was explained that the solidification morphology of solid and powder materials is similar. However, the effective thermal conductivity is different, which can result in different build deposition. Since solid substrates have homogeneous properties, heat conduction is uniform in all directions, resulting in hemispherical isotherms and

weld profiles. However, in powders, thermal conductivity may vary depending on the compactness and particle size and distribution (Alkahari et al., 2012). Effective thermal conductivity of powder material is controlled by the proportion of the powder compactness (air gap), particle sizes and morphology (Tolochko et al., 2003). The way the heat propagates within the material determines the shape of weld pool.

A study by (Alkahari et al., 2012) showed that the thermal conductivity of materials increases with increasing powder particle sizes. The larger the particle sizes, the higher the thermal conductivity, due to high conductive heat transfer between the powder particles. They mentioned that such a condition only apply when the total air gap per unit area is constant. In this condition, the effect of air gaps between powder particles becomes insignificant. In reality, such assumed conditions may not be achievable. In real conditions, by using collections of powder particle of finer sizes, it becomes denser and compacted together and therefore the ratio of air gaps to the powder volume decreases (Desmond and Weeks, 2013). In most cases the thermal conductivity of solid materials is greater than powders for the same type of material (Pinkerton and Li, 2004) The thermal conductivity of powder approaches that of solids for the same material when the surface contact takes place between the melted powder particles (Gusarov et al., 2007). However in real conditions melt flow is another efficient way of transporting the heat (Childs et al., 2005). This means that despite poor contact between individual particles, the heat exchange is possible if liquid metal surrounds particles. Therefore, considering multiple reflections, absorptivity and heat transfer by liquid, greater weld profiles should be achieved in powders than in solids.

3.6.2 Welding regimes in solid and powder melting

There are three welding regimes in laser welding of solid materials, which are conduction, transition and keyhole (see Section 3.1). There is a lot of speculation on the welding regime in powder beds in the laser community.

Some authors claim that powder bed fusion processes is similar to laser cladding and it is a conduction process (King et al., 2014; Toyserkani, E. et al., 2005). This is mainly determined based on the weld profile. Identification of welding regime in powder melting may be more complex than in solid materials due to inhomogeneous properties of powders. In this section, comparison of existing information for powder melting regime identification is presented. Some of the examples of similarities and differences between solid and powder melting are shown in Table 3-8. In this table, studies on solid and powder melting were compared in terms of conditions required to achieve the forms of welding regimes available. In solid melting, three welding regimes can be seen with necessary conditions. In powder melting, there is no indication the existence of vaporisation and plasma formation in powder melting. Based on the experience of welding of solid materials the threshold interaction parameters for vaporisation can be identified. In solid melting, plasma and vapour plume is a good indication of the transition or keyhole regime. It is adequate to assume that to achieve good quality deposits powder melting should be considered as a conduction welding problem. Due to the complexity of the processes and inhomogeneous properties of powders, there is a threshold between conduction and keyhole regime.

Table 3-8: Comparison of existing information for powder melting regime identification

Properties	**Powder melting**		**Solid melting**		
	Conduction regime	Keyhole regime	Conduction regime	Transition regime	Keyhole regime
Metal vaporisation	No/Yes unclear[1]		No[2]	Yes[2]	Yes[3]
Plasma formation	No/Yes(Kruth et al., 2004)[1]		No[2,4]	No information	Yes[5,6]
Heat flow pattern	3-dimensional heat flow is desirable[7]		3-dimensional[8]	No information	2-dimensional[8]
Surface temperature	Above melting but below vaporisation		Ideally below vaporisation[2,5]	No information	Above vaporisation[5,9]
Process stability	No information		More stable than keyhole	Dynamic	Dynamic
Interaction parameters	No adequate information for wide range of beam diameters		Below 10^6 W/cm^2 (depends on beam diameter and interaction time)	Vary with interaction parameters and beam diameters	Above 10^6 W/cm^2 (depends on beam diameter and interaction time)
Aspect ratio (depth/width)	AR of ≤0.5[1] is desirable		AR ≤0.4[2,4]	AR of 0.4 to 0.6[2,4]	AR≥ 0.6[2,4]
Likelihood of defects	Defects are not desirable		No	No	Keyhole porosity, spatter

1.(Kruth et al., 2004); 2.(Assuncao, E. et al., 2012); 3.(Wang et al., 2007); 4.(Sánchez-Amaya et al., 2009); 5.(Fuerschbach P.W. and Eisler G.R., 2002); 6. (Suder, 2012); 7.(Hauser, 2003); 8.(Sayegh, 1998); 9.(Ion, J.C., 2005);

The processing regime has a big implication on the quality and productivity. Because all the issues related to vaporisation, such as melt expulsion, spatter, vapour pressure the process should be maintained within the conduction regime. This is because the productivity and resolution requirements often dictate the use of small beam diameters with high power density, conditions which are very prone to vaporisation. Profiles of deposited tracks suggest conduction welding, however in some studies evidence of evaporation (Kruth et al., 2004) and keyhole (King et al., 2014) was found. In the same study, a powder-bed fusion of powder melting was classified has a conduction welding, as shown in Figure 3-16 (King et al., 2014). The regimes of powder-bed fusion process in both cases were based on bead profile (Eagar and Tsai, 1983; King et al., 2014). Figure 3-16a shows conduction profile with lower power density and bigger beam diameter while Figure 3-16b is a keyhole build profile of higher power density and smaller beam diameter. Thus, the applied energy is very high for the build profile in the keyhole regime. Considering the laser power, scanning speed and beam diameters used, the parameters suggest the power density used is beyond the threshold for conduction regime. It seems that because of the extreme processing conditions i.e. small beam diameters, fast processing speeds and inhomogeneous properties of powders, the threshold between conduction and keyhole regime is narrow and the process may easily switch between both.

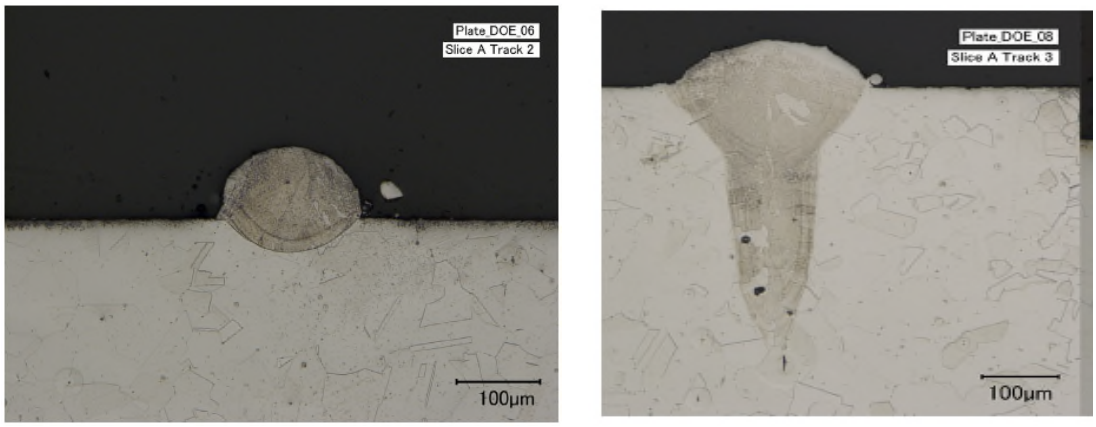

Figure 3-16: The cross section of a powder track fused by laser power of 150 W with different beam diameters (a) conduction regime (beam diameter = 0.15 mm and scan speed = 188 mm/s) and (b) keyhole regime (beam diameter = 0.052 mm and scan speed = 100 mm/s)(King et al., 2014)

3.7 Melting and penetration efficiency

In solid melting of materials, a portion of the applied energy is absorbed while some are reflected. Thus, only some portion of absorbed energy is utilised for melting and rest is dissipated and considered as losses. Melting efficiency is the ratio of the energy utilised for melting to form the fusion zone to the net absorbed energy. Normally, in any welding processes, it is desired to maximise melting efficiency. In laser processing, the total absorbed energy is distributed between energy utilised for fusion, conduction loss, evaporation, formation of heat affected zone, and plasma plume formation. In conduction welding and powder melting, the common form of energy losses are conduction and convection. The contribution of convection is often assumed to be negligible as compared to conduction losses (Greses, J. et al., 2003; Kruth et al., 2004). Thus, the energy of fusion and absorbed energy by the heat affected zone (HAZ) are equivalent to the net absorbed energy by the solid or powder, as given in Equation 9. The energy necessary to achieve the fusion zone depends on the pool volume melting rate ($t_s A$) and material properties, as shown in Figure 3-17 (Badrossamay and Childs, 2007; Fuerschbach and Eisler, 1999;

Greses, J. et al., 2003). This suggests that melting efficiency of solid and powder melting can be compared with the weld and build geometry in terms melt area, as in Equation 12. The difference in the profiles could be because of difference in material properties.

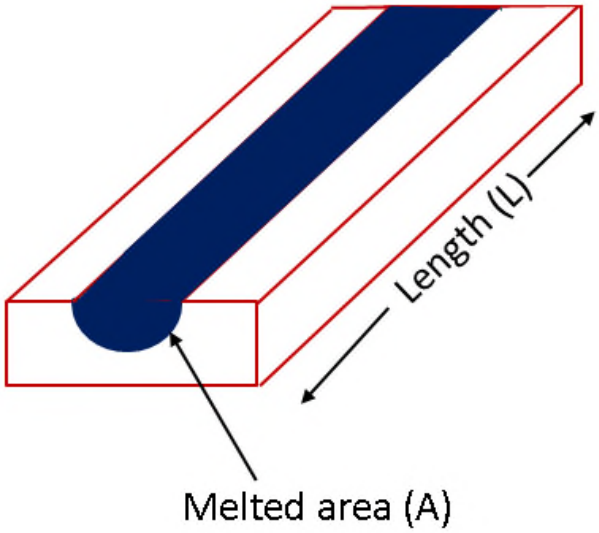

Figure 3-17: Schematic projection of weld bead geometry

$$E_{absorbed} = E_{fusion} + E_{cond} \tag{9}$$

$$E_{absorbed} = \rho V_{fusion}[C_{pm}(T_m - T_{room}) + H_f] + \rho V_{cond}[C_{ps}(T_{cond} - T_{room})] \tag{10}$$

$$\text{Melting efficiency } (M_{eff}) = \frac{Energy\ for\ fusion}{Net\ absorbed\ energy} \tag{11}$$

$$\text{Melting efficiency } (M_{eff}) = \frac{\rho V_{fusion}[C_p(T_m - T_{room})}{P * t} \tag{12}$$

$E_{absorbed}$ is the energy absorbed by the substrate

E_{fusion} is the energy required to melt a volume of metal

E_{cond} is the energy loss due to heat conduction

$C_{pm}, heat\ capacity\ of\ melting(680\ J(kgK)^{-1});\ T_m, melting\ temperature\ of\ the\ plate\ (1510\ K); T_{phase}, phase\ transformation\ temperature\ (1200\ K);\ T_r, room\ temperatureof\ the\ plate\ (300\ K); H_f, heat\ of\ fusion\ (2500000\ Jkg^{-1});\ V, melt\ volume(melt\ cross\ sectional\ area * length\ of\ the\ plate)and\ \rho, density\ of\ mild\ steel(7800\ kgm^{-3}), C_{ps}, heat\ capacity\ of\ solid(466\ J(kgK)^{-1}$(Greses, J. et al., 2003)

Melting efficiency examines the response of the material response to laser energy in terms of melt area, bead length and material properties. Alternative method of comparing material response to applied laser energy spot is with the penetration efficiency. Penetration efficiency is the ratio of depth of penetration to the applied laser spot energy, as given in Equation 13 (Assuncao E., 2012). Penetration efficiency is very useful to compare two or different materials in terms of depth of penetration when the same laser energy is applied.

$$Penetration\ efficency = \frac{Depth\ of\ penetration}{Laser\ spot\ energy}\ (\frac{mm}{J}) \quad (13)$$

3.8 Summary

The current method of characterising the build profile in powder melting is based on the engineering approach. Furthermore, the welding regime of powder melting switches between conduction and keyhole when system parameters are used. This makes it difficult to understand the process and improve the quality of built parts. Every powder machine is developed based on individual design, which further makes the transferring data between different machines difficult.

Thus, there is no adequate understanding of the process and parameters controlling the build profile are unclear. This is because there is no direct relationship between the system parameters and the resulting bead profile. The resulting bead profile is defined by the thermal cycle, which depends on the interaction parameters and material type and properties. The build profile is a result of complex balance between surface tension, vaporisation pressure, temperature gradient, melt flow etc. In laser welding, there are three welding regimes: conduction, transition and keyhole. The welding regimes depend on the pressure of vaporisation and surface tension and applied interaction parameters, which vary with the system parameters. The use of interaction parameters that are independent of the optical set-up have helped to improve welding process. In keyhole welding to achieve similar welds profile and with similar quality, power density and specific point energy were used to control the weld depth and weld width with interaction time. Furthermore, the material properties, such as absorptivity, conductivity, and material type and laser wavelength can also influence the build profile.

This study proposes the use of the interaction parameters of power density, interaction time and specific point energy to characterise powder melting. FLMIPs should enable us to improve and understand the bead formation independently of the laser system. Furthermore, it allows a better understanding of the effect of beam diameter and improvement of data transferability between different machines. Due to lack of adequate information about the effect of interaction parameters in conduction welding, the initial study concentrated on the interaction parameters controlling weld bead profile in conduction welding. Subsequently, parameters controlling build profile in powder melting were also investigated.

4 General experimental set-up and methods

4.1 Set-up used for solid and powder melting with large beam diameters (0.60 –5.50 mm)

4.1.1 Laser source

An IPGYLR-8000 continuous wave (CW) fibre laser with an output power of 8 kW and a wavelength of 1.07 µm was used to manufacture the bead-on-plate welds. The laser beam delivery system consisted of an optical fibre with a diameter of 300 µm and a collimating lens with a focal length of 125 mm. Focusing lenses with focal lengths of 250 mm, 680 mm and 1000 mm which resulted in spot sizes of 0.61mm, 1.70 mm and 2.35 mm respectively were used (see Table 4-1). Additional experiments were conducted with focusing lens of 250 mm out of focus position to achieve a wider range of beam diameters.

A Primes GmbH Focus monitor was used to determine the beam characteristics namely, beam diameter, focus position and divergence angle. Beam caustics data were also determined to find appropriate defocusing distance needed to achieve a particular beam diameter. To prevent laser head from back reflection, the optical head was tilted at 10^{o}, as shown in Figure 4-1 during the experiments. This set-up was used for both solid and powder melting.

Table 4-1: Measured propagation properties of laser beams for different optical set-ups

Focusing lens (mm)	Beam diameter (mm)	Rayleigh length (mm)	Divergence angle (mrad)
250	0.61	6.60	92.50
680	1.70	36.48	44.16
1000	2.35	91.80	25.42

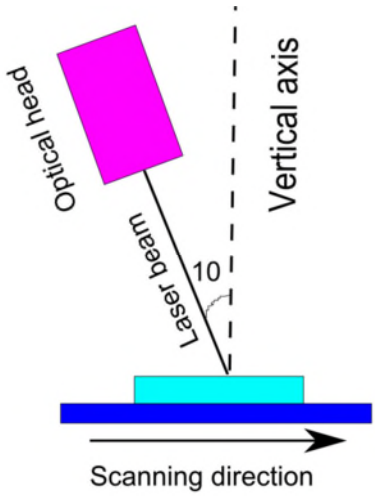

Figure 4-1: Laser head tilted at an angle of 10^{o} to prevent back reflection

4.1.2 Motion and clamping set-up for high power laser in solid melting

The translation of the laser beam over the workpiece was achieved with a six-axis Fanuc M700i B45 robot coupled with a single axis translation stage, as shown in Figure 4-2. The samples were clamped using a clamping system at both ends.

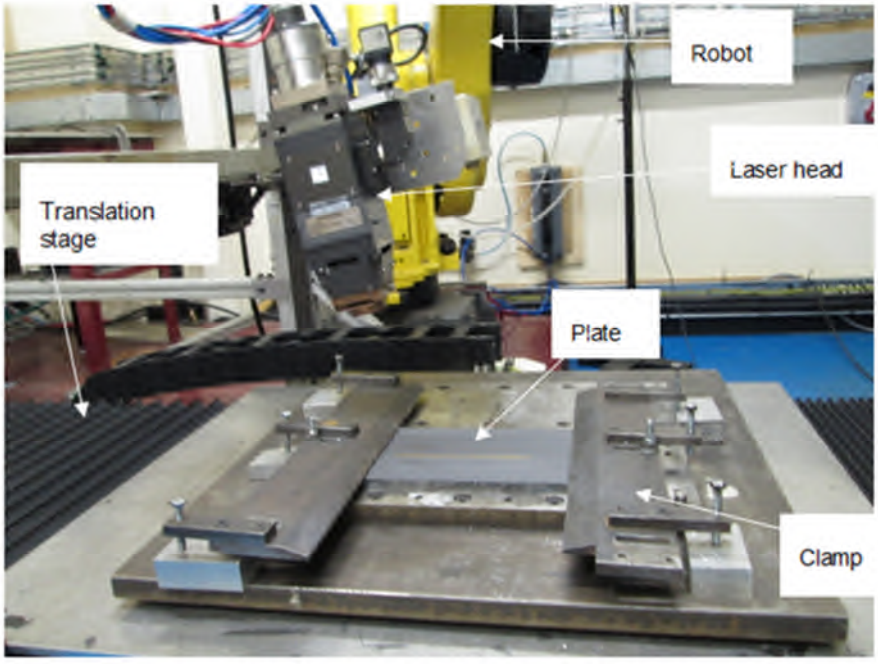

Figure 4-2: Experimental set-up used for laser welding

4.1.3 Processing chamber for powder melting (without shielding)

The processing chamber was used for powder melting with high power laser. The processing chamber used was a custom-made enclosure. The set-up consisted of the constructed chamber box, system control unit and sample motion mechanism. The laser beam was delivered to the workpiece through an optical window allocated in the top surface of the chamber, as shown in Figure 4-3. In the initiall experiments conducted in solid and powder melting, the effect of shielding gas was not significant on the bead profiles with large beam diameters. So, no shielding gas was used for solid and powder melting with large beam diameters.

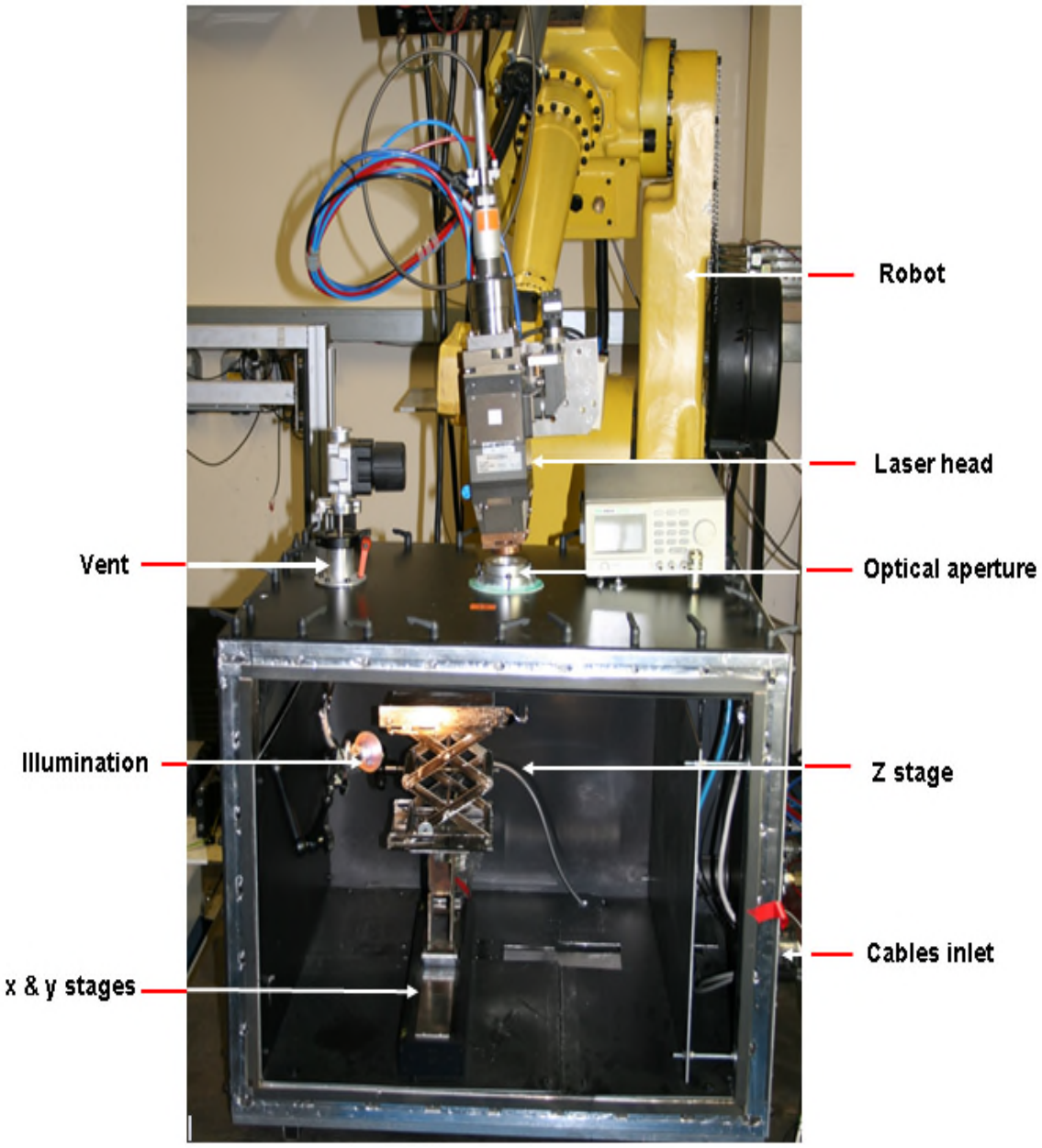

Figure 4-3: Experimental set-up used for large beams

4.2 Set-up used for solid and powder melting with small beam diameters (0.10 mm)

4.2.1 Low power lasers

An SPI fibre laser (JK500FL) with maximum output power of 500 W and a wavelength of 1.07 µm was used. Laser beam delivery system consisted of an optical fibre with a diameter of 300 µm and a collimating lens with a focal length of 115 mm. Focusing lenses with focal lengths of 300 mm, which resulted in spot sizes of 0.10 mm was used. To prevent laser head from back reflection, the optical head was tilted at 10^{o}. The set-up was used for both solid and powder melting.

4.2.2 Processing chamber for solid and powder melting (with shielding)

Similar set-up as shown in Figure 4.3 was also used for solid and powder melting with small beam diameters. Except that, the chamber was airtight with argon gas. Argon gas was supplied through the air knife to provide oxygen free environment and to protect the optical window from contamination. The shielding gas was used for the process because of the small conduction welds been produced and some welds are also in keyhole regime. The oxygen level maintained was less than 500 ppm. Low power laser from SPI was used for this experiment.

4.3 Commercial powder bed machine (with shielding)

Renishaw AM250 machine with a fibre laser having a maximum output power of 200 W was used. The theoretical spot size of this laser system is 0.07mm. Note that, in this case, the real beam diameter could not be measured due to time limitation. The Renishaw laser works on the principle of a pseudo pulsed laser. The exposure time is the period of interaction between the laser beam and the

material. The point distance is the distance between two successive ends of the laser spot. There was no overlap between the successful spots because the beam diameter used equals the point distance. The interaction time was taken as the exposure time. With this system, only a few welds in solid steel were produced.

4.4 Material: analysis, composition, preparation and processing

4.4.1 Solid melting

S275 mild steel of 250 mm x 160 mm x 12 mm thick was used. The nominal chemical composition of the S275 mild steel plates used is shown in Table 4-2. All the plates were thoroughly cleaned with acetone solution prior to welding. Then the samples were coated with graphite spray. This is to minimise variations of the absorptivity of the laser radiation.

Table 4-2: Nominal chemical composition of S275 mild steel used in this thesis

Material	**Elemental composition (wt %)**						
S275 mild steel	Fe	C	Si	Mn	Cr	Ni	Cu
	98.28	0.14	0.30	1.16	0.05	0.02	0.05

4.4.2 Powder material

The powder materials used in this study was nitrogen atomised pure iron supplied by Sandvik Osprey Ltd. Table 4-3 shows the nominal chemical compositions of the as-received pure iron. The average particle size of the powder was less than 150 μm. This powder was selected due to its close composition to the solid steel used in this work.

Table 4-3: As-received nominal chemical composition of the pure iron

Elements	Fe	C	Mn	Si
wt %	99.0	0.10	0.40	0.50

Figure 4-4 shows the particle size particle distribution of the iron powder used. The powder material was used in as-received condition without sieving. The powder materials were treated with minimum exposure to the atmosphere to reduce the absorption of moisture and prevent its contamination.

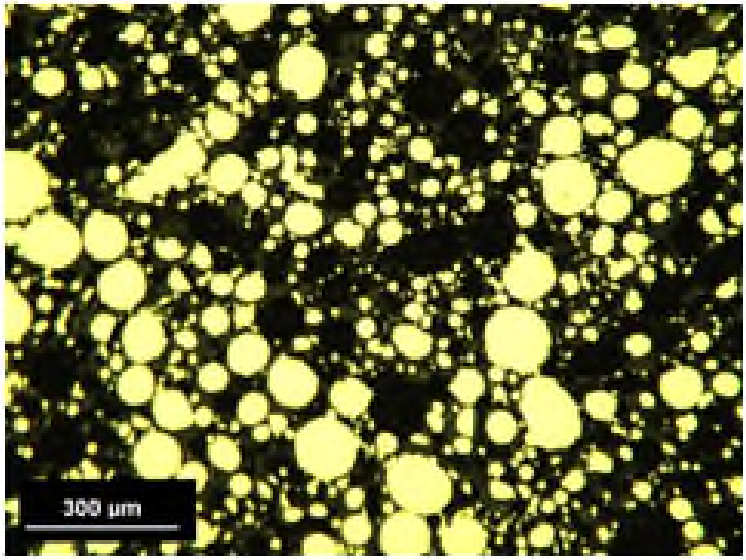

Figure 4-4: Particle size of the pure iron powder used in this work

The same material S275 mild steel was used as substrate material for powder melting as for conduction welding. Grooves of different depths ranging from 0.20 mm to 1.00 mm were machined in the base plates (see Figure 4-5). The width and length of each groove was 10 mm x 90 mm respectively. The groove depths served as the layer thickness for the powder melting process. The grooves were later cleaned with acetone solution. It was allowed to dry and then

manually filled with powder. Shown in Figure 4-6 is an example of a groove with 200 µm depth.

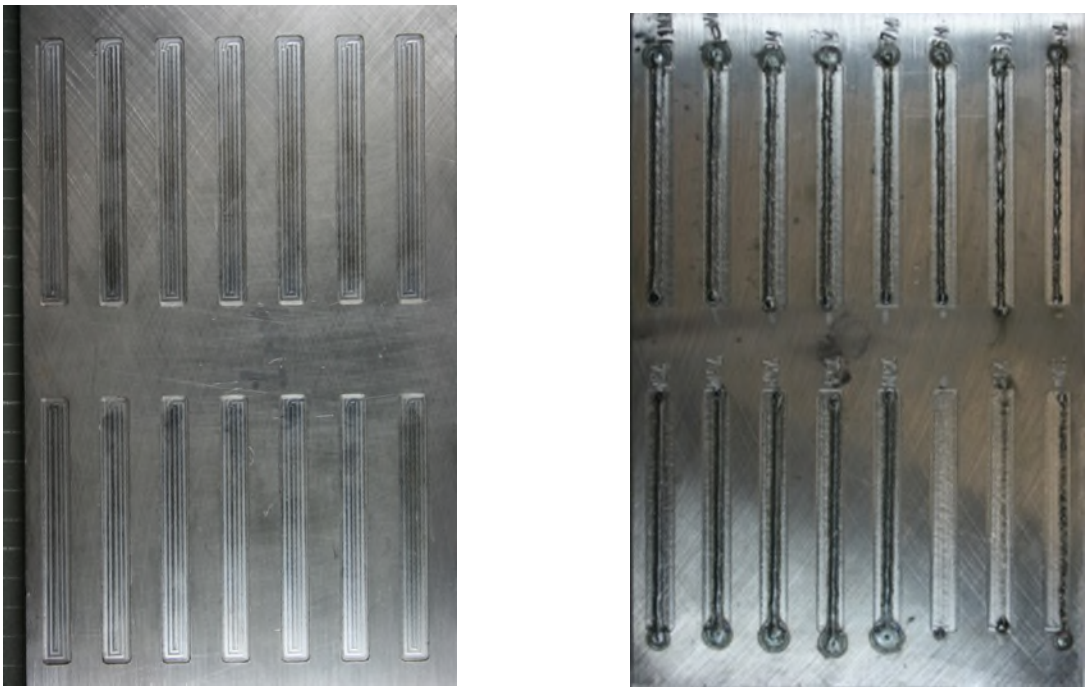

Figure 4-5: Substrate plates a) milled substrate with groove depth of 0.50 mm and b) substrate with deposited tracks

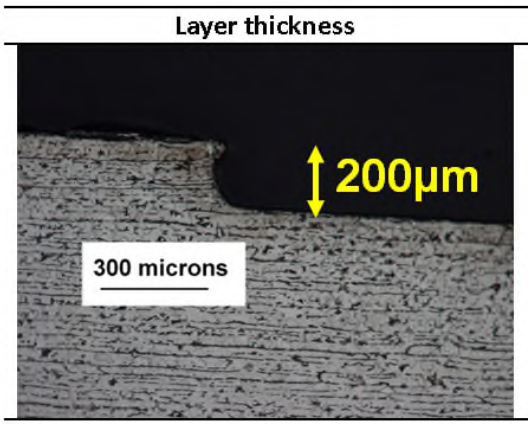

Figure 4-6: An example of groove with a depth of 200 µm before being filled with powder

One of the objectives of this study is to compare solid and powder melting. The depth of penetration (d) and weld width (ww) in solid melting was compared with build height (BH) and build width (BW) in powder melting as shown in Figure 4-7. The aspect ratio of weld bead profile is defined as the ratio of depth of penetration to the weld width (d/ww) and build layer aspect ratio is given as ratio of build height to the build width (BH/BW)

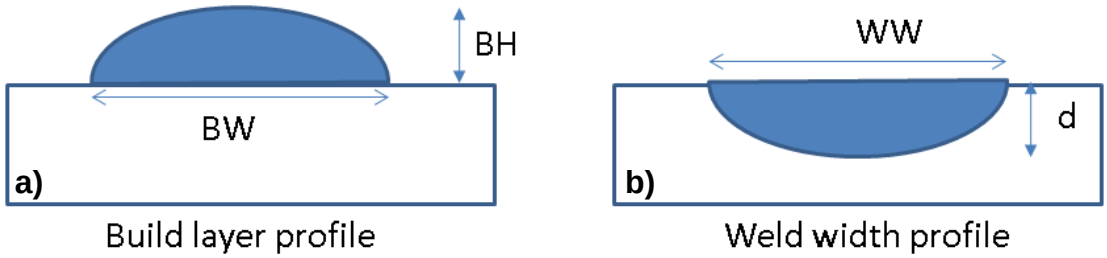

Figure 4-7: Schematic representation of bead profiles to be measured a) build layer and b) weld bead

4.5 Preparation of samples for metallographic inspection

The same procedure was used for the bead on plate welds and the deposited powder layers. The samples cross sections were taken at a half-length of each bead. All the samples were ground and polished using a grinding machine with grinding papers of grades 240 µm, 1500 µm and 2500 µm. The polishing was carried out with a 3 µm diamond paste. Subsequently, the final stage of polishing was carried out with a silica suspension of 0.05 µm. To reveal the cross sectional images of the samples were etched with 2% Nital solution.

4.6 Software used for samples measurement

The image processing and measurements were done with AxioVision LE64 software. The measurement errors of the bead profile, associated with the systematic error of focusing of the optical microscope were in the order of ± 0.05 mm for all the range of magnifications used. Each sample was measured three times and the average was used.

4.7 Analysis of samples measurement errors

The second trial of experiments was carried to examine the variation in the depth of penetration of the welds produced. Welds were produced to achieve conduction profile and sectioned longitudinal section as in Figure 4-8 to observe the variation in the weld depth. The weld depths are very consistent.

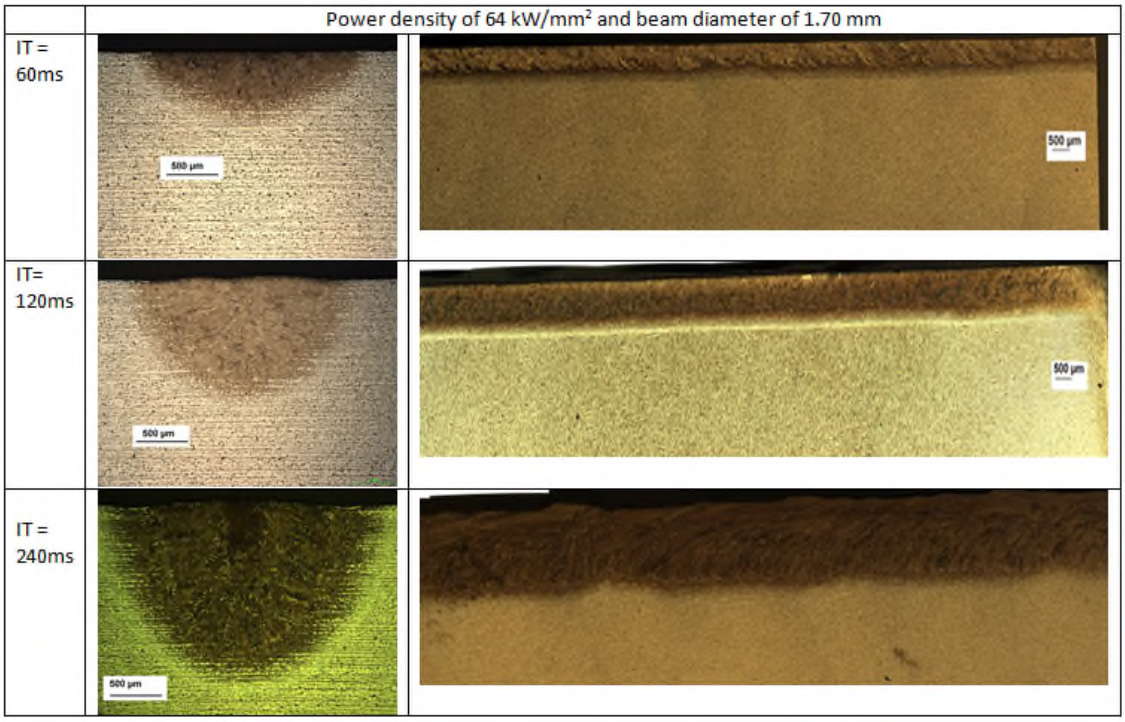

Figure 4-8: Analysis of the errors of weld depth along the longitudinal sectioning

5 Solid melting: Investigation of laser material interaction parameters in conduction welding with medium and large beam diameters

The objectives of this chapter are

- To investigate the basic laser material interaction parameters that control the weld bead profile and melting efficiency in conduction welding over a wide range of beam diameters.
- To investigate equivalent parameter to power factor in conduction regime

5.1 Research approach

To achieve this objective, a range of beam diameters between 0.07 mm and 5.50 mm was used to achieve different combinations of interaction parameters of power density, interaction time, specific point energy and energy density. Shown in Figure 5-1 is the research approach adopted in this study. Different lasers were used for different regimes depending on the beam diameter needed. The beam diameters greater than 1.00 mm were considered medium or large. Hence, laser with an output of 8 kW was used. For the beam diameters less than 1.00 mm were regarded to be small, lower laser power were used, one from Renishaw company and the other from SPI Fibre Lasers.

In Figure 5-1, studies have been carried out with medium and large beam diameters for the keyhole regime (Suder, W.J. and Williams, S., 2014; Suder, W.J. and Williams, S.W., 2012). Work is ongoing for the investigation of interaction parameters that control bead profile for very small beam diameters in keyhole regime by another researcher. Also, the transition between the keyhole and conduction has been investigated (Assuncao E. et al., 2012; Assuncao, E., Ganguly, S., Yapp D. and Williams, 2010). The current study is on the investigation of interaction parameters that control the weld profile with a wide range of beam diameters for conduction regime and powder melting.

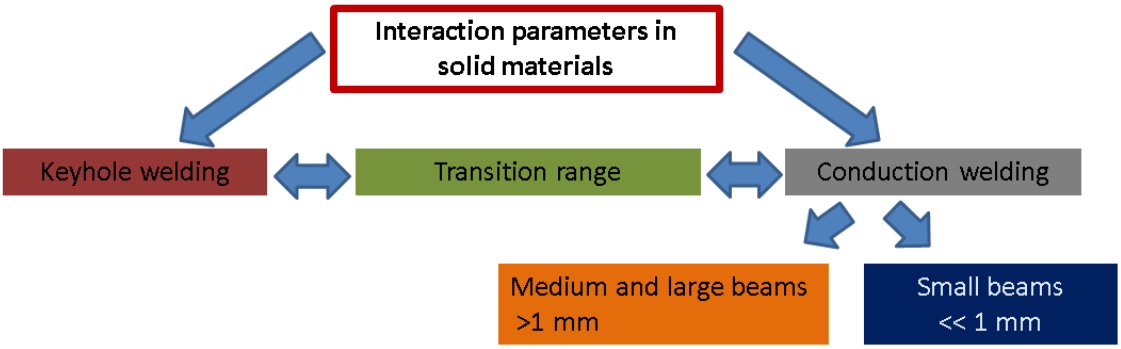

Figure 5-1: Classification of beam diameters for research approach

Studies carried out in this chapter aimed at using interaction parameters to understand the behaviour of bead profile. The detail of the experimental procedure and results are described. The beam diameters medium and large were investigated in this chapter.

5.2 Experimental procedure

5.2.1 Investigation of constant power density (P_d) and specific point energy (E_{SP}) on the weld bead profile

In keyhole welding, it was shown that constant power density and specific point energy control the depth of penetration and interaction time controls weld width for different beam diameters (Suder, W.J. and Williams, S.W., 2012). To investigate if the same behaviour can be observed in conduction welding, an experiment with constant power density and specific point energy and different beam diameters was performed. The welding parameters were adjusted to a given beam diameter according to Equation 1 and Equation 3 to obtain constant power density and specific point energy respectively. The interaction time was obtained according to Equation 2. Other experiments were carried out for a range of power densities and specific point energies of pairs 55.1 kW/cm^2 and 215J; 64.0 kW/cm^2 and 251 J; and 75.0 kW/cm^2 and 294 J in that combination.

$$Power\ density\ P_d = \frac{4P}{\pi D_B^2}\ [Wm^{-2}] \quad (1)$$

$$Interaction\ time\ t_i = \frac{t_s}{D_B}[s] \quad (2)$$

$$Specific\ point\ energy\ E_{SP} = P_d \cdot t_i \cdot \frac{\pi D_B^2}{4}[J] \quad (3)$$

5.2.2 Investigation of constant power density (P_d) and interaction time (t_i) on weld bead profile

In Section 5.2.1, the effect of constant power density and specific point energy on the weld bead geometry was investigated. This current section examines the effect of constant power density and interaction time (product is energy density) on weld geometry for large beam diameters. The welding parameters were adjusted to a given beam diameter according to Equation 1 and Equation 2 to obtain constant power density and interaction time respectively. The approach was investigated for other power densities of 22.9 kW/cm^2, 25.5 kW/cm^2 and 28 kW/cm^2. Furthermore, the effect of increasing beam diameter at constant power density and interaction times was examined on the weld geometry. This was also carried out with the same power densities and interaction times.

5.2.3 Investigation of constant energy density (E_d) across a wider range of beam diameters

This experiment was conducted at constant energy density (product of power density and interaction time). The energy density was maintained constant while changing the beam diameter. This will enable investigation of constant energy density across a wider range of beam diameters. The beam diameters used were between 0.60 mm to 5.50 mm. Laser power and travel speed were adjusted to each of the beam diameters projected on the workpiece surface to

attain power densities of 33.1 kW/cm^2 and 45.1 kW/cm^2 and interaction time of 120 ms, according to Equation 1 and Equation 2 respectively.

5.2.4: Investigation of power density (P_d) and interaction time on melting efficiency (M_{eff})

The following experiments were carried out to understand the effect of interaction time and power density on melting efficiency. Two levels of power densities of 41.5 kW/cm^2 and 64 kW/cm^2 were obtained by applying laser power to the beam diameter of 1.80 mm. The travel speed was varied to obtain the interaction time between 4 ms and 200 ms for the two levels of power densities. The effect of beam diameters on the melting efficiency was investigated at six levels of 0.60 mm to 5.50 mm. The same welding parameters investigated in Section 5.2.3 were used. The melting and penetration efficiencies were calculated according to Equation 12 and Equation 13 respectively. The melt areas and depths of penetration measured from the macrographs were used in these equations.

$$\text{Melting efficiency } (M_{eff}) = \frac{\rho V_{fusion}[C_p(T_m - T_{room})}{P * t} \quad (12)$$

$$\text{Penetration efficiency} = \frac{Depth\ of\ penetration}{Laser\ spot\ energy}\ (\frac{mm}{J}) \quad (13)$$

5.2.5: Calculation of melt energy and conduction losses

To evaluate the proportion of energy utilised for melting to the energy dissipated for conduction losses within the bulk of the material, an analytical solution of heat equation was used (Ashby and Easterling, 1984).

$$T(z,t) = T_0 + \left[\frac{(AP/t_s)}{2\pi\lambda[t(t+t_0)]^{1/2}}\right] \cdot \exp - \left(\frac{(z+z_0)^2}{4\alpha t}\right) \quad (14)$$

where T_0 is the room temperature; P is the laser power; t_s is the travel speed; A is the absorptivity; λ is the thermal conductivity; t is the time; z is the depth below the surface; α is the thermal diffusivity and t_o is given by

$$t_o = \frac{D_B^{\ 2}}{16\alpha} \tag{15}$$

After differentiating Equation 14 with respect to time and rearranging the peak temperature T_{peak} achieved in each thermal cycle can be determined from (Ashby and Easterling, 1984)

$$T_{peak} = T_0 + \frac{2A(P/t_s)}{e\pi\rho c(z+z_0)^2} \tag{16}$$

with

$$z_0 = \left[\left(\frac{\pi^{1/2}}{e}\right)\cdot\left(\frac{\alpha D_B}{C_1 2t_s}\right)^{1/2}\cdot\frac{D_B}{2}\right]^{1/2} \tag{17}$$

where C_1 is a constant.

Equation 16 was used to calculate temperature as a function of depth below the laser spot, as shown in Figure 5-2. A uniform hemispherical weld profiles were assumed to simplify the calculation. First, the melt depth was calculated based on the welding parameters used in the experiments (see Figure 5-2). The melt depth was considered to correspond to an isotherm of 1500°C. The distance between the surface and the 1500°C isotherm was assumed to be molten metal (z melt). Then the area of melt pool (S melt) was calculated, based on melt depth (z melt) with the assumption of a hemispherical weld profile. The value of absorptivity in Equation 16 was adjusted to achieve the same melt area as in the experimental welds. In the next step, an isotherm for a temperature of 200°C was determined from Equation 16. The depth at which temperature was between 1500°C and 200°C was taken as the conduction losses depth (z loss). Based on this the area of conduction losses (S loss) was calculated with the

assumption of hemispherical isotherms. Then the energies utilised for melting (T>1500°C) and conduction losses (1500>T>200°C) were determined from:

$$E_{Melt} = \left[\frac{1}{2}\pi(z_{Melt}^2)L\rho\right]\left[C_{pm}(T_1 - T_0) + H_m\right](J) \quad (18a)$$

$$E_{Loss} = \left[\frac{1}{2}\pi(z_{Loss}^2)L\rho\right]\left[C_{ps}(T_1 - T_{200})\right](J) \quad (18b)$$

where E_{melt} is the energy for melting; E_{loss} is the energy utilised for conduction losses; Z_{melt} is the depth of melt zone; Z_{loss} is the depth of conduction losses zone; *L* is the length of weld; ρ is the density; C_{pm} is the heat capacity for melting; C_{ps} is the heat capacity for solid, *T* is the temperature and H_m is the enthalpy of melting.

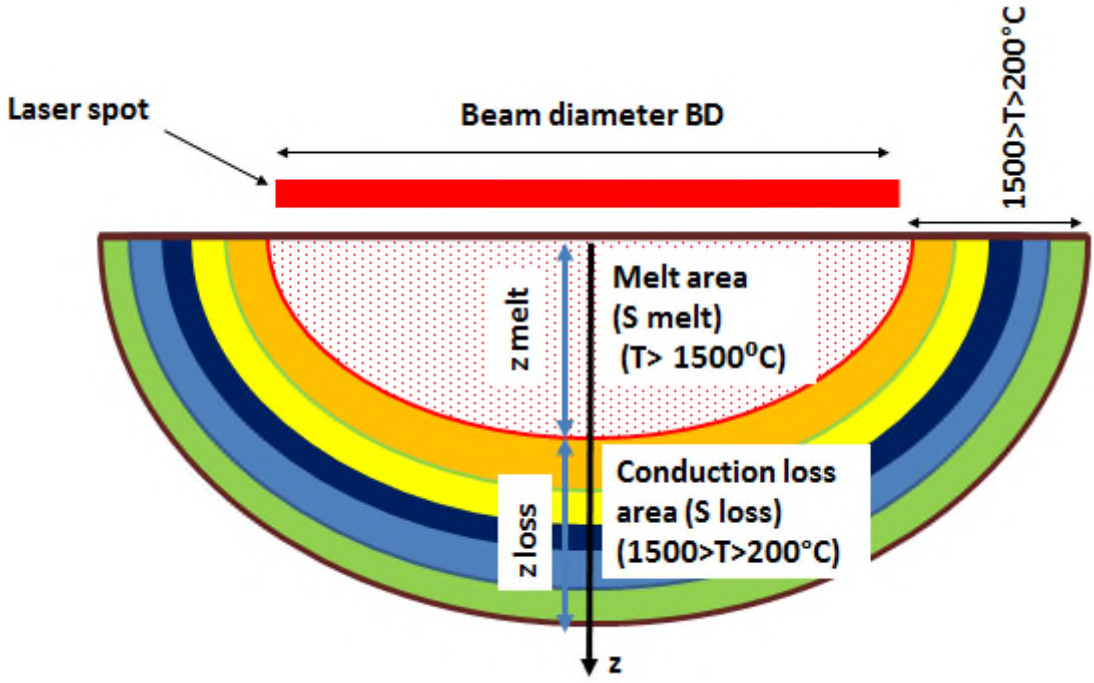

Figure 5-2: Calculation of melt area and conduction loss based on Equation 18

5.3 Results

5.3.1 Investigation of constant power density (P_d) and specific point energy (E_{SP})

Experiments conducted in Section 5.2.1 investigate if constant power density and specific point energy control the weld profile in conduction welding, independently of the beam diameter, as reported for keyhole regime (Suder, W.J. and Williams, S.W., 2012). The laser power and travel speed were adjusted to maintain constant power density and specific point energy, as shown in Table 5-1. Figure 5-3 shows the macrographs of bead-on-plate welds obtained. In these macrographs, it can see that both the weld width and depth of penetration vary with beam diameter, despite a constant power density and specific point energy. The same data are plotted in Figure 5-4. It can be seen that the depth of penetration changes with beam diameter. The same trend was observed for all ranges of power density and specific point energy. This suggests that the conduction regime does not respond to the applied laser energy in the same way as keyhole regime.

Table 5-1: Parameters used to investigate the effect of constant power density (41.5 kW/cm^2) and specific point energy (161 J) on weld geometry

D_B (mm)	t_i (ms)	t_s (mm/s)	P (kW)
1.00	480	2.00	0.34
1.50	240	6.00	0.68
2.00	120	17.00	1.36
2.90	60	47.70	2.68

$D_B\,(mm)$	1.00	1.20	1.50	1.80	2.00	2.40	2.90
$t_i\,(ms)$	480	345	240	160	120	86	60
162J & 41.5 kW/cm^2							

Figure 5-3: Macrographs of bead-on-plate welds at constant power density and specific point energy for different beam diameter D_B

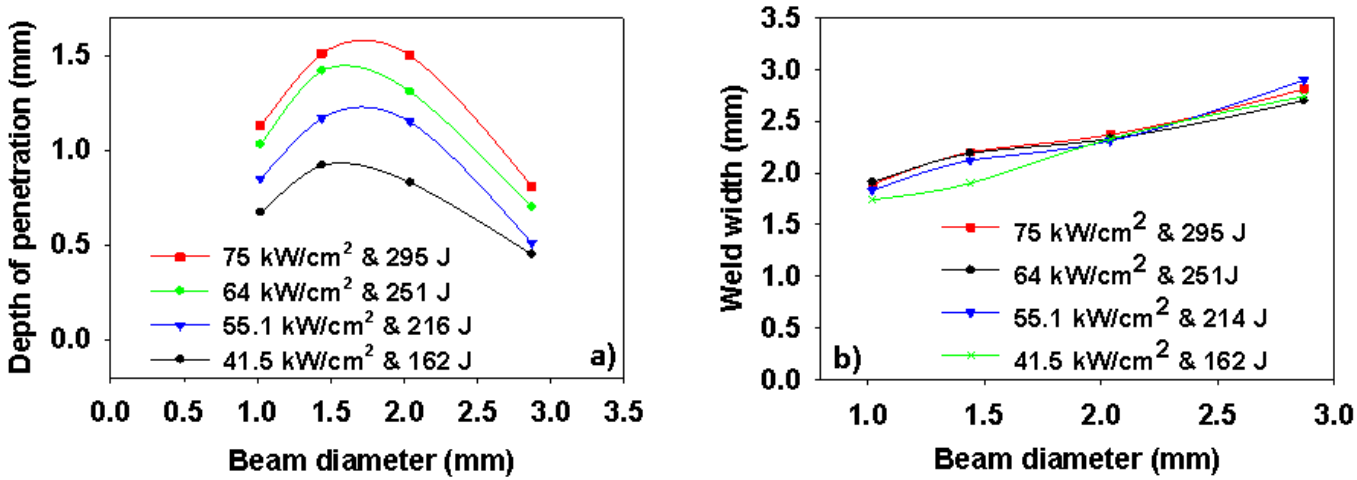

Figure 5-4: Effect of beam diameter (interaction time) on a) depth of penetration and b) weld width

5.3.2 Investigation of constant power density and interaction time

Figure 5-5 shows the macrographs of the bead-on-plate welds produced with constant power density and interaction time for three beam diameters, according to parameters shown in Table 5-2. It can be seen in Figure 5-6 that the depth of penetration is similar and only for an interaction time of 480 ms where there is a small discrepancy. In the case of 480 ms, the depth of penetration slightly increases with increasing beam diameter, despite constant power density and interaction time. It is worth noticing that at this interaction time the weld profiles exhibit aspect ratio of 0.4, which suggest transition regime. It is confirmed that apart from the interaction time of 480 ms, the depth of penetration is proportional to the interaction time and power density (product is energy density) and is independent of the beam diameter. At this range, the interaction time has greater effect on penetration than the power density.

Table 5-2: Parameters used to investigate effect of beam diameter on weld geometry at constant power density (20.4 kW/cm^2) and interaction time (D_B - beam diameter, t_s - travel speed and t_i - interaction time). Additional power density investigated is 22.9. 25 and 28 kW/cm^2

D_B (mm)	P (kW)	t_s(mm/s)	$t_i(ms)$
4.00	2.56	66.00	60
		33.20	120
		16.67	240
		8.33	480
5.00	4.00	83.33	60
		41.70	120
		20.80	240
		10.40	480
6.00	5.76	99.50	60
		49.80	120
		25.00	240
		12.50	480

$D_B(mm)$	4.00	5.00	6.00
$t_i = 60ms$	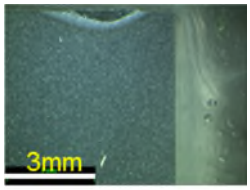	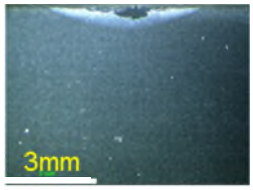	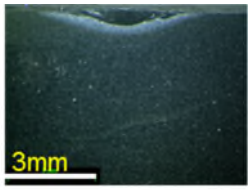
$t_i = 120ms$	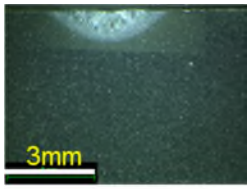	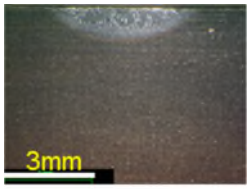	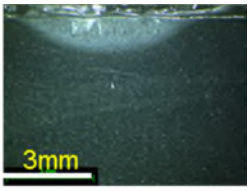
$t_i = 240ms$	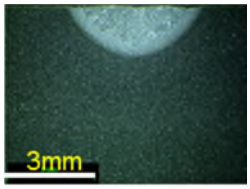	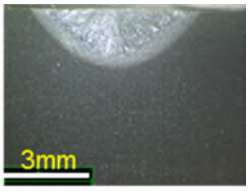	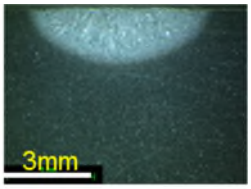
$t_i = 480ms$	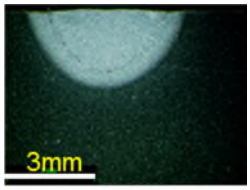	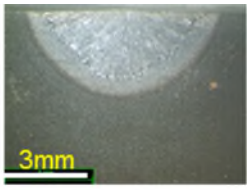	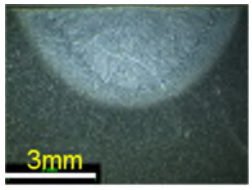

Figure 5-5: Macrographs of bead-on-plate welds with different beam diameter at constant power density (20.4 kW/cm^2) and different interaction times

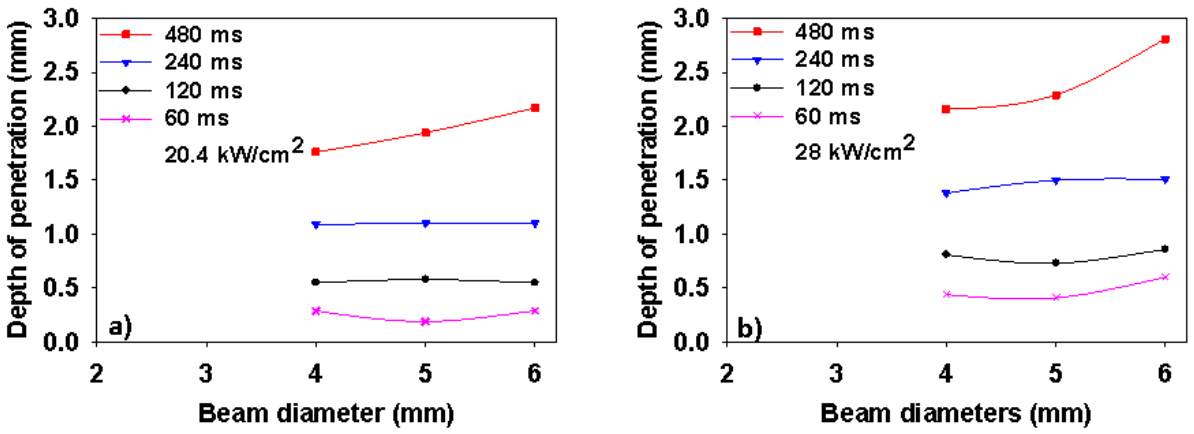

Figure 5-6: Effect of beam diameter on the depth of penetration at constant interaction time and power density of a) 20.4 kW/cm^2 and b) 28 kW/cm^2

In Figure 5-7, the same results are plotted as a function of interaction time and power density. The depth of penetration increases linearly with increasing interaction time and is independent of the beam diameter. Only for the interaction time of 480 ms is there a discrepancy (Figure 5-7a). When compared to the power density in Figure 5-7b, it can be seen that the effect of interaction time on depth of penetration is much greater than the effect of power density, which is typical for conduction regime. The relative increase of penetration with interaction time is 0.65 and with power density is 0.47. This suggests that the weld profile in conduction regime is more dependent on the interaction time, which is attributed to the time needed for the heat to be transferred from the laser interaction point to the bulk material and generate melting.

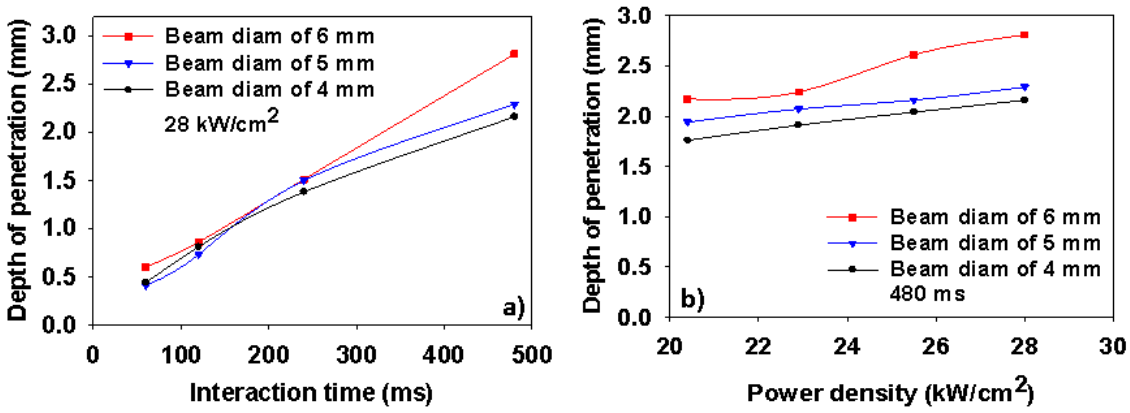

Figure 5-7: Effect of interaction time (a) and power density (b) on depth of penetration

To further test, the effect of power density and interaction time the range of beam diameters was extended, as shown in Table 5-3. Beam diameters from 0.60 mm to 5.5 mm were used and constant power density and interaction time was achieved by adjusting the welding parameters for each beam. From macrographs presented in Figure 5-8 and Figure 5-9, it can be seen that initially the depth of penetration is dependent on the beam diameter and then at certain point it becomes independent of it. The data are plotted in Figure 5-10 for two power densities. For large beam diameters, the depth depends only on power

density and interaction time. As the beam diameter is reduced below 2.9 mm the beam diameter has a significant effect on the depth. This suggests that the material response is also dependent on the heat source size, which links it to the specific point energy. The weld width, on the other hand is entirely controlled by the beam diameter, as shown in Figure 5-11. In all cases, the weld width approached the beam diameter projected on the workpiece.

Table 5-3: Parameters used to investigate the effect of beam diameter on weld geometry at constant power density and interaction time (product is energy density) (D_B) beam diameter, (P) - laser power and (t_s) -travel speed)

$D_B(mm)$	$P(W)$	$t_s(mms^{-1})$	$P(W)$	$t_s(mms^{-1})$
	41.5 kW/cm^2 & 120 ms (5.0 kJ/cm^2)		33.1 kW/cm^2 & 120 ms (4.0 kJ/cm^2)	
0.60			100	5.13
1.00			260	8.36
1.50	680	0.70	540	12.00
2.00	1360	1.10	1080	17.00
2.90	2685	1.50	2140	23.82
4.00	5220	2.00	4160	33.31
5.00			6500	41.00
5.50			7870	46.00

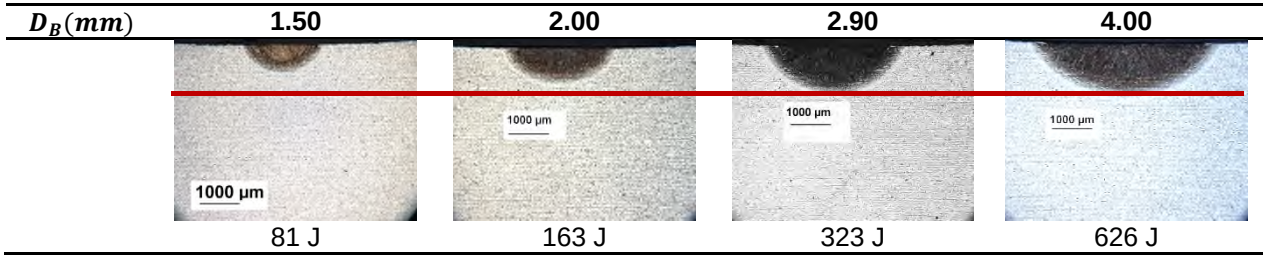

Figure 5-8: Bead-on-plate welds produced at constant power density of 41.5 kW/cm^2 and interaction time 120 ms (energy density of 5.0 kJ/cm^2) a range of beam diameter

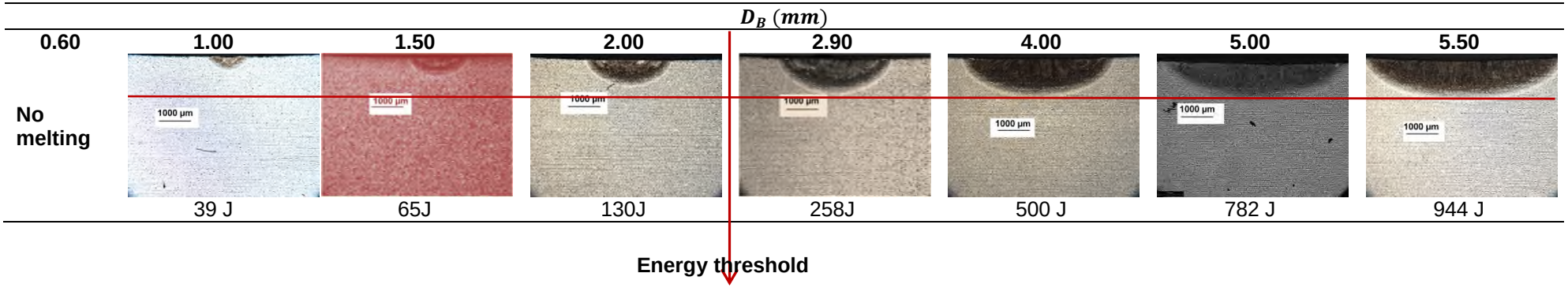

Figure 5-9: Bead-on-plate welds produced at constant power density of 33.1 kW/cm^2 and interaction time 120 ms (energy density of 4.0 kJ/cm^2) a range of beam diameter

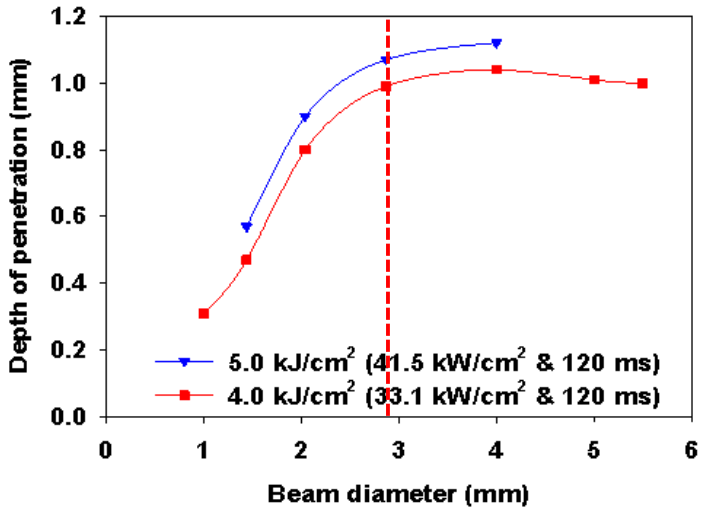

Figure 5-10: Effect of beam diameter on the depth of penetration at constant power density and interaction time

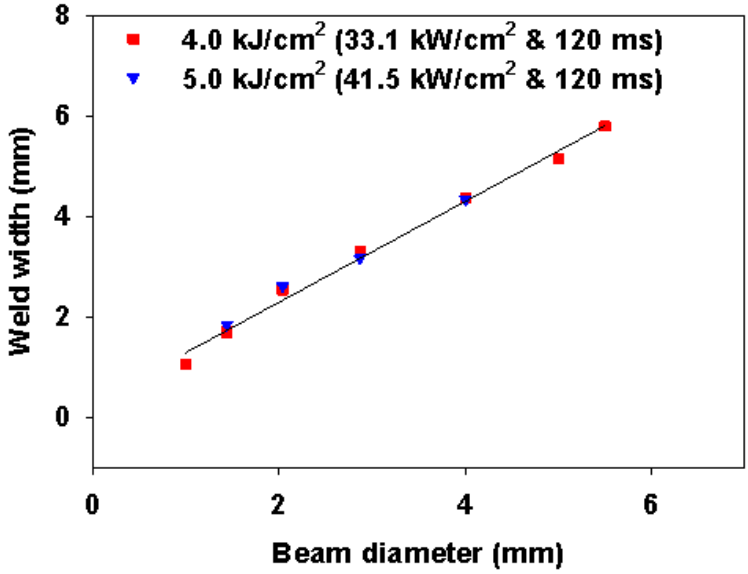

Figure 5-11: Effect of beam diameter on the weld width at constant power density and interaction time

5.3.3 Melting efficiency with medium and large beam diameters

To investigate the effect of power density and interaction time on melting efficiency, experiment with a range of interaction times and power densities was carried out, as described in Section 5.2.4. Figure 5-12 shows the macrographs of the build-on-plate welds produced with a beam diameter of 1.80 mm. The melting efficiency in the conduction welding depends on both the power density and interaction time, as shown in Figure 5-13. In the figure, the travel speed was varied to achieve different interaction times. The effect of interaction time is much greater than the effect of power density. The melting efficiency first increases and then decreases again with increasing interaction time. The maximum melting efficiency was recorded for interaction time of 25 ms (Figure 5-13).

Figure 5-14 shows the penetration and melting efficiency as a function of interaction time. Penetration efficiency is the ratio of depth of penetration to the applied energy. The same trend was observed for penetration efficiency as melting efficiency with both reaching maximum value for the same interaction time. It is important to mention that the melt area was used to calculate the melting efficiency and depth of penetration was used to calculate the penetration efficiency. This clearly indicates that change in melting efficiency of conduction welding might be linked to penetration efficiency, which indicates a fixed relationship between the melt area and depth of penetration.

Table 5-4: Welding parameters used to investigate the effect power density and interaction time on melting efficiency with beam diameter 1.80 mm

$P(W)$	$P_d\,(kW/cm^2)$	$t_s\,(mm/s)$	$t_i\,(ms)$
1033	41.50	145.80	12.20
		75.00	23.70
		50.50	35.20
		25.70	69.40
		19.30	92.10
		15.50	114.80
		10.40	169.50
		8.92	197.80

Power density (kW/cm^2)	Interaction time (ms)				
	12	25	35	92	115
64.0	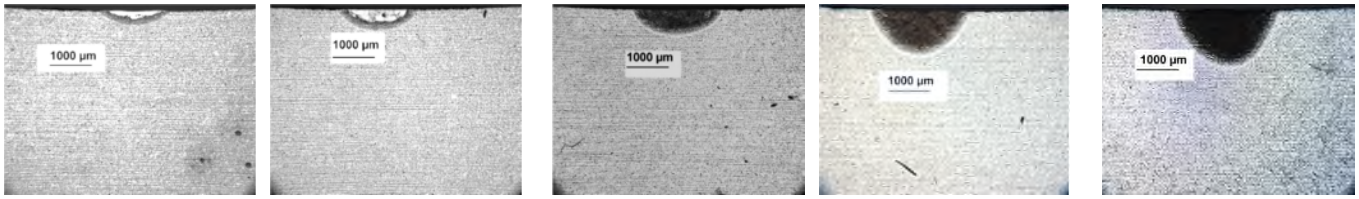				
41.5	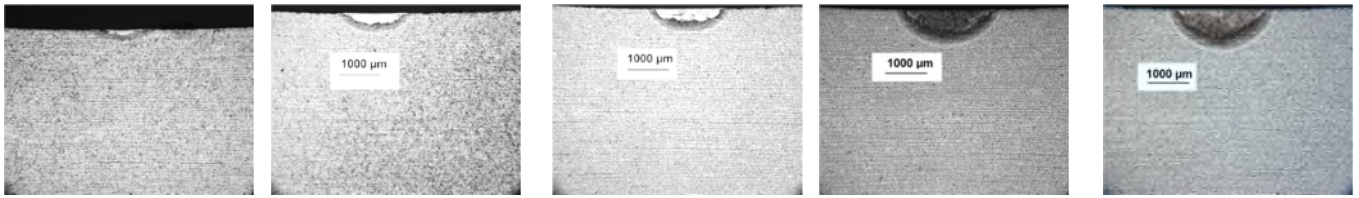				

Figure 5-12: Macrographs of bead-on-plate welds used to investigate the effect of interaction time and power density on melting efficiency

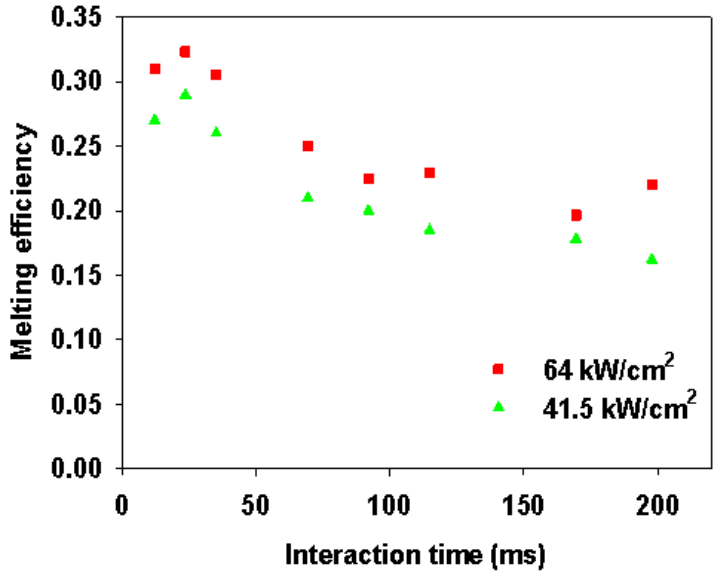

Figure 5-13: Dependence of melting efficiency on the interaction time for two levels of power density and constant beam diameter of 1.80 mm

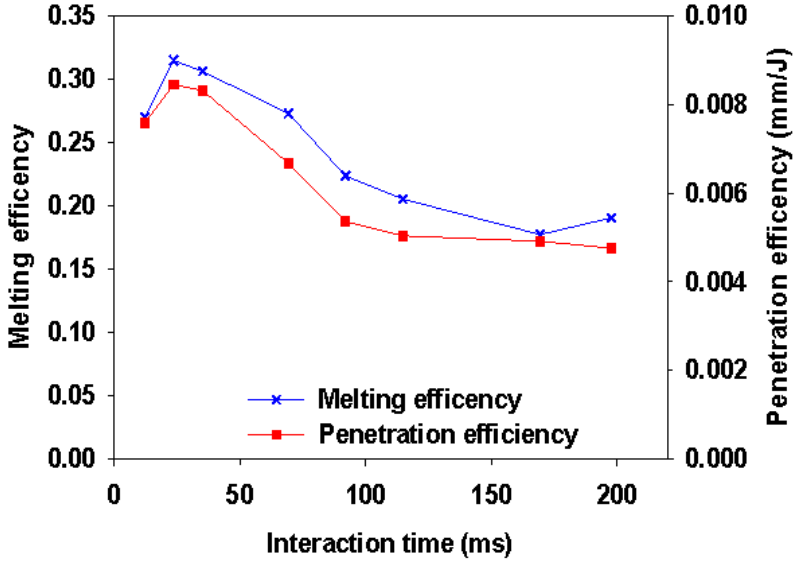

Figure 5-14: Melting efficiency and penetration efficiency as a function of interaction time at constant power density of 52 kW/cm^2 and beam diameter of 1.80 mm

The effect of beam diameter on the melting efficiency at constant power density and interaction time is presented in Figure 5-15. The corresponding macrographs are shown in Figure 5.8 and Figure 5.9 (see page 73). It can be seen that for both power densities the melting efficiency increases with increasing beam diameter. The maximum melting attained with this combination of interaction parameters is 25%. This is due to longer interaction time of 120 ms. The influence of power density depends on a beam diameter used. For a beam diameter of 1.50 mm, the melting efficiency increased from 10% to 15% when the energy density was increased from 4.0 kJ/cm^2 to 5.0 kJ/cm^2. However, with bigger beams, the effect of energy of energy density is insignificant.

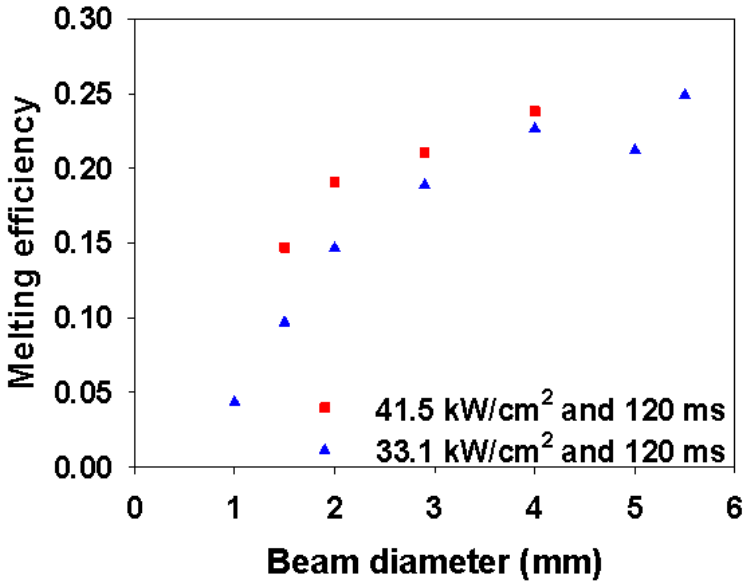

Figure 5-15: Melting efficiency as a function of beam diameter at constant power density and interaction time

5.4 Discussion

The main objective of this chapter was to investigate parameters that control the weld bead geometry in conduction welding. The first experiment examined if constant power density and specific point energy control the depth of penetration in conduction welding independently of the beam diameter, as reported for keyhole welding (Suder, W.J. and Williams, S.W., 2012). The depth of penetration and melt area varied with beam diameter (see Figure 5.3 in page 70), which is in contrast to keyhole welding. Conduction regime is controlled by the power density and interaction time, as shown in Figure 5.6. This suggests significant differences between the responses of the material in these two regimes. Keyhole regime is a vaporisation driven process and hence the power density plays the most important role and the interaction time is less significant. As reported by Suder and Williams, the depth of penetration in keyhole regime is proportional to power density and specific point energy (Suder, W.J. and Williams, S.W., 2012). The specific point energy describes a discrete energy in a given laser size domain for a given interaction time in CW laser welding. In another means, it confines the size of a domain over which a particular energy density is applied. Both power density and specific point energy determine the rate of vaporisation, which translates directly into the depth of a keyhole. In another study, it was shown that the depth of penetration is proportional to a power factor, which is a simplified product of power density and specific point energy (Patschger A. et al., 2013b; Suder, W.J. and Williams, S., 2014). This shows that the keyhole regime is a one-dimensional process where the depth of penetration can be increased without increasing the weld width. In this case, the laser power has to be increased only by a factor of two when beam diameter is doubled to maintain a constant depth of penetration (Patschger A. et al., 2013b; Suder, W.J. and Williams, S., 2014).

In conduction welding, the heat has to be transferred into the material via conduction, which is a relatively slow process. As shown in Figure 5.6 and Figure 5.7, the depth of penetration in conduction is strongly dependent on the interaction time (slope of 0.65) and a less dependent on the power density

(slope 0.47). This is attributed to the process dynamics. There is a time required for the heat to conduct from the laser interaction point to the material. Therefore, the longer the interaction time, the greater the size of melt pool and weld depth. Although the rate of increase of depth with increasing interaction time is greater than with increasing power density, but the power density is also important. A certain minimum power density is required to achieve melting. Therefore, any change of interaction time at low power density will have no effect on the weld geometry.

The weld profile in conduction regime is controlled by the energy density, which controls the energy flux and the surface temperature. This means that to maintain a constant depth of penetration the laser power has to be quadrupled when beam diameter increases by a factor of two. Beam diameter, on the other hand, controls the size of domain over which heat is applied and hence the weld width. Therefore, the weld width in conduction welding is proportional to the beam diameter.

It was anticipated that the energy density could provide a simple phenomenological model to control depth of penetration and weld profile with variable beam diameters, similarly as the power factor in keyhole regime (Suder, W.J. and Williams, S., 2014). However, as shown in Figure 5.6, at longer interaction times (480 ms) the process is dependent on the beam diameter. This can be attributed to the change of welding regime from conduction to transition or keyhole. With increasing interaction time, the workpiece is exposed to the laser radiation for a longer time, thereby increasing the peak temperature. However, at a certain point, the boiling point of material will be exceeded leading to a change of welding regime. This is shown in Figure 5-16 where all data from Figure 5.6 are plotted as a function of energy density. In conduction regime, the process is independent of the beam diameter and all curves merge but at a certain point the beam diameter starts influencing the depth of penetration. At this point the transition regime commences where vaporisation starts governing the process and the power density and specific point energy become dominant (Assuncao, E. et al., 2012; Suder, W.J. and

Williams, S.W., 2012). This suggests that depending on the processing regime different parameters control weld profile.

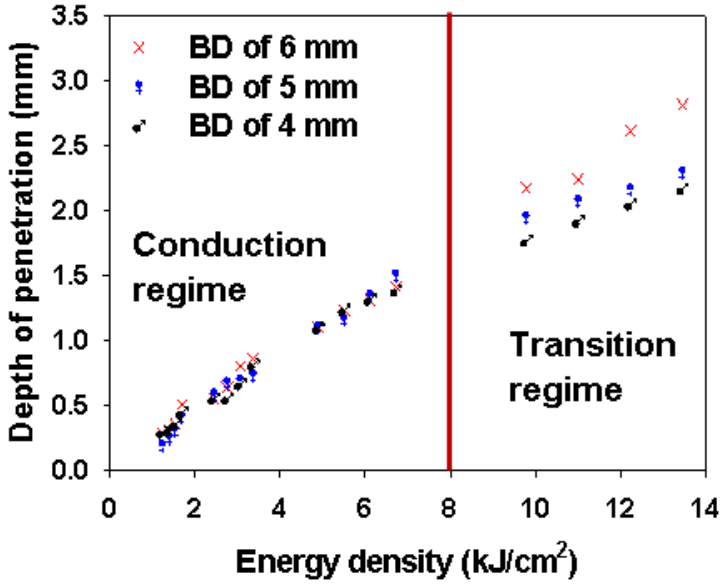

Figure 5-16: Effect of energy density on the depth of penetration in different welding regime and beam diameter

To investigate the effect of power density and interaction time (product is energy density) ultimately a further experiment on a wider range of beam diameters was carried out (Figure 5-8 to Figure 5-11). It turned out that the material response is not only dependent on the welding regime but also in the range of beam diameters. Even in pure conduction regime, the weld depth is dependent on the beam diameter when beam is smaller than 2.90 mm (see Figure 5-10). In this operating regime, the process is not only controlled by the power density and interaction time but also by the beam diameter. This suggests that the process is less efficient with small beams than with big beams due to greater conduction losses. A certain amount of heat is dissipated for lateral thermal conduction into the bulk material. All the heat conducted into the workpiece but not contributing to the melting is considered as a loss. These

losses are proportional to the contact surface between the melt pool and the bulk solid material, as shown schematically in Figure 5-17. The size of this surface is proportional to the size of the melt pool i.e. depth and width, which in pure conduction welding should be proportional. The energy utilised for melting, on the other hand, is proportional to the melt volume. At a certain point, below a certain critical beam diameter, the conduction losses will be so high with respect to the applied energy that no melting of material will occur, as shown in Figure 5-9 for beam diameter of 0.60 mm. This means that the ratio of energy dissipated in the bulk material to the energy utilised for melting decreases with increasing beam diameter. In Figure 5-17, the ratio of the surface area to the melt volume measured from macrographs from Figure 5-9 is shown. The process efficiency decreases rapidly when the ratio of the contact surface area to melt volume of fusion zone is above beam diameter of 2.0 mm. This is the main reason why the process is more efficient with larger beams.

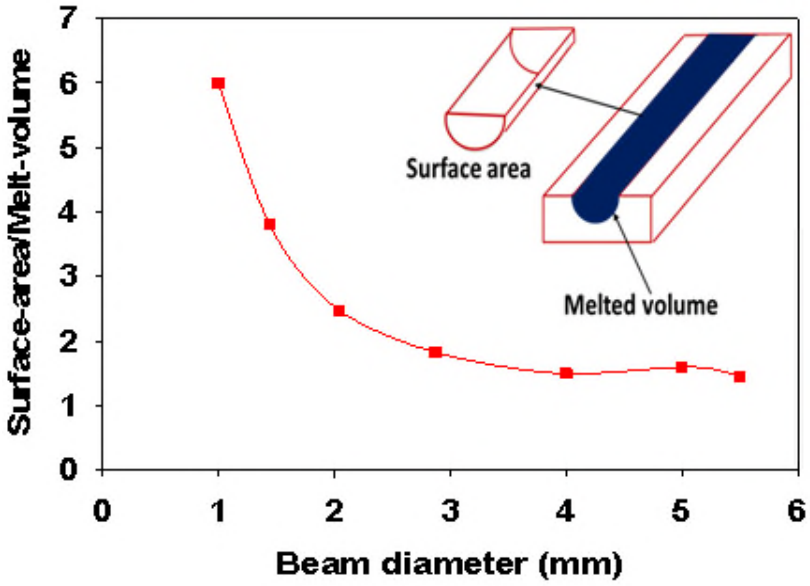

Figure 5-17: Ratio of surface area to melt to volume measured from macrographs in Figure 5-8 and Figure 5-9 (constant power density and interaction time)

Relationship between the energy lost and energy utilised for melting was calculated using an analytical solution of the heat equation, as described in the Section 5.2.5 (Ashby and Easterling, 1984). The area of melting (T>1500°C) and the area of conduction losses (1500>T>200°C) were estimated from a one-dimensional temperature distribution (see Equation 15). The ratio of energy loss to the energy utilised for melting for different beam diameters and processing conditions from Figure 5-9 is shown in Figure 5-18. The data confirm the hypothesis of a greater proportion of conduction losses for small beam diameters. This implies that it may be difficult to achieve pure conduction welds with small beams. Any attempt to increase the input energy to overcome these losses is likely to result in vaporisation and keyhole regime. Therefore, the change of processing regimes is more rapid with small beams.

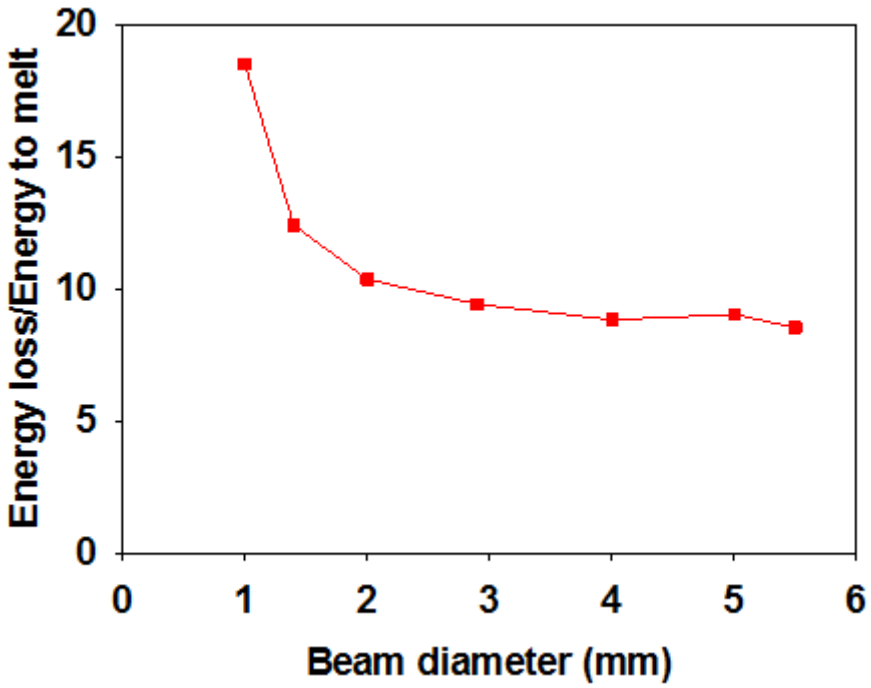

Figure 5-18: Ratio of energy for melting to the energy for conduction losses calculated based on the Equation 16

This is also confirmed by the melting efficiency presented in Figure 5-13. The melting efficiency is higher at shorter interaction times and bigger beam diameters. At short interaction times, there is less time for heat to transfer inside the material and losses are lower. Therefore, it is only possible to achieve conduction welds at short interaction time with small beams. However, too short interaction time does not provide enough energy for melting. Therefore initially melting efficiency increases with increasing interaction time (Figure 5-13). The effect of beam diameter on melting efficiency can also be explained by the ratio of heat utilised for melting to conduction losses based on heat equation (Figure 5-18). The proportion of conduction losses decreases with increasing beam diameter, therefore, melting efficiency is higher with bigger beams.

A maximum melting efficiency of 0.32 (Figure 5-13) was obtained in this study for interaction time of 25 ms, which is close to the theoretical maximum melting efficiency of 0.34 for conduction welds (Fuerschbach and Eisler, 1999; Fuerschbach, 1996).

6 Solid melting with small beam diameters (0.07-0.10 mm)

All results reported in Chapter 5 were focused on medium and large beam diameters. This current chapter investigates the effect of interaction parameters on melting of solid with beam diameters commonly used in powder bed machines, that are beam diameters between 0.07 to 0.10 mm (see Tables 6-1 and 6-2). Some samples were produced in Welding Engineering and Laser Processing Centre (WELPC), Cranfield University. Some samples were also produced on a commercial powder bed machine at Renishaw.

6.1 Experimental procedure for small beam diameter

The first experiment was carried out with a fibre laser (JK500FL) with maximum output power of 500 W. In this experiment, an enclosure was used with the laser head located out of the enclosure. Argon gas was used to shield the welding environment to prevent oxidation, which may affect the welds. The laser head was focused to obtain a beam diameter of 0.10 mm (100 µm) with the process set-up described in Section 4.2. The laser power and travel speed were adjusted to a given beam diameter to achieve different levels of power density and interaction time. The welding parameters for a power density of 3570 kW/cm^2 are presented in Table 6-1. Additional power densities investigated were 640 kW/cm^2, 1150 kW/cm^2, 1660 kW/cm^2, 2160 kW/cm^2, 2670 kW/ cm^2 and 5350 kW/cm^2.

Table 6-1: Welding parameters used to investigate effect of interaction parameters on weld geometry (D_B – beam diameter, P – laser power and t_s -travel speed, E_d – energy density and t_i – interaction time)

$t_i(ms)$	$P(W)$	$t_s(mms^{-1})$	$E_d(kJmm^{-2})$	$E_{SP}(J)$
1		100.0	3.60	0.28
2		50.0	7.10	0.56
4	280	25.0	14.20	1.12
6		16.7	21.30	1.68
8		12.5	28.50	2.24
10		10.0	35.60	2.80

The second experiment conducted at Renishaw was carried out with a beam diameter and point distance of 0.07 mm (70 µm). Laser powers of 180 W and 200 W were used. The travel speed was varied between 500 mm/s and 1800 mm/s. The details of the welding parameters investigated with a laser power of 180 W are presented in Table 6-2. The exposure time was used as the interaction time.

Table 6-2: Welding parameters used in the powder bed machine for solid melting (beam diameter of 0.07 mm and point distance is 0.07 mm)

$t_i(\mu s)$	$P_d(kWcm^{-2})$	$P(W)$	$t_s(mms^{-1})$
50			1400
60			1170
70			1000
80	4680	180	880
90			780
100			700
110			640
120			580
130			530
140			500

6.2 Results

Shown in Figure 6-1 and Figure 6-2 are some of the beads on plate welds produced with a beam diameter of 0.10 mm. Figure 6-1 shows the welds produced with increasing power density at constant interaction time. The power density was increased from 1530 kW/cm^2 to 2550 kW/cm^2. Figure 6-2 shows the welds produced with increasing interaction time at constant power density. In this case, the interaction time used ranged between 1 ms to 2 ms. Note that compared to large beam diameters presented in Chapter 5 here power density was higher and interaction time shorter. This was required to minimise conduction losses and increase the rate of energy input in order to achieve melting. The macrographs indicate that both power density and interaction time have effect on the depth of penetration and weld width. Figure 6-1 shows that by nearly doubling the power density at constant interaction time, the depth of penetration increases by nearly 100% and weld width by 50%. The results in Figure 6-2 show that depth of penetration and weld width also increase with interaction time. That is, increasing interaction time from 1.0 ms to 2.0 ms at a power density of 2040 kW/cm^2 increased both depth of penetration and weld width by approximately 20%, as shown in Figure 6-2. Figure 6-3 and Figure 6-4 show the detail of the bead-on-plate welds produced. Only the welds that exhibited conduction profile are presented in Figures 6-5 to Figure 6-8.

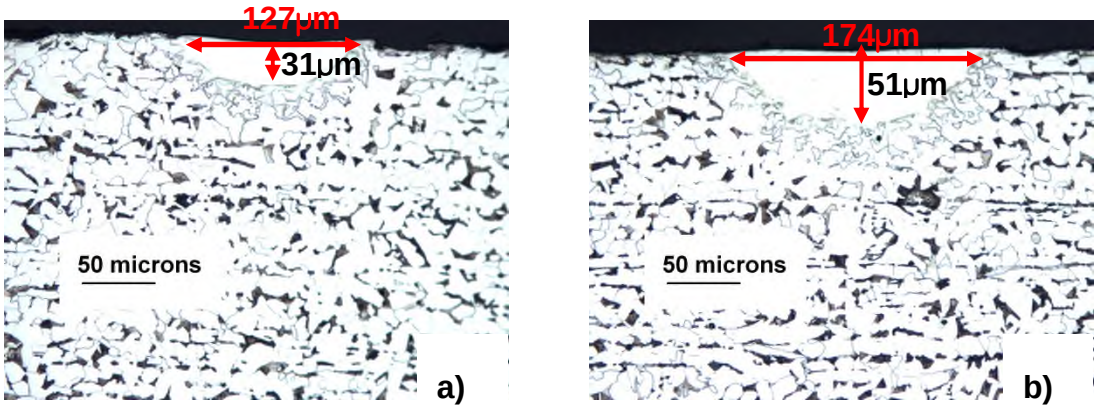

Figure 6-1: Macrographs of conduction welds produced with a beam diameter of 0.10 mm and interaction time of 1.25 ms at power densities of a) 1530 kW/cm^2 and b) 2550 kW/cm^2

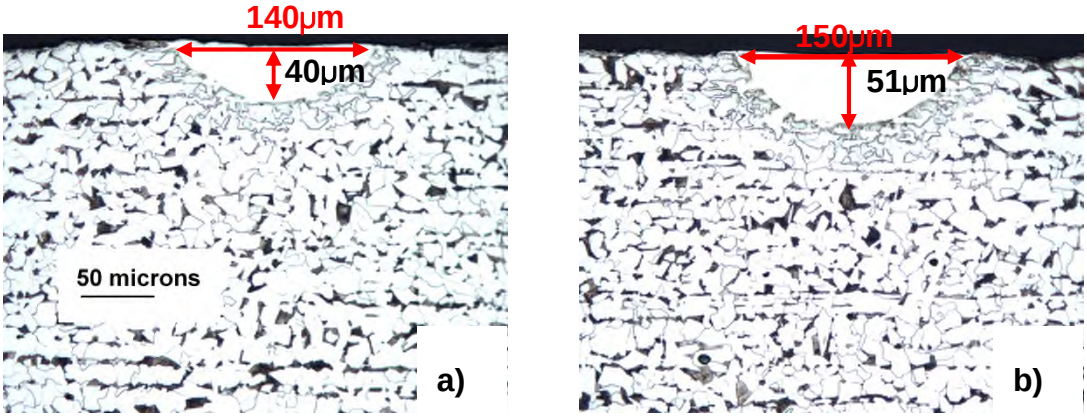

Figure 6-2: Macrographs of conduction welds produced with a beam diameter of 0.10 mm and power density of 2040 kW/cm^2 at interaction times of a) 1 ms and b) 2 ms

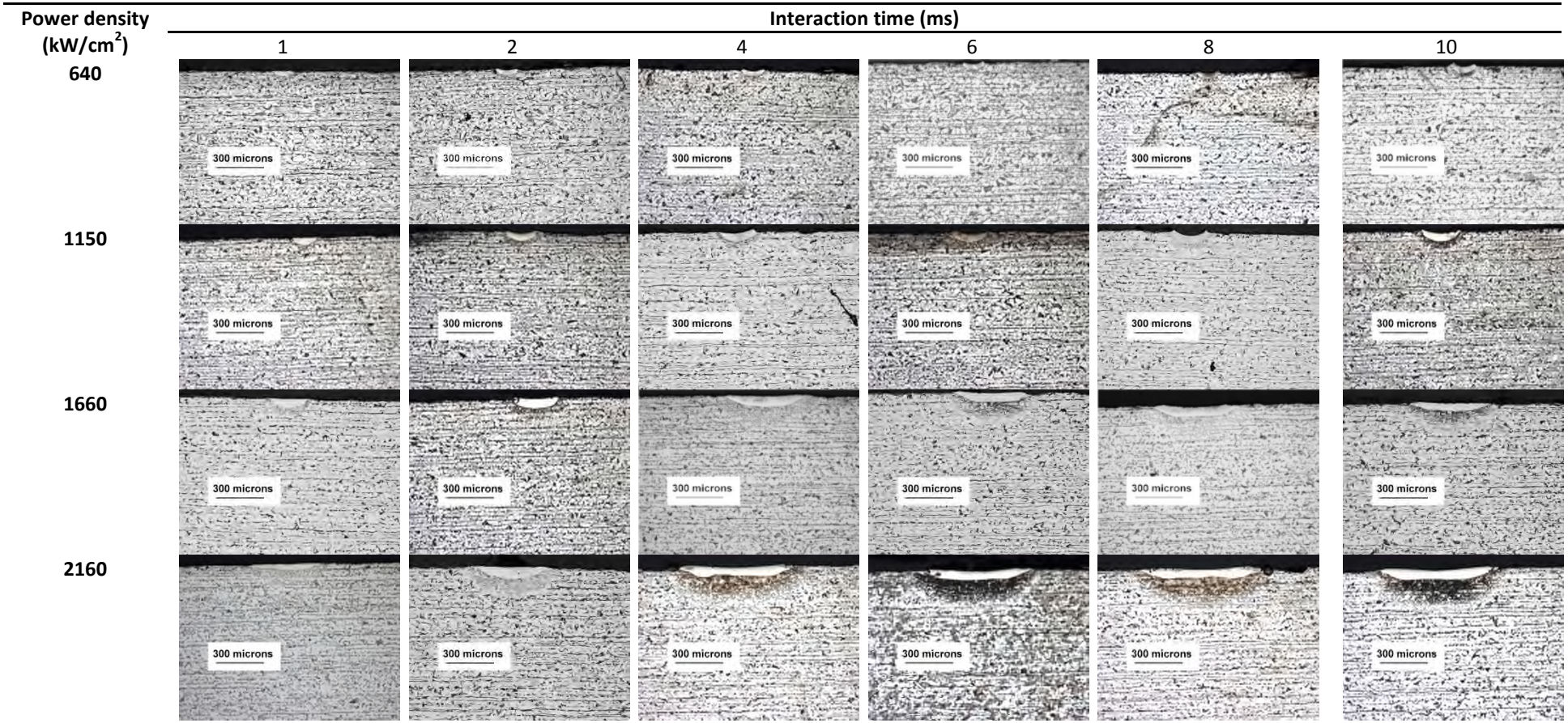

Figure 6-3: Macrographs of the bead on plate welds with different combination of interaction times and power densities (the same macrograph is on page 136)

Power density (kW/cm^2)	Interaction time (ms)				
	1	2	4	6	8
2670	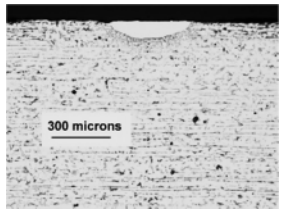	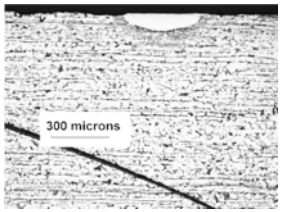	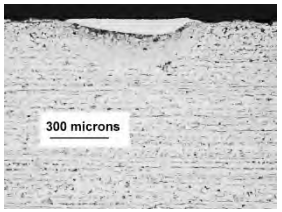	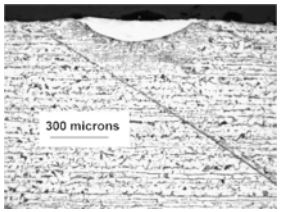	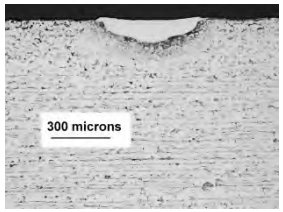
3570	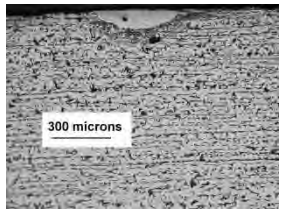	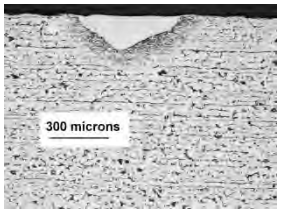	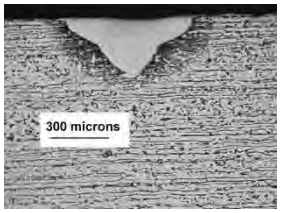	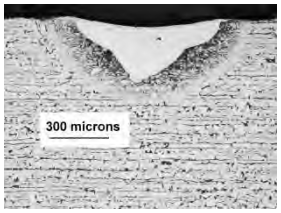	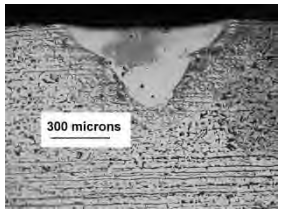
5350	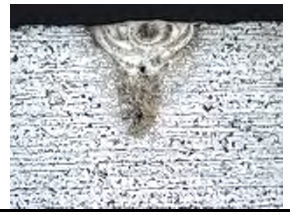	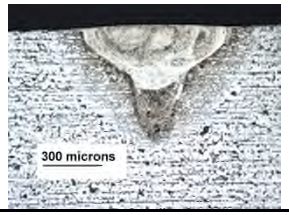	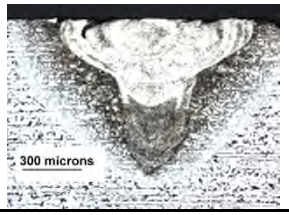	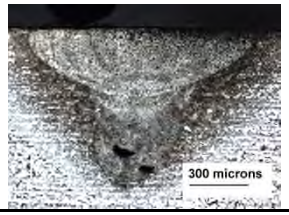	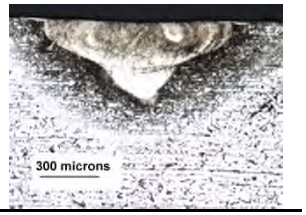

Figure 6-4: Macrographs of the bead-on-plate welds in solid steel produced with different combination of interaction parameters (the same macrograph is on page 137)

Figure 6-5 to Figure 6-8 show the dependence of depth of penetration and weld width on power density and interaction time. The depth of penetration and weld width increased with increasing power density, as shown in Figure 6-5 and Figure 6-7 respectively. A small increase of depth of penetration and weld width can be seen with increasing interaction time, as shown in Figure 6-6 and Figure 6-8. Interesting to notice is the fact that the weld width increases rapidly above 1150 kW/cm^2 power density (Figure 6-7) and 2 ms interaction time (Figure 6-8). The weld width in those cases is much wider that the beam diameter on the workpiece. Figure 6-9 shows the relationship between the aspect ratio and the energy density for the build-on-plate welds produced with beam diameter of 0.10 mm. The build-on-plate welds produced spread across the three welding regimes of conduction, transition and keyhole with most welds in conduction regime.

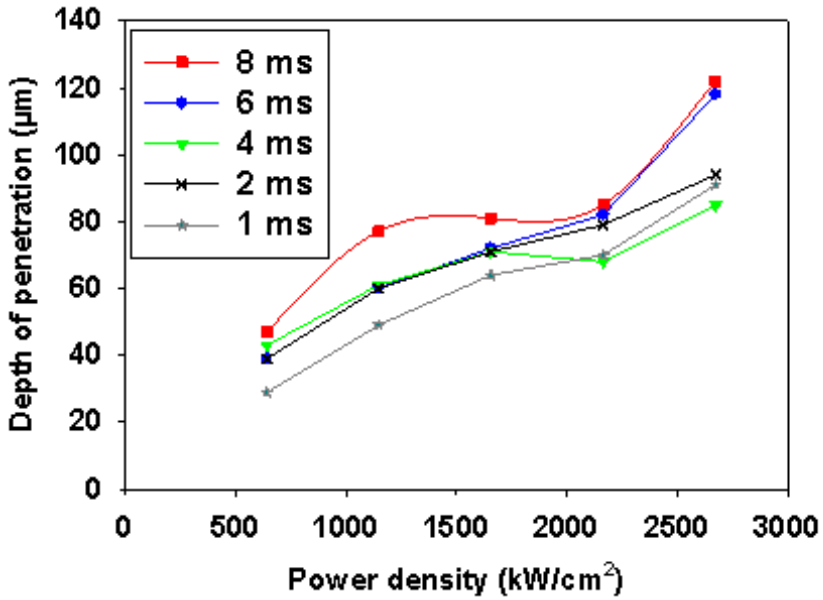

Figure 6-5: Effect of power density on the depth of penetration for different interaction times

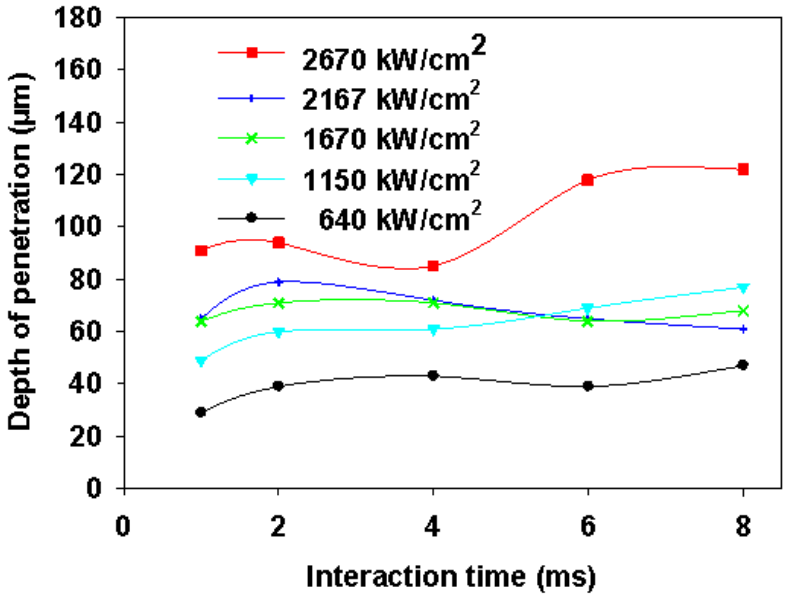

Figure 6-6: Effect of interaction time on depth of penetration for different power densities

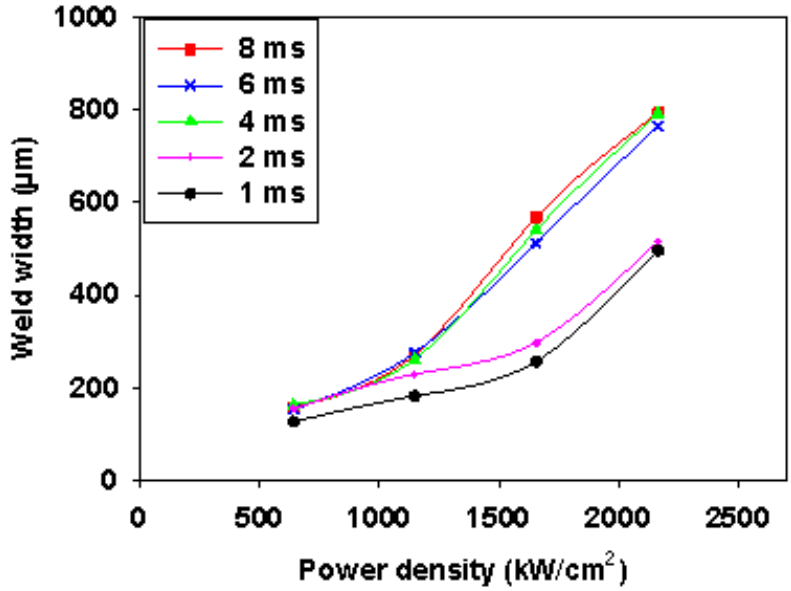

Figure 6-7: Effect of power density on weld width for different interaction times

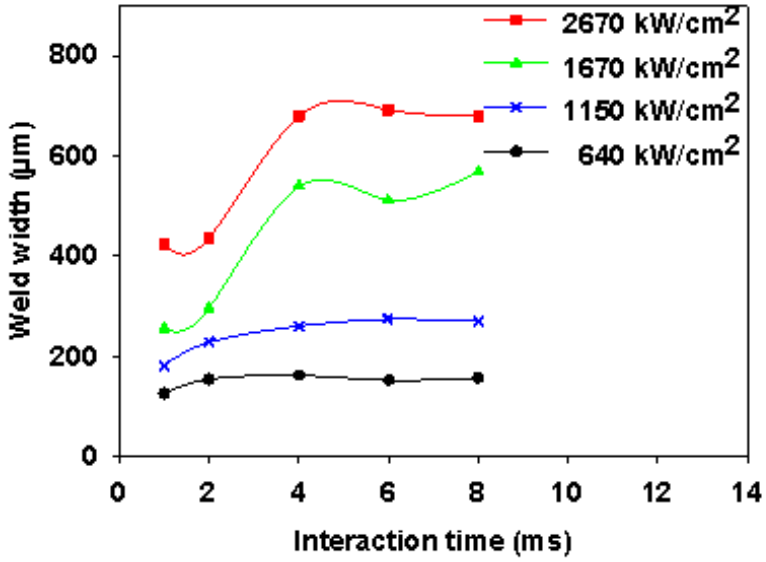

Figure 6-8: Effect of interaction time on weld width for different power densities

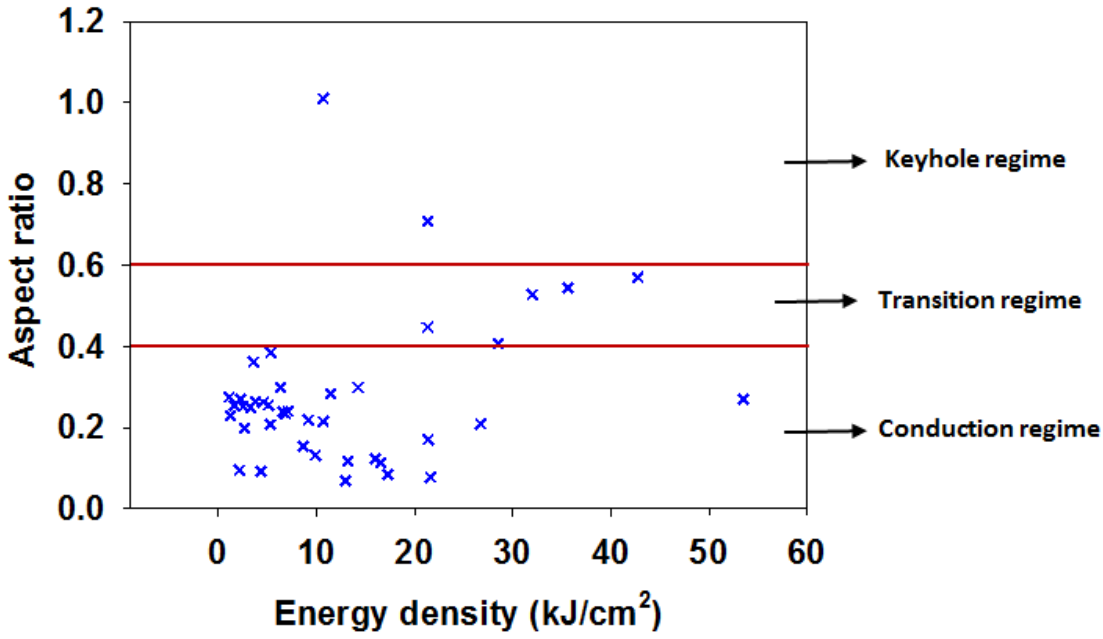

Figure 6-9: Aspect ratio (depth/width) as a function energy density with a beam diameter of 0.10 mm

Figures 6-10 shows the macrographs of samples produced using a commercial powder bed with a beam diameter of 0.07 mm for different power densities and interaction times. The macrographs indicate that the smaller the beam diameter, the more it is difficult to achieve conduction welds. In addition, the smaller the beam diameter becomes, the higher the power density is required to achieve melting. There is a narrow window of optimum interaction time for conduction welds. If the interaction time is too short no melting is achieved, then at 50 µs small conduction welds appeared, but further increase of interaction time resulted in vaporisation and keyhole regime. This is indicated in the plot of aspect ratio (depth/width) as a function of energy density in Figure 6-11. The figure indicates that most of the welds are in keyhole regime with the aspect ratio exceeding 0.6 (Assuncao, E. et al., 2012). The remainder are in transition regime of 0.4 to 0.6. The threshold values for keyhole and conduction were determined based on the ratio of depth of penetration to weld width.

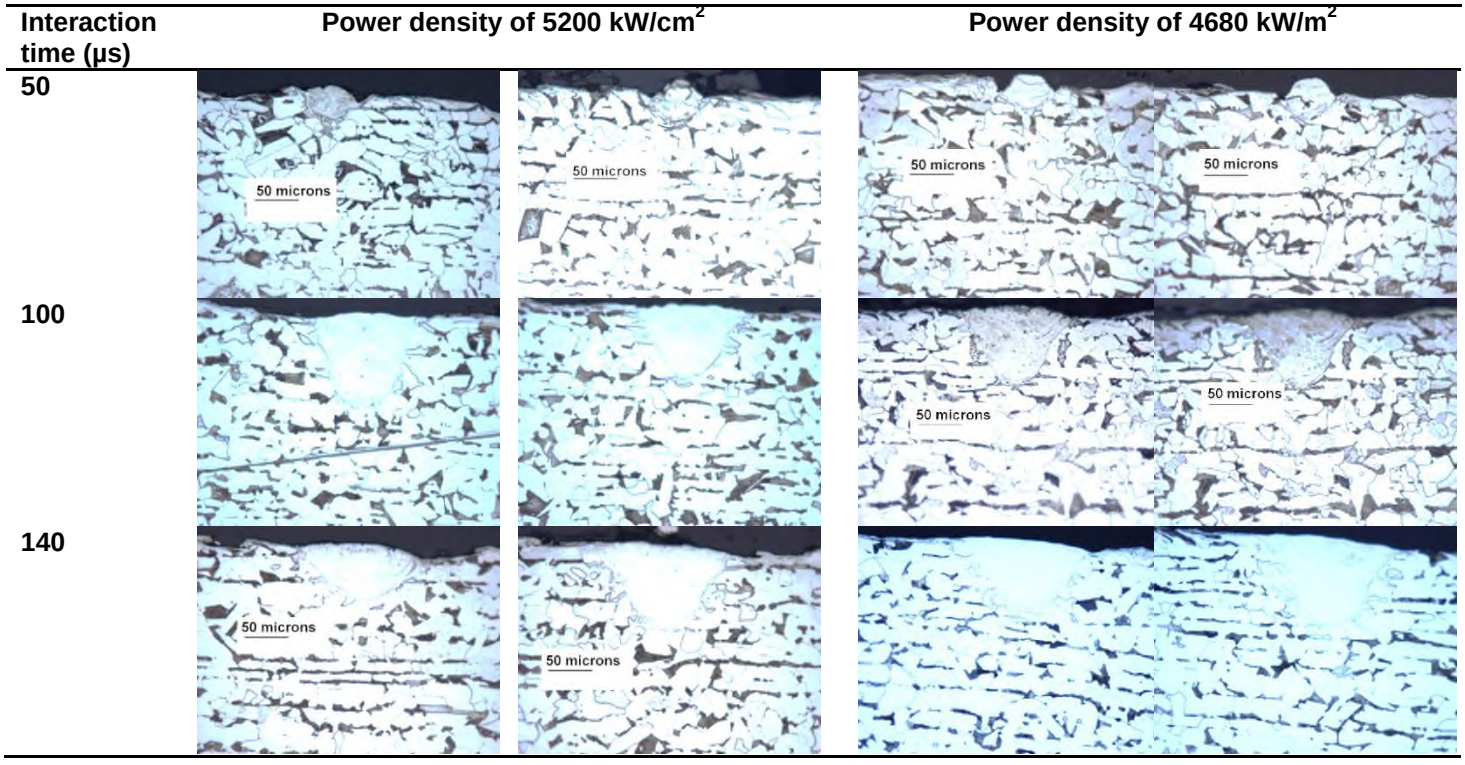

Figure 6-10: Macrographs of bead-on-plate welds produced with a beam diameter and point distance of 0.07 mm for different power densities and interaction times

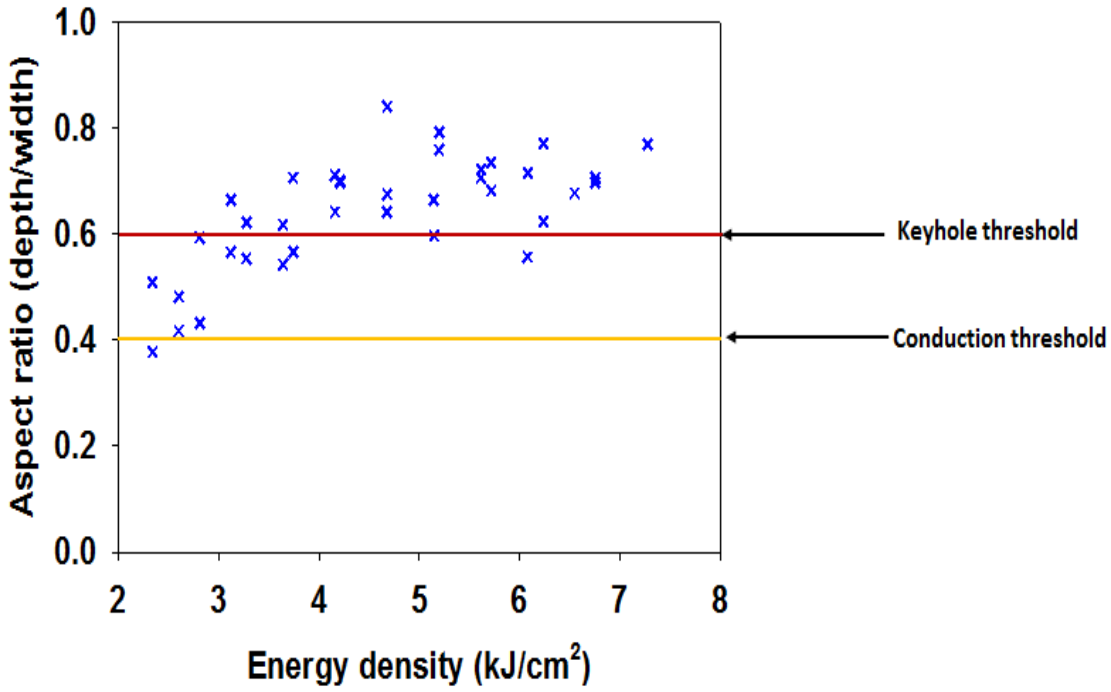

Figure 6-11: Aspect ratio (depth/width) as a function energy density with a beam diameter of 0.07 mm

The depth of penetration and weld width increased linearly with increasing interaction time at constant power density, as shown in Figure 6-12 and Figure 6-13 respectively. Note that the interaction time used were much shorter compared to the results presented in Figure 6-6.

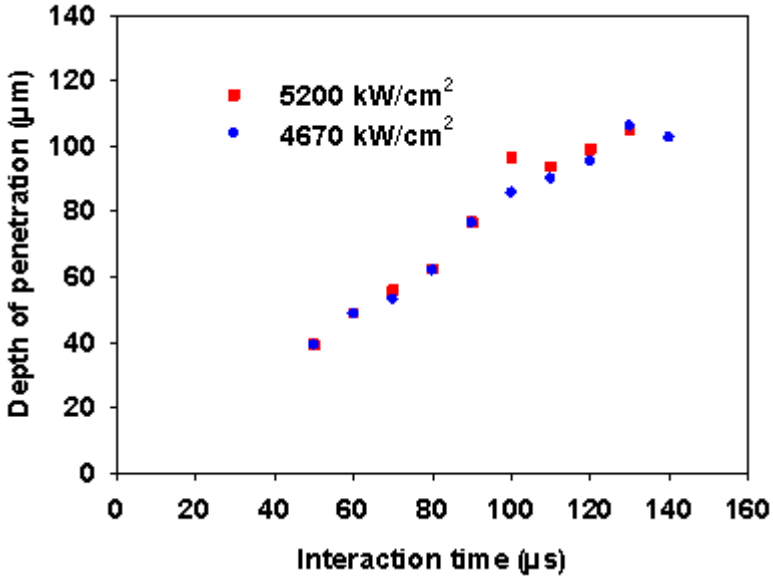

Figure 6-12: Dependence of depth of penetration on interaction time at constant power density

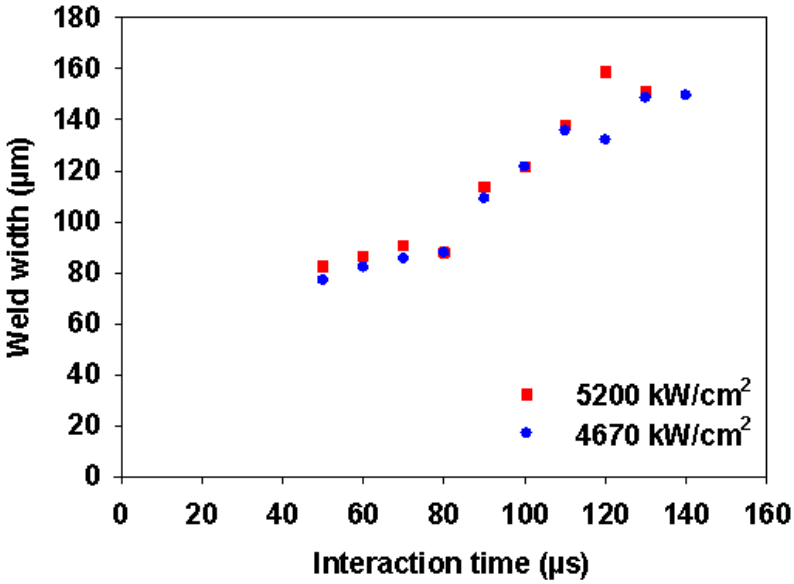

Figure 6-13: Dependence of weld width on interaction time at constant power density

Figure 6-14 shows bead on plate welds produced with energy density of 4.0 kJ/cm^2 and beam diameters of 0.10 mm. Pure conduction welds were achieved with this energy density comparison to those in Figure 6-10.

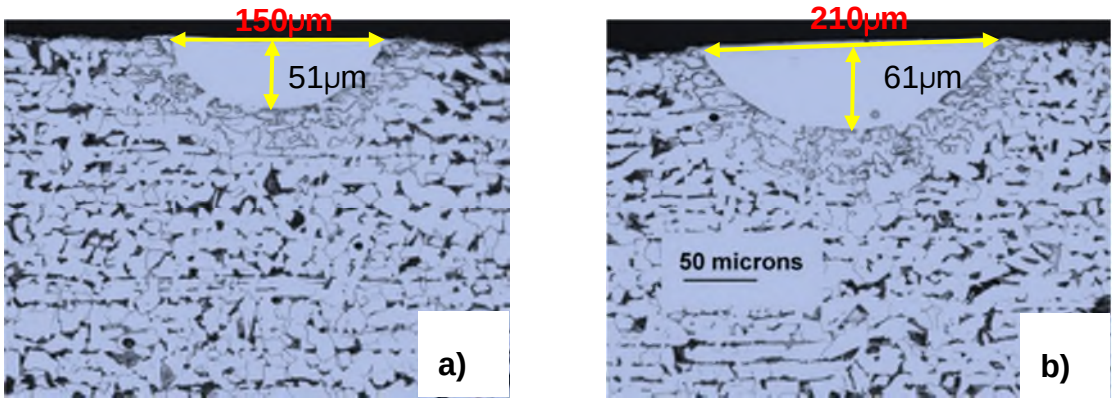

Figure 6-14: Bead-on-plate welds of conduction profile with an energy density of 4.1 kJ/cm^2 for (a) power density of 2040 kW/cm^2 and interaction time of 2.0 ms and (b) 3000 kW/cm^2 and interaction time of 1.40 ms

6.3 Discussion

In Section 5.3 of Chapter 5, it was observed that for large beam diameters, the depth of penetration was controlled by interaction time and power density and was independent of the energy. However, below a certain beam diameter, the depth of penetration started to decrease with decreasing beam diameter at constant power density and interaction time due to high conduction losses (see Figure 5-9). This means that at a certain small beam diameter, it is not possible to achieve melting of material with such a combination of interaction parameters. Note that in that case it was not possible to achieve melting with a beam diameter of 0.60 mm (Figure 5-9 in Section 5-3). However, in contrast to this in Figure 6-1 and Figure 6-2 there are pure conduction welds produced with a beam diameter of 0.10 mm. The welds were produced with a similar level of energy density, but for much high power density and shorter interaction time, as shown in Figure 6-15.

$D_B(mm)$	0.60	1.00	1.50	4.00
$P_d = 33.1 kWcm^{-2}$ $t_1 = 120ms$ $E_d = 4 kJcm^{-2}$	No melting			

Bead-on-plate welds produced at a constant energy density of 4.0 kJ/cm^2 with bigger beams. Note: Figure 5-9 of Section 5-3

$D_B(mm)$	0.10	0.07
$P_d = 2040 kWcm^{-2}$ $t_1 = 2ms$ $E_d = 4 kJcm^{-2}$	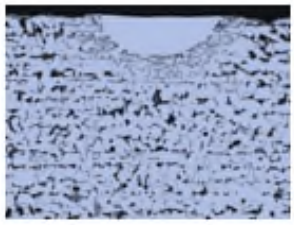	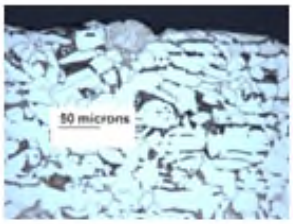

Figure 6-15: Bead-on-plate welds produced at constant energy density of 4.0 kJ/cm^2 (small beams)

This suggests that selection of parameters for conduction welding is very sensitive to the size of the beams. It was shown, based on an analytical solution of the heat equation, in Chapter 5 that the ratio of energy utilised for melting to the energy dissipated to the bulk material decreases with decreasing beam diameter. This means that conduction losses take a very significant proportion of laser energy when using small beam diameters. In order to achieve melting and reduce conduction losses with small beam diameters, the interaction time has to be reduced to a minimum. As shown in Figure 6-15, shorter interaction time resulted in less conduction losses, which led to a good conduction weld, even with this small beam diameter. However, to provide enough energy at this short interaction time a relatively high power density was required. In powder bed with a beam diameter of 0.07 mm even more extreme conditions were

needed to achieve conduction weld (Figure 6-10). However, at these high power densities and short interaction times, there is a greater risk of exceeding vaporisation and switching to keyhole regime. In fact, the threshold power density for melting and vaporisation is higher for small beam diameters and short interaction times, as reported by (Assuncao, E. et al., 2012), but the transition between conduction and keyhole is much narrower, as compared to big beams. This means that difficulty of achieving steady state conduction welds increases with decreasing beam diameter and in practice either no melting or a sudden keyhole occurs (Fuerschbach and Eisler, 1999).

As observed in Figure 6-5, Figure 6-6 and Figure 6-11, the interaction parameters that control depth of penetration for small beam diameters are power density and interaction time. Similarly, the weld width depends on the power density and interaction time as suggested in Figure 6-7, Figure 6-8 and Figure 6-13. However, for small beam diameters, the power density has a greater effect on the weld bead profile unlike in large beam diameters where the effect of interaction time was more significant. Normal conduction welds are time dependent, which is attributed to the time required for the heat to conduct from the laser-interaction point to the inner regions of the material. Conduction heat transfer is relatively slower compared to vaporisation or convection heat flow. However, the high conduction losses with small beam diameters make the process response differently. In this case, an increase of interaction time results in a simultaneous increase of energy input and conduction losses, hence the change of the weld profile is low. The only way to increase the absorbed energy in the material and to create more melting is by increasing power density, that is the rate of energy input. Therefore, depth of penetration is more responsive to variation of power density than interaction time for small beam diameters.

The weld width for large beam diameters was proportional to the size of beam diameter on the surface of workpiece. However, the results of the smaller beam diameters indicate that the weld width can be greater than the beam diameter. Also, in this case the weld width is very dependent on the interaction time (see Figure 6-3), unlike for big beams. Small beam diameters behave like a point

source profile where the weld width becomes wider than the beam diameter compared to the medium or large beam diameters, which can be approximated by a disc source. This is likely to be attributed to strong heat loss through the thickness, which promotes lateral expansion of fusion zone with increasing energy density, or by a rapid melt flow.

Shown in the analysis of the aspect ratio of the bead on plate welds achieved on a commercial powder bed indicated that most of them were in transition and keyhole regime, as presented in Figure 6-11. In keyhole regime, the increase of depth of penetration is greater than weld width, hence the aspect ratio greater than 0.6. In pure conduction regime, the rate of increasing depth of penetration and weld width is equal, but for small beam diameters and short interaction times, the conduction window is narrow.

7 Relationship between energy distribution and weld bead geometry

The size of the projected beam on the workpiece and the energy distribution profile defines the response of the material to the applied laser heat. The use of galvo-scanners to manipulate laser beam across the working envelope is the most popular choice in powder bed technology. This is due to fast scanning requirement of the process. However, one of the downsides of galvo-scanners is a distortion of the projected laser spot, which varies continuously during the processing. Consequently, the quality of deposited beads and the process efficiency cannot be uniform due to change in beam shape that affects the interaction parameters. Therefore, the objective of this chapter is to examine the influence of a change in shape of the projected beam and its energy distribution on the weld bead profile of conduction welds.

7.1 Beam profiles

7.1.1 Laser beam distortion with galvo-scanner due to the slide angle

Galvo-scanner utilise mirrors to deflect the beam, which changes shape of the projected spot on the workpiece, as shown in Figure 7-1. Random changes in the beam shape can induce different interaction parameters i.e. power density, interaction time and specific point energy. This will result in different melting characteristics of the build profiles. It is anticipated that an increase of the beam inclination by 45^{o} can cause a decrease in the power density by 30% and an increase of interaction time by 40% due to elongation of the beam, despite constant travel speed and laser power. This happens as the beam changes from usual circular shape to an elliptical shape, with a greater surface area.

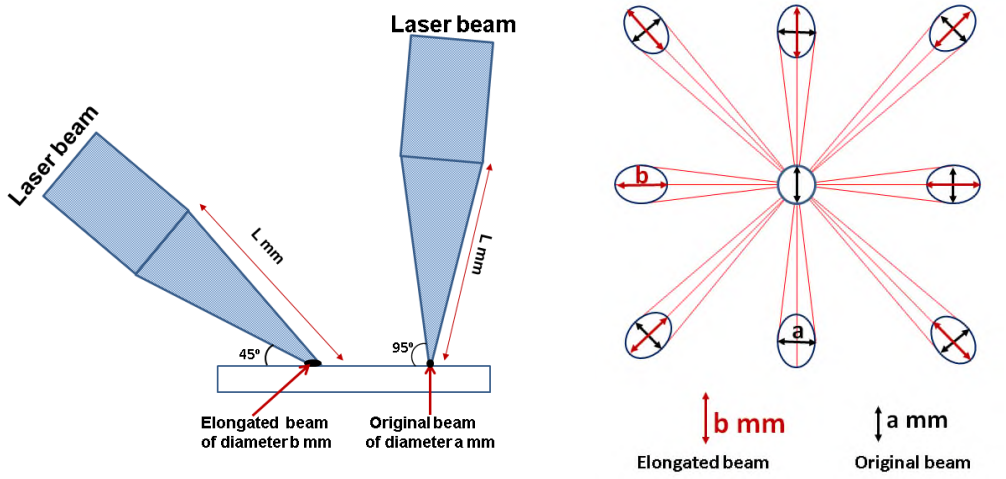

Figure 7-1: Schematic representation of the effect of the incident angle on the projected spot size

From Figure 7-1, if “a” is the original beam diameter for an undistorted beam and “b” the beam diameter for the distorted beam (45^{o} inclination angle)

$$b = a\sqrt{2}mm \tag{18}$$

From Equation 1, the power density P_d for circular beam of diameter “a” mm is given by

$$P_{d1} = 4\frac{P}{\pi a^2} \tag{19}$$

For a beam of ellipse configuration of radii x and y where $a = 2x$ and $b = 2y$ power density is given by

$$P_{d2} = 2\frac{P\sqrt{2}}{\pi a^2} \tag{20}$$

$$P_{d1} : P_{d2} = 2 : \sqrt{2} \tag{21}$$

From Equation 2, the interaction time (t_i) for beam of diameter a mm is given by

$$t_1 = \frac{a}{t_s} \tag{22}$$

Similarly for beam of diameter b mm

$$t_2 = a\frac{\sqrt{2}}{t_s} \tag{23}$$

$$t_1 : t_2 = 1 : \sqrt{2} \tag{24}$$

7.2 Experimental procedure

7.2.1 Effect of shape of projected laser beam on weld bead profile

This experiment examined the effect of beam distortion and welding direction on the weld bead geometry in conduction welding. The laser beam at the workpiece was elongated by applying a tilting angle of 45° to the laser head. This was then compared with a reference sample achieved with a circular beam. The welding parameters and the change to the corresponding interaction parameters are given in Table 7-1. The interaction parameters of power density and interaction time were calculated according to Equations 19 and 20. Note that in the case of reference sample a small tilt of 5º was applied to prevent the laser head from back reflection.

Table 7-1: Variation of fundamental laser material interaction parameters caused by inclination of the beam at constant laser power and travel speed

Degree of distortion (º)	Beam diameter (mm)	Elongated length (mm)	Spot area (mm^2)	Power density (kW/cm^2)	Interaction time (ms)	Energy density (kJ/cm^2)
5	1.37	1.37	1.47	61.00	120.0	7.32
45	1.37	1.94	2.10	43.30	170.0	7.36
45	1.37	1.37	2.10	43.30	120.0	5.20

7.2.2 Effect of spatial energy distribution on weld geometry

In this experiment, welding cases with out-of-focus conditions were compared with welds achieved at the focal point for the same nominal beam diameters. Laser beams with diameters of 1.70 mm and 2.35 mm used in focal points were applied to produce a series of bead on plate welds. Then, these reference welds were compared with a set of welds achieved using 250 mm focusing lens but defocused in such a way to obtain the same beam diameters of 1.70 mm and 2.35 mm. For both cases, the same laser power was applied to obtain power density of 17. 8 kW/cm^2 and 33.1 kW/cm^2 for beam of diameters 1.70 mm 2.35 mm respectively. The change of focal distance resulted in a change of power density distribution from the flat top-hat to a pseudo-Gaussian. This enabled comparison between the welds achieved with the same nominal beam diameters but different power density distributions. The details are shown in Table 7-2.

Table 7-2: Beam properties of different optical set-ups

Focusing lens (mm)	Focusing distance (mm)	Beam diameter (mm)	Rayleigh length (mm)	Laser power (kW)	Peak intensity (kW/cm^2)
250	Defocused by 20	1.70	6.45	1.45	171.3
250	Defocused by 28	2.40	6.07	0.80	44.0
680	Focused	1.70	37.48	1.45	94.19
1000	Focused	2.40	91.84	0.80	26.40

7.3 Results

7.3.1 Effect of laser beam distortion on weld bead profile

In the first experiment, the laser beam was inclined by 45° and the resulting welds were compared with the reference with a marginal inclination of 5º. Figure 7-2 shows the macrograph of the control sample (reference). Figure 7-3 shows the macrographs of the bead-on-plate welds produced at higher inclination angle for different welding directions. The weld shapes, depth of penetration and the weld width change with the inclination angle and welding direction, despite the same welding parameters. Distortion of the projected beam elongates in one direction, which changes the power density and energy distribution.

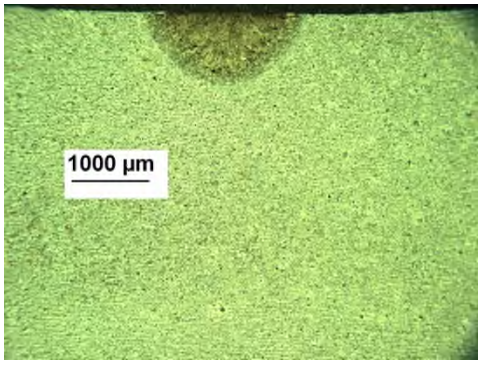

Depth = 0.73 mm, width = 1.76 mm and area = 0.77 mm^2

Figure 7-2: Control sample

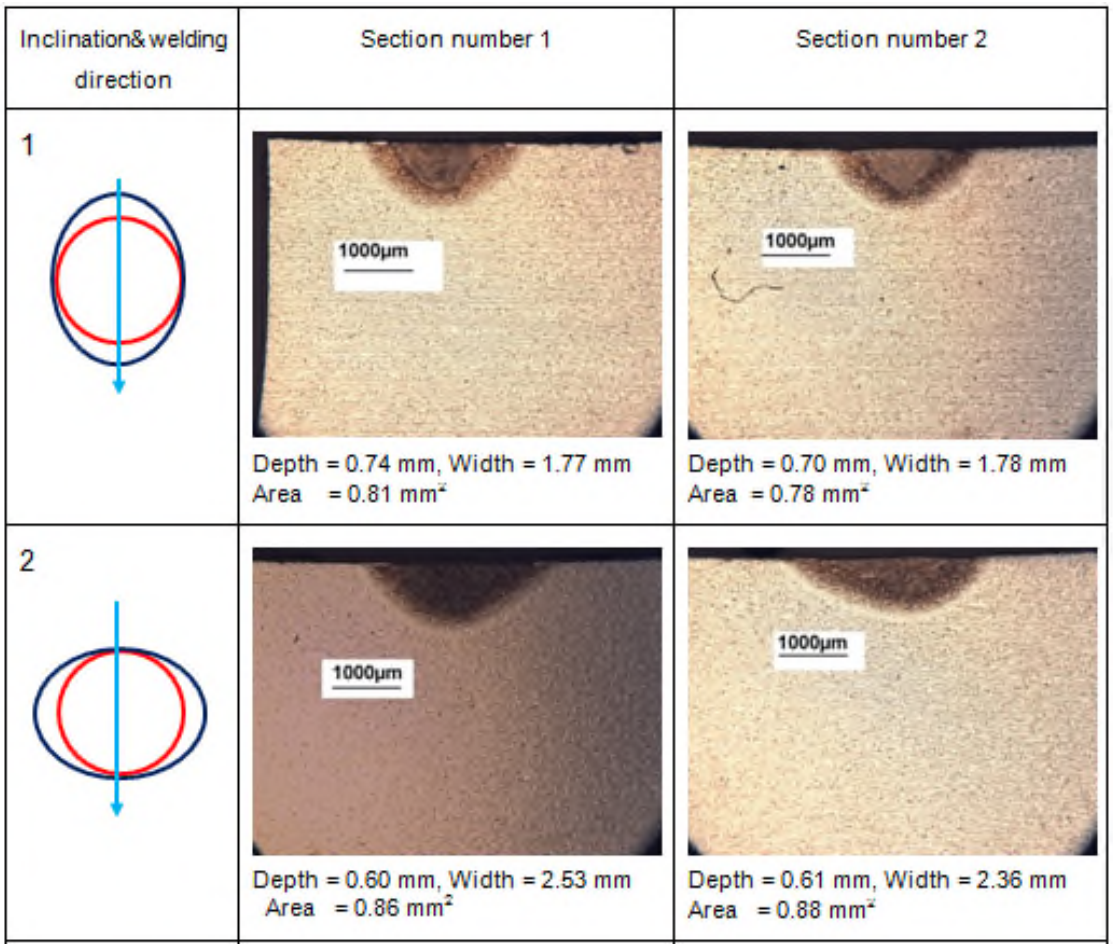

Figure 7-3: Macrographs of bead-on-plate welds produced at an inclination of 45°, laser power of 0.9 kW, travel speed of 0.69 m/min and beam diameter of 1.40 mm (Note: the light blue line indicates the welding direction, the royal blue circle is the elongated beam and red circle is the original beam)

The depth of penetration is higher for the welds produced with the elongation in the welding direction (direction 1), as compared to the transverse inclination to the welding direction (direction 2). The effect of beam elongation on weld bead profile is more complicated when welding direction is changing. The welds produced with the elongated beam in the welding direction exhibited narrower weld widths compared to the welds with the beam elongated in the transverse direction to the welding direction (direction 2). Therefore, the ratio of depth of penetration to the weld width varies depending on the inclination angle and

welding direction. The aspect ratio of the of control sample and with the elongated beam towards the welding direction exhibited higher aspect ratio compared to welds produced with beam elongated in the transverse direction. The shape of the control sample is more symmetrical, as compared to the distorted beams for the same laser power and travel speed.

7.3.2 Effect of energy distribution on weld beam profile

In this experiment, focused and defocused beams were compared for the same nominal beam diameters. The macrographs for the beam diameter of 2.35 mm are in Figure 7-4. A significant difference in the weld profiles can be seen. This is confirmed in Figure 7-5 and Figure 7-6. For both cases, a greater penetration was achieved with defocused beams, as compared to the focused ones. A difference in penetration up to 12% is shown for the beam diameter of 1.70 mm, and even greater difference of 24% for the beam of 2.35 mm. This can be attributed to the difference in the distribution of power density between focused and defocused beams. As shown in Figure 7-6, there is no significant difference in the weld width between defocused and focused beams at the weld surface. The melt area depends on the beam shapes. The defocused beam has higher melt area than the focused beam, as shown in Figure 7-7.

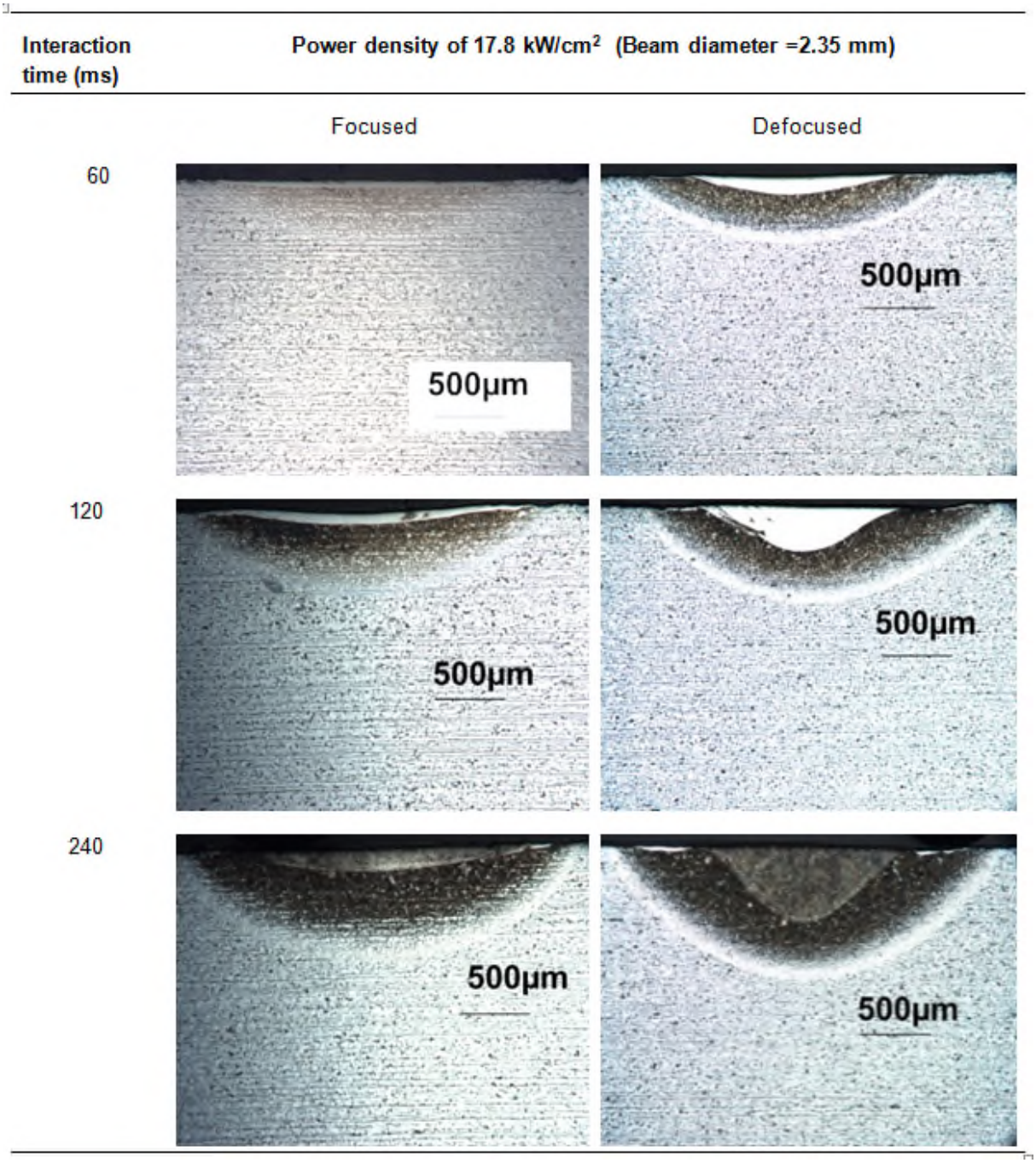

Figure 7-4: Macrographs of bead-on-plate welds produced with focused and defocused beams for the same nominal beam diameter at constant power density of 17.8 kW/cm^2 and different interaction times

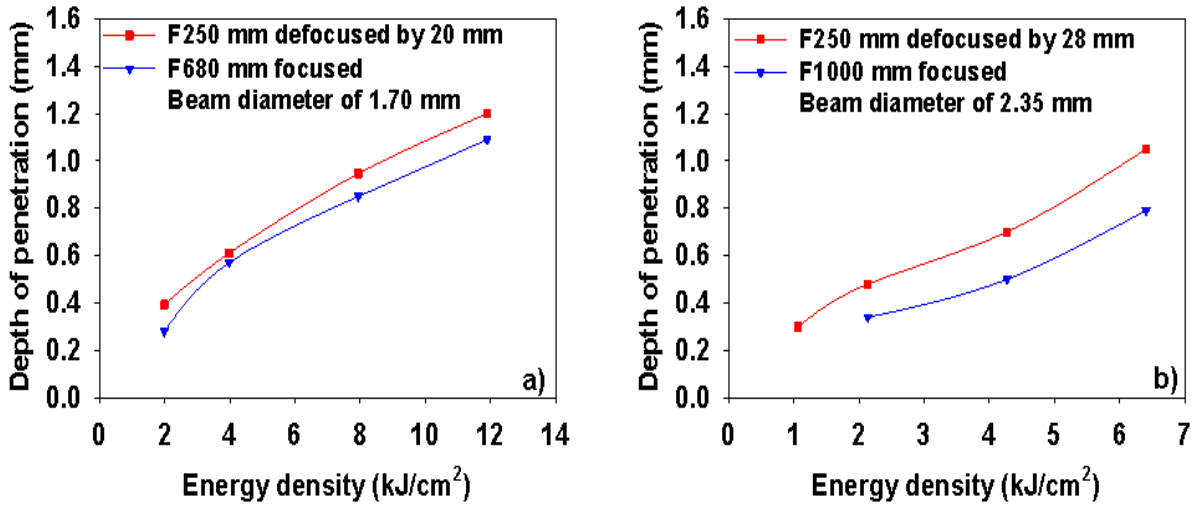

Figure 7-5: Depth of penetration with focused and defocused beams for the same nominal beam diameter: a) 1.70 mm and b) 2.35 mm

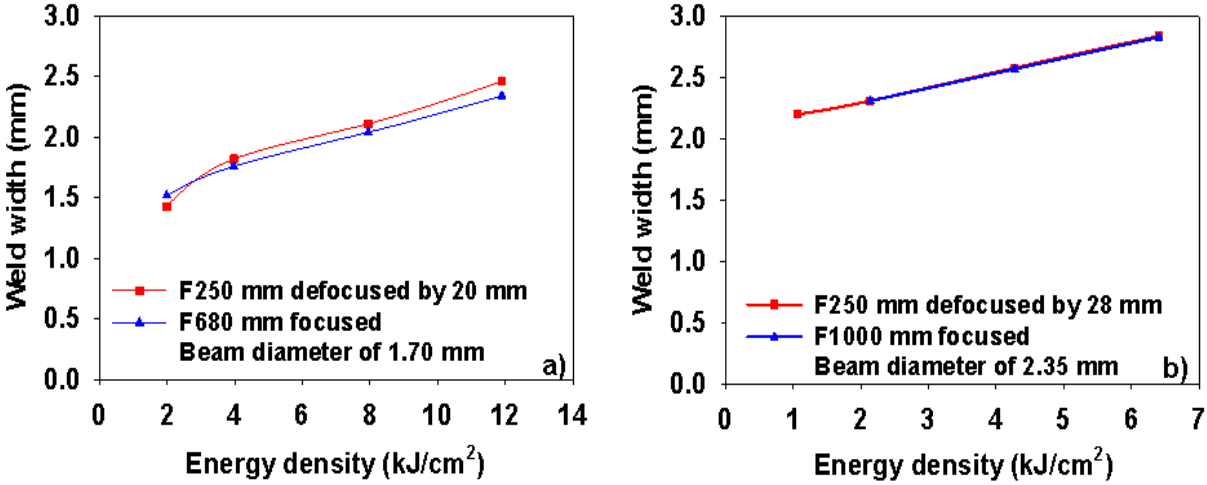

Figure 7-6: Weld width with focused and defocused beams for the same nominal beam diameter a) 1.70 mm and b) 2.35 mm

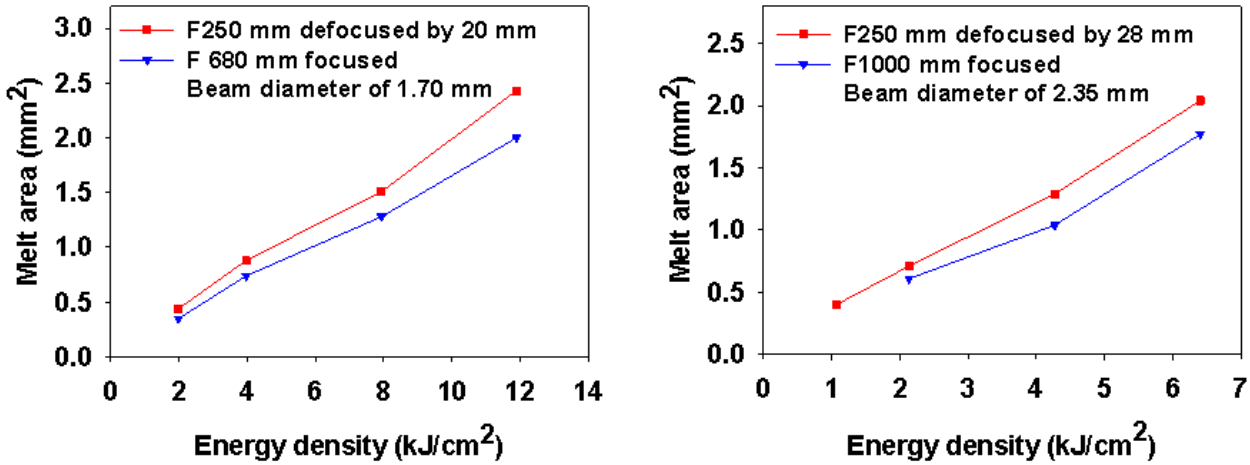

Figure 7-7: weld width with focused and defocused beams for the same nominal beam diameter a) 1.70 mm and b) 2.35 mm

7.4 Discussion

To melt a workpiece, a certain amount of energy is required. The weld bead in a particular material with certain thermophysical properties is a response of the material to a particular thermal cycle, which is determined by the spatial and temporal energy distribution of the heat source. The effect of changing the spot shape was investigated. The intention was to simulate distortion of a laser beam by a galvo-scanner, and its influence on the weld profile. In Figure 7-3, it was observed that the depth of penetration and weld width varied with the inclination angle and welding direction when using constant laser power and travel speed, due to change in beam shape.

The results indicate that the depth of penetration and weld width of the control sample is similar to the welds produced in the elongated beam towards a welding direction, as shown in Table 7-3. A change of the beam shape on the workpiece has a profound effect on the fundamental interaction parameters, which all depend on the beam diameter. Travelling in the elongation direction at

constant laser power and travel speed resulted in a drop of the power density and an increase of the interaction time and specific point energy. However, as shown in Table 7-3, these two offsetting effects led to the same energy density, and therefore the weld profiles between the reference sample and the elongated in welding direction are similar, in terms of depth and width. In contrast, travelling across the elongation direction produced wider and shallower welds, as compared to the reference sample (see Figure 7-3). In this case, the power density dropped and the interaction time and specific point energy were the same. The weld width increased due to widening effect of the beam diameter, which was compensated by the drop of penetration. The depth of penetration decreased in the transverse direction because of the drop in power density at constant interaction time (Table 7-3) leading to a lower energy density. In Chapter 5.0 (see Section 5.3.2), it was shown that the energy density controls depth of penetration and the beam width controls the fusion zone width. Therefore, any change to the energy density and beam width will be reflected on the weld profile.

Table 7-3: Effect of beam inclination angle on fundamental interaction parameters and weld profile

Degree of distortion (º)	Beam length (mm)	Beam width (mm)	SP Energy (J)	Power density (kW/cm^2)	Int time (ms)	Energy density (kJ/cm^2)	Weld depth (mm)	Bead width (mm)
5	1.37	1.37	108	61.00	120.0	7.32	0.73	1.76
45	1.94	1.37	155	43.30	170.0	7.36	0.72	1.77
45	1.37	1.97	109	43.30	120.0	5.20	0.60	2.45

This is consistent with a previous study done by Tang et al (Tang et al., 2004). They examined the accuracy of building a part during prototyping by direct laser sintering system. Different sources of errors were identified. The most significant cause of error was the variation of laser spot shape across the

workpiece by the laser scanner. Therefore, compensation parameters by the software were developed to correct for the errors resulting from distortion of galvo-scanner and theta lens. The build parts fabricated with and without compensation factor were compared. The galvo-scanner with a standard F-theta lens caused significant deviation of the part dimensions ranged from 2 to 21% compared to the actual dimension. However, with the compensation procedure, the deviation was 0.1 to 5.5 %. The laser spot size used in the experiment was 0.60 mm. This suggests that despite the use of an F-theta lens, the effect of distortion is very significant, which could be more evident with large beam diameters.

This shows that in powder beds with galvo-scanners the fusion characteristics may continuously change when laser beam is moved across the workpiece, if no compensation procedure is applied. The simulation of beam distortion in this work caused a deviation of 21 % in depth of penetration and 43 % in weld width. Although in standard powder beds beam diameters used are much smaller than in this case (1.70 mm) and the effect may not be as great in this case, but the relative difference in change of weld profile should be the same. The problem should be greater when building bigger powder bed machines, which will require galvo-scanners with longer focal length optics.

Use of the system parameters, such as laser power and travel speed to characterise the weld bead profile in welding is inadequate due to the effect of beam diameter. In this study, it was found that the weld bead profile is dependent on the beam shape, and power density distribution. It was shown in Figure 7-4 that the spatial distribution of energy affects the weld profile even for the same energy applied. Focused beams, in this case, had a top-hat power density distribution and defocused beams exhibited a pseudo-Gaussian profile. The pseudo-Gaussian beam resulted in higher peak intensity at the centre point, with gradually decreasing intensity towards the circumference of the laser spot. The top-hat intensity distribution profiles, on the other hand, resulted in a more homogenous distribution of energy across the surface of laser spot, leading to more homogenous temperature profiles. Thus, all welds achieved

with defocused beams exhibited a higher depth of penetration and melt area (Figures 7-5 and 7-7) with no significant difference in weld width (Figure 7-6), than the welds achieved with a focused beam.

The temperature reached in the melt pool is a function of absorbed power density. The pseudo-Gaussian beam profile in the defocused case resulted in a higher temperature in the centre of melt pool due to higher peak intensity and greater temperature gradient, as compared to the focused beam case (Figure 7-5). This high temperature gradient can induce strong convection and even initiate evaporation, which leads to an increase of depth of penetration. However, more uniform power density of the of the top-hat beam led to more uniform weld profiles. With smaller beams, the difference in temperature gradients is less significant. Therefore, the difference in weld profiles was smaller for the beam diameter of 1.70 mm (Figure 7-5) than for 2.40 mm. It was shown that in keyhole welding that involves high power density and smaller beam diameters, the effect of beam shapes on depth of penetration is less significant (Kaplan, 2011; Volpp, 2012). This was attributed to the fact that the central region of the beam does not play important role in material interaction. In keyhole welding or conduction welding with smaller beam diameters, the temperature gradients are lower and the melt flow plays an important role in homogenising temperature distribution. This suggests that in powder bed additive manufacturing with small beams the intensity profile, i.e. top-hat or Gaussian may play a secondary role in the formation of bead profile.

8 Comparison between solid and powder melting

In this study, powder melting is compared with solid melting for different beam diameters. The interaction parameters investigated in solid melting in Chapters 5.0 and 6.0 were applied in powder melting for the comparison. This is to understand the fusion characteristics of powder of different bulk properties and solid material of homogeneous particle sizes. The first part of this chapter investigates the interaction parameters that control the build profile in powder melting. The second part compares the melting characteristics between powder and solid. The overall objectives of this chapter are:

- To compare the weld bead profile (depth of penetration, weld width and melt area) of solid melting with the build layer (build height, build width and build area) of powder melting;
- To identify welding regime in powder bed additive manufacturing

The fundamental laser material interaction parameters used in this chapter are power density and interaction time. Section 3.3 of Chapter 3.0 (see pages 19 and 20) discussed the details of these interaction parameters.

8.1 Research approach

In Chapter 5.0, the effect of interaction parameters and beam diameter on the weld bead profile was investigated in S275 low carbon steel. The investigation was carried out with a wide range of beam diameters. The first group consisted of large beams of 4.0 mm to 6.0 mm. A similar approach used in Chapter 5.0 was adopted for the powder melting in this chapter. The same beam diameter and interaction parameters were used. The details of the experimental set-up including the powder properties are given in Chapter 4.0.

In the second group of experiments, solid and powder melting with small and large beam diameters will be compared. This is to understand the fusion characteristics of powder of different bulk properties and solid material of homogeneous particle sizes. Experiments conducted with small and large beam

diameters in Chapters 5.0 and 6.0 are compared to the powder melting of this chapter. The layer thickness will serve as the substrate. The depth of penetration, weld width and melt area of solid melting will be compared to build height, build width and build area of powder melting in that order. Shown in Figure 4-7 of Chapter 4.0 (see page 58) are the forms of the bead profiles to be compared for solid and powder melting.

8.2 Experiments conducted in powder melting with different range of beam diameters

8.2.1 Large beam diameters

In solid melting to achieve power densities of 25.5 kW/cm^2 and 28 kW/cm^2, the laser power was adjusted to the spot size projected on the workpiece according to Equation 1. Similarly, to achieve interaction times between 60 ms and 480 ms, travel speed was varied with the beam diameter according to Equation 2 (see Section 5.2.2). The same conditions of interaction parameters with these beam diameters were obtained for powder melting. In this experiment, beam diameters of 4.0 mm and 5.0 mm and groove thicknesses of 0.50 mm and 1.00 mm were used. The groves were filled with powder, which was then fused with the laser energy, as shown in Figure 4-7. Therefore, the groove depths serve as the layer thicknesses in powder melting.

8.2.2 Small beam diameter

In a powder bed machine, it is common practice to use small beam diameters. In this section, the melting behaviour of solid and powder material is compared with a beam diameter of 0.10 mm, which is comparable to the conditions used in commercial powder bed machines (Buchbinder et al., 2011). The experiment was conducted to compare the bead-on-plate profile in solid melting with build layer profile in powder melting to consolidate further the understanding of powder fusion with the smaller beam.

The power density was varied by changing the laser power at constant beam diameter. Different interaction times were obtained by varying the travel speed from 10 mm/s to 130 mm/s according to Equation 2. Similar conditions used in solid melting were replicated in powder melting, including shielding gas, optical set-up and welding enclosure, as described in Section 6.1.

8.3 Results

8.3.1 The parameters controlling build profile in powder melting

8.3.1.1 Effect of interaction parameters on the build profile

Effect of interaction time on the build profile at constant power density

In Section 8.2.1, experiments were conducted to investigate the effect of interaction parameters on build profile for large beam diameters. Table 8-1 shows the details of the welding parameters and interaction parameters used. Figure 8-1 and Figure 8-2 show the effect of interaction time on the build height and build width at constant power density. In the experiment, layer thicknesses of 0.50 mm and 1.00 mm were used. Figure 8-1a and Figure 8-2a consisted of additional experimental data points to better understand the trend of the results. In Figure 8-1a & b and Figure 8-2a & b, there was no fusion for interaction time of 60 ms. Therefore, these points have been omitted. It can be seen in Figure 8-1 that the build height shows no significant difference from the layer thickness at constant beam diameter and power density. This means that the build height is less dependent on the interaction time.

Table 8-1: Parameters used to compare bead profile in solid melting with build layer profile in powder melting at power density of 25.5 kW/cm^2

$BD\ (mm)$	$P\ (kW)$	t_s(mm/s)	$t_i(ms)$
4.00	2.56	66.00	60
		33.20	120
		16.67	240
		8.33	480
5.00	4.00	83.33	60
		41.70	120
		20.80	240
		10.40	480
6.00	5.76	99.50	60
		49.80	120
		25.00	240
		12.50	480

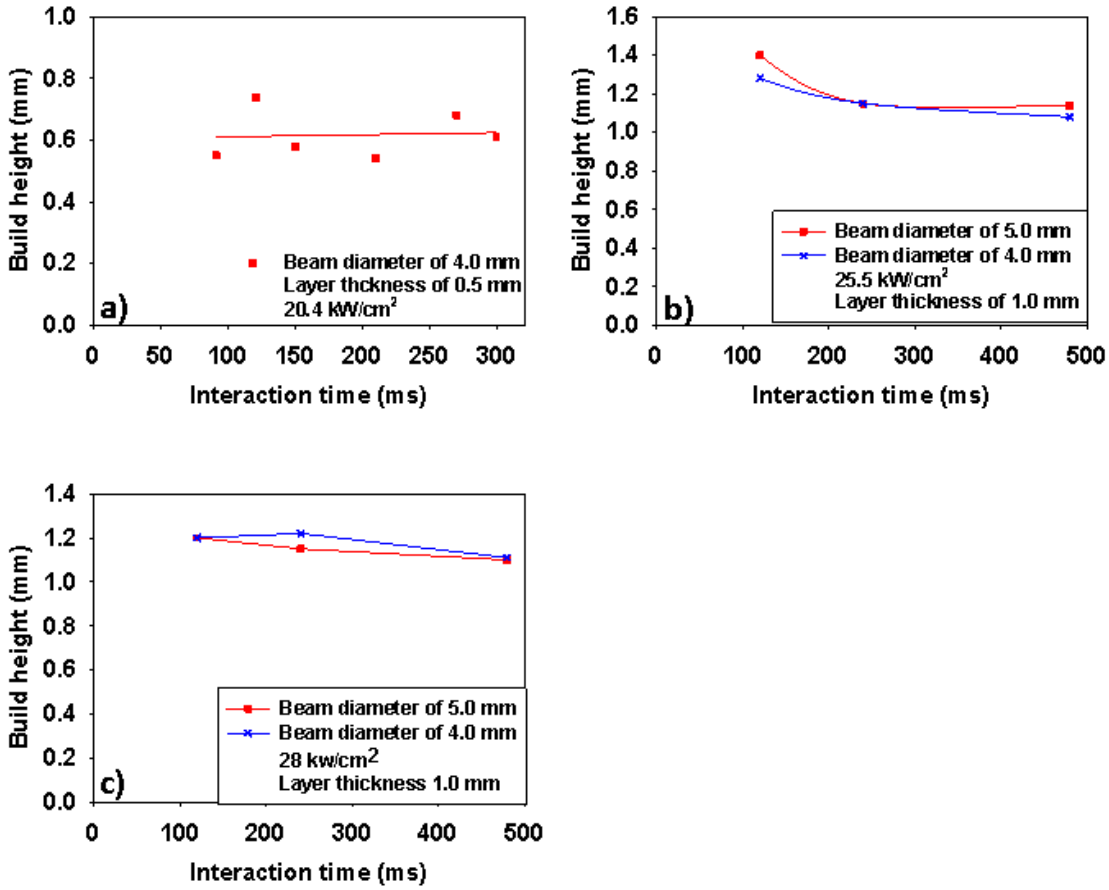

Figure 8-1: Effect of interaction time on the build height at constant power density of a) 20.4 kW/cm^2 b) 25.5 kW/cm^2 and c) 28 kW/cm^2

Figure 8-2 shows that the build width increases significantly with increasing interaction time. Similar to solid melting (see Figure 5-11 in page 74) with large beam diameters, the build widths in powder melting also saturates when the width approached the beam diameter.

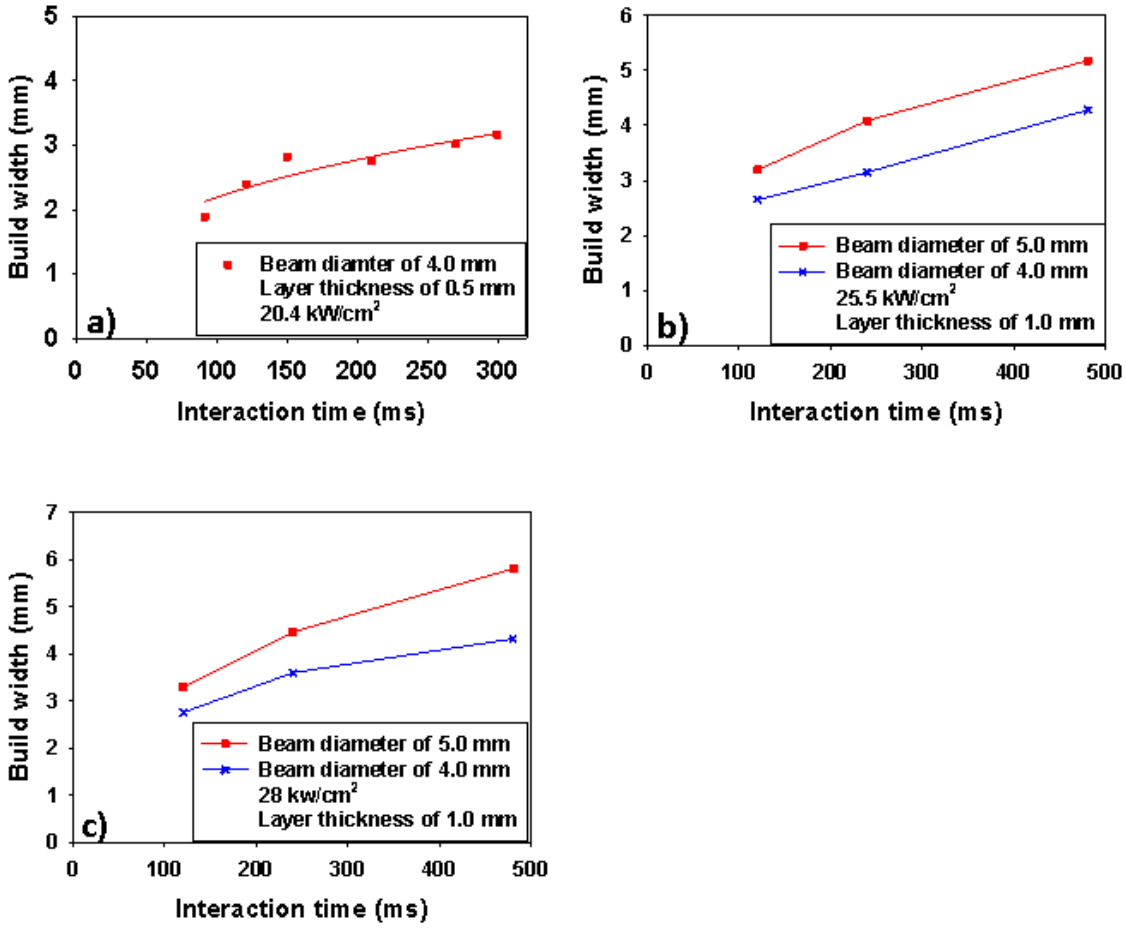

Figure 8-2: Effect of interaction time on the build width at constant power density of a) 20.4 kW/cm^2, b) 25.5 kW/cm^2 and b) 28 kW/cm^2

Figure 8-3 shows the macrographs of build layers produced at constant power density and layer thickness. The dilution is increased by 0.70 mm into the substrate due to an increase of interaction time for the condition shown.

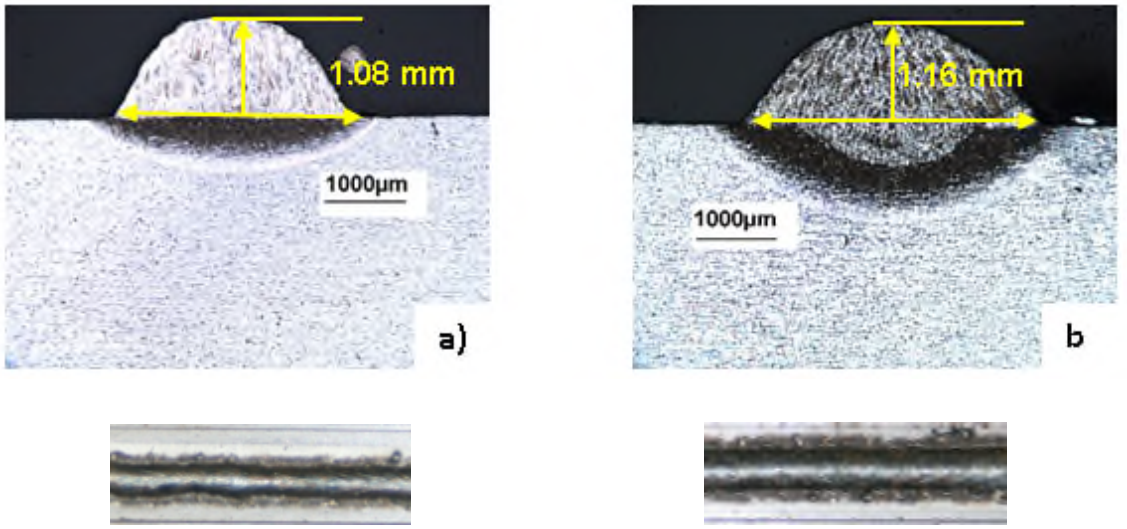

Figure 8-3: The effect of interaction time on the build height and width at constant beam diameter of 4.0 mm, power density of 28 kW/cm^2 and layer thickness of 1.0 mm; a) 120 ms (3.4 kJ/cm^2) and b) 240 ms (6.7 kJ/cm^2)

Influence of power density on build profile at constant interaction time

Figure 8-4 and Figure 8-5 show the effect of power density on the build height and width respectively, for large beam diameters. Figure 8-4 indicates that the effect of power density on the build height is insignificant for all levels of the interaction times investigated in this work. Unlike in solid melting where for large beam diameters the weld width was almost constant despite increasing power density. In powder, the power density affects the build width, as shown in Figure 8-5.

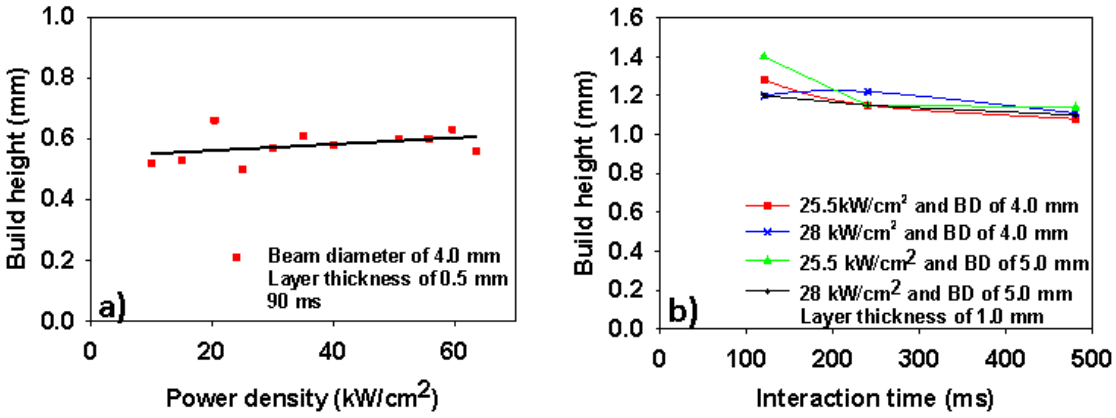

Figure 8-4: Effect of power density on the build height at constant interaction time

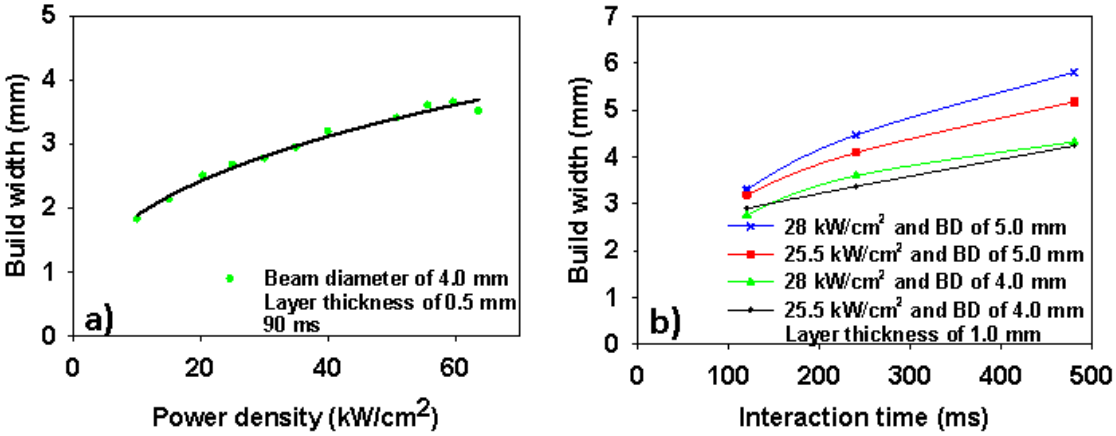

Figure 8-5: Effect of power density on the build width at constant interaction time for different beam diameters

8.3.1.2 Influence of layer thickness on build profile

Previous results have shown that the effect of power density and interaction time is less significant on the build height. Figure 8-6 shows the macrographs of built layers at energy density of 3.4 kJ/cm^2(28 kW/cm^2 and 120 ms) when the layer thickness is increased. The macrographs show good bonding between the deposited layer and the substrate. This figure indicates that at constant energy density the build height increases with increasing layer thickness from 0.5 mm to 1.0 mm by a factor of two, but at the same time the dilution of powder into the

substrate significantly decreased. The dilution depth in the powder of layer thickness 0.50 mm is 0.10 mm. The build width shows no significant difference with increasing layer thickness. The similarity in the build width is also visible in the top view of the build profiles shown in Figure 8-6. In addition, the aspect ratio of the build profile increased by a factor of two.

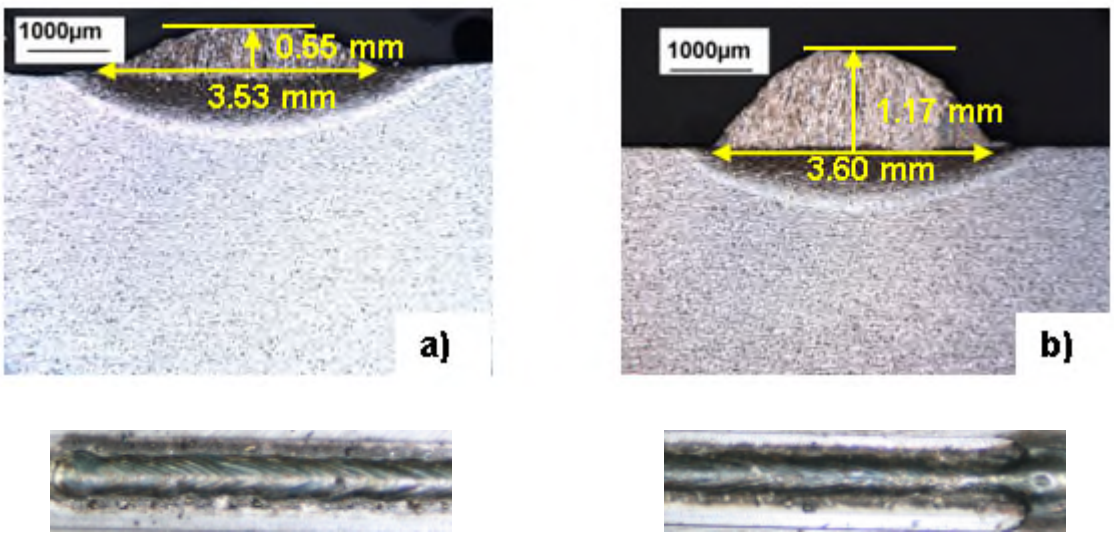

Figure 8-6: Effect of powder layer thickness on the build profile at constant energy density of 3.4 kJ/cm^2 and beam diameter of 5.0 mm; a) 0.50 mm and b) 1.00 mm

8.3.1.3 Beam diameter

Section 8.2.1 also examined the effect of beam diameter on build profile. This enables identification of parameters that control build height in powder melting. Figure 8-7 shows the effect of beam diameter on the build height and width at constant energy density and layer thickness. The layer thickness used was 1.00 mm. When the beam diameter was increased from 4.00 mm to 5.00 mm, no significant effect on the build height was seen at this energy density. The same trend was observed for a layer thickness of 0.50 mm. The dilution in the substrate is similar. However, the build width increased with increasing beam diameter and thus the build area, as shown in Figure 8-7 for a powder thickness

of 1.00 mm. Thus, the aspect ratio of the build profile decreases with increasing beam diameter.

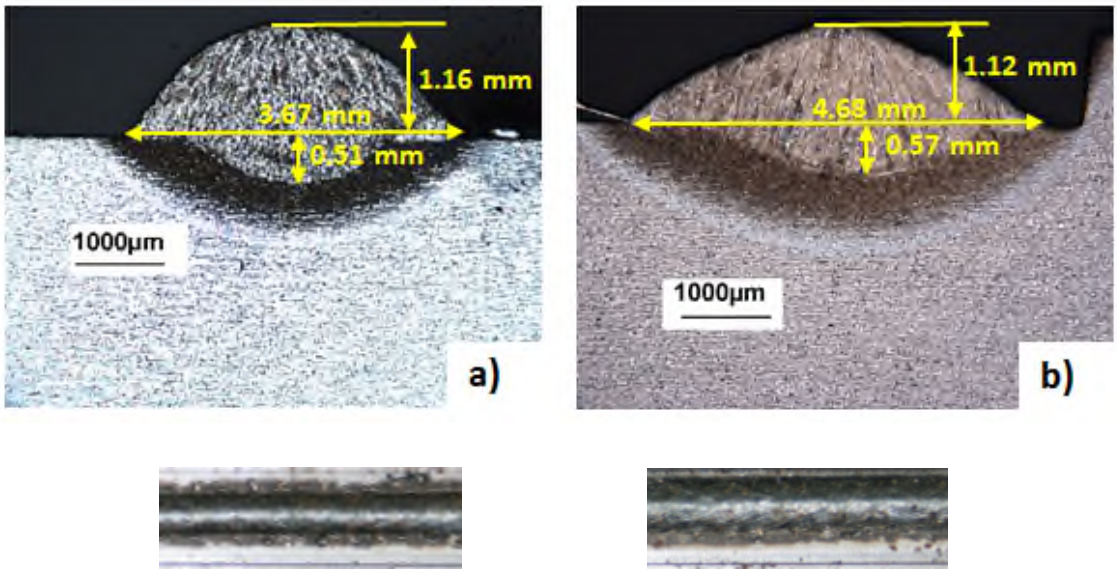

Figure 8-7: Effect of beam diameter of a) 4.00 mm and b) 5.00 mm on track profile in powder melting with energy density of 6.7 kJ/cm^2 (28 kW/cm^2 and 240 ms) and layer thickness of 1.0 mm

8.3.2 Comparison of weld profile between solid and powder melting with large beam diameters

One of the objectives of this study was to compare the melting behaviour of homogeneous solid material and powder particles of non-homogeneous distribution. Results of experiments conducted in Chapter 5.0 for solid melting and powder melting of this chapter were used for the comparison. In Figure 8-8, the bead profile of a weld in a solid material is compared with the profile of a fused track in powder for a constant energy density and beam diameter. It can be seen that in solid melting, a depth of penetration of 0.74 mm was achieved, but in powder melting a powder layer thickness of 1.17 mm could be fused to the substrate for the same laser parameters. Figure 8-9 also confirmed such a trend. For the same energy density, the build height is slightly higher than the depth of penetration.

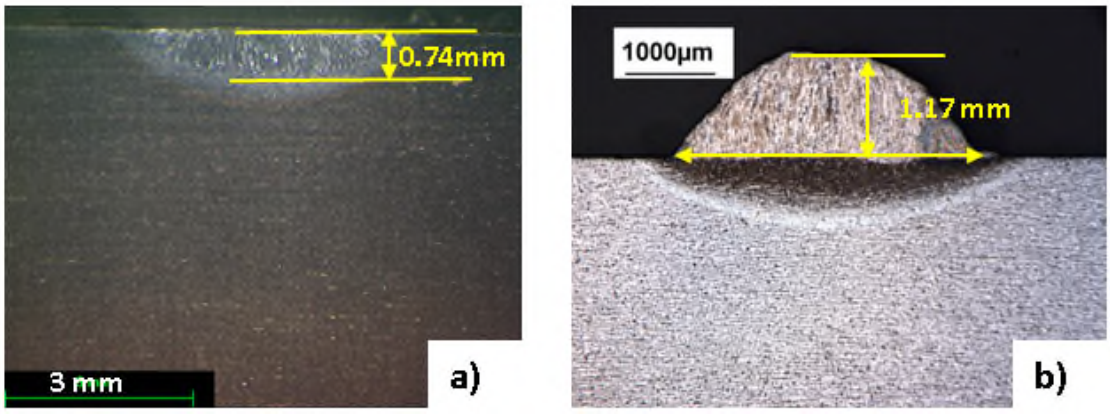

Figure 8-8: Comparison of the depth of penetration with build height at a constant energy density of 3.4 kJ/cm^2 (28 kW/cm^2 and 120 ms) and beam diameter of 5.00 mm for a) solid melting and b) powder melting

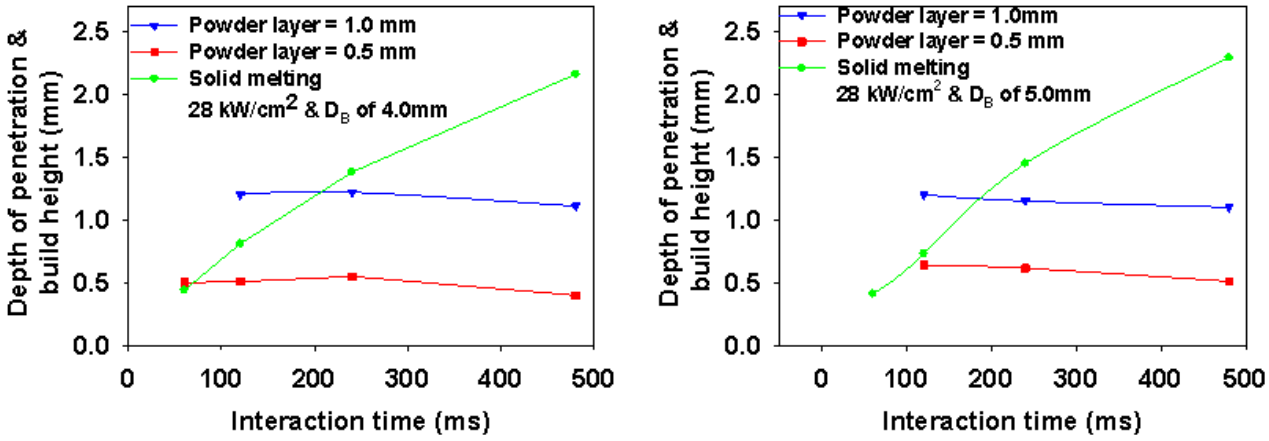

Figure 8-9: Comparison of the depth of penetration with build height at a constant energy density and layer thickness for beam diameters of a) 4.0 mm and b) 5.0 mm (Note: green lines are penetration in solid melting)

Figure 8-10 shows the comparison of weld and build widths. In the previous figures also, the comparison between solid and powder was shown. The weld width is the same as the build width. Figure 8-11 also confirmed the trend for a wider range of parameters. The weld width is slightly higher than the build width at lower energy density for both beam diameters. However, at higher energy

density, there is no significant difference in the weld width and build width, as shown in Figures 8-11.

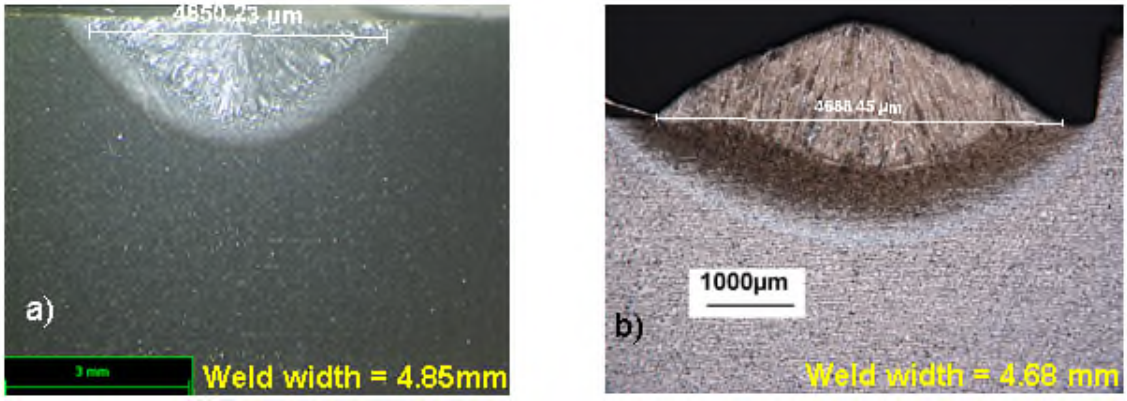

Figure 8-10: Comparison of weld width with build width produced with energy density of 6.7 kJ/cm^2 (28 kW/cm^2 and 240 ms) and beam diameter of 5.00 mm a) solid melting and b) powder melting

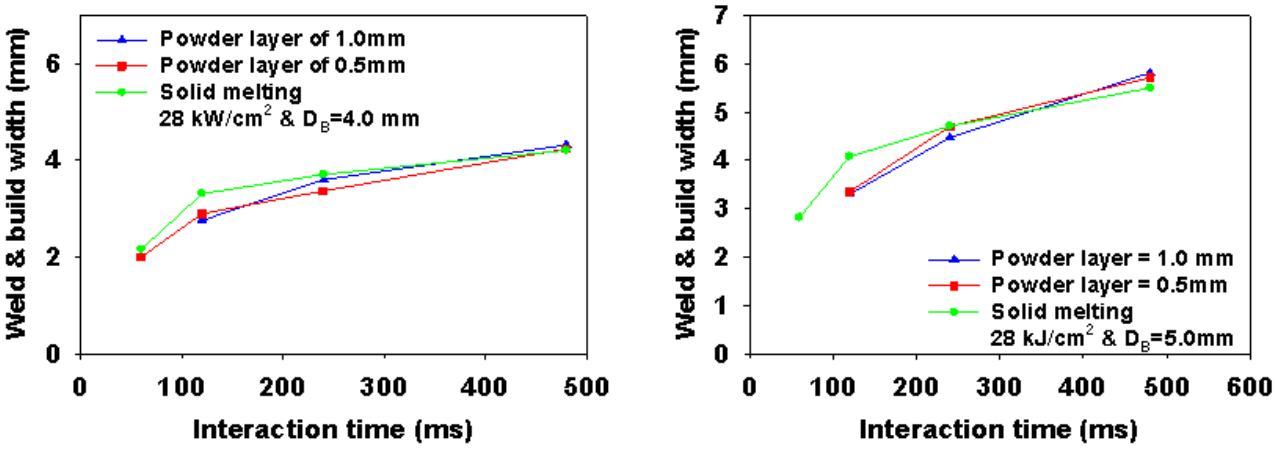

Figure 8-11: Comparison of weld width in solid melting with build width in powder melting produced with different beam diameters of a) 4.0 mm and b) 5.0 mm

8.3.1 Comparison of weld profile in solid and powder melting for small beam diameters

This section shows the results of solid and powder melting produced with beam diameters of 0.10 mm. Table 8-2 shows the welding parameters and corresponding interaction parameters investigated. Figures 8-12 and 8-13 show the macrographs of the build layers produced with the interaction parameters investigated.

Table 8-2: Parameters used to compare solid and powder melting with beam diameter 0.10 mm and power density of 640 kW/cm^2

t_i (ms)	t_s (mms^{-1})	E_d (kJ/cm^2)
1	100.0	0.60
2	50.0	1.30
4	25.0	2.50
6	16.7	3.80
8	12.5	5.10
10	10.0	6.40

There are four main regions of the build layers. The first region is where there is no melting but heating of the powder. This occurs at a low power density of 640 kW/cm^2 and a short interaction time of 1.0 ms. In the second region, there is a melting of the powder layer, however, due to insufficient heating the wetting of the molten powder with the substrate is inadequate and the deposited bead attains a ball shape due to strong surface tension. In the third region, there is a significant melting of the powder layer deposited. The built layers produced form a circular cross section with little wetting between the built layer and the substrate. The portion of the build width fused into the substrate is smaller than the diameter of the deposits. The build height and the width of the deposits are greater than the layer thickness. The fourth region is where there a complete melting of powder and smooth deposits. In this region, the power density used was between 1660 kW/cm^2 to 5350 kW/cm^2. The track profile also depends on

the interaction times. The build profile gets more stable when interaction time is increasing. Table 8-3 shows a summary of the four regions. In this table, a region where stable build profile was obtained is marked in yellow.

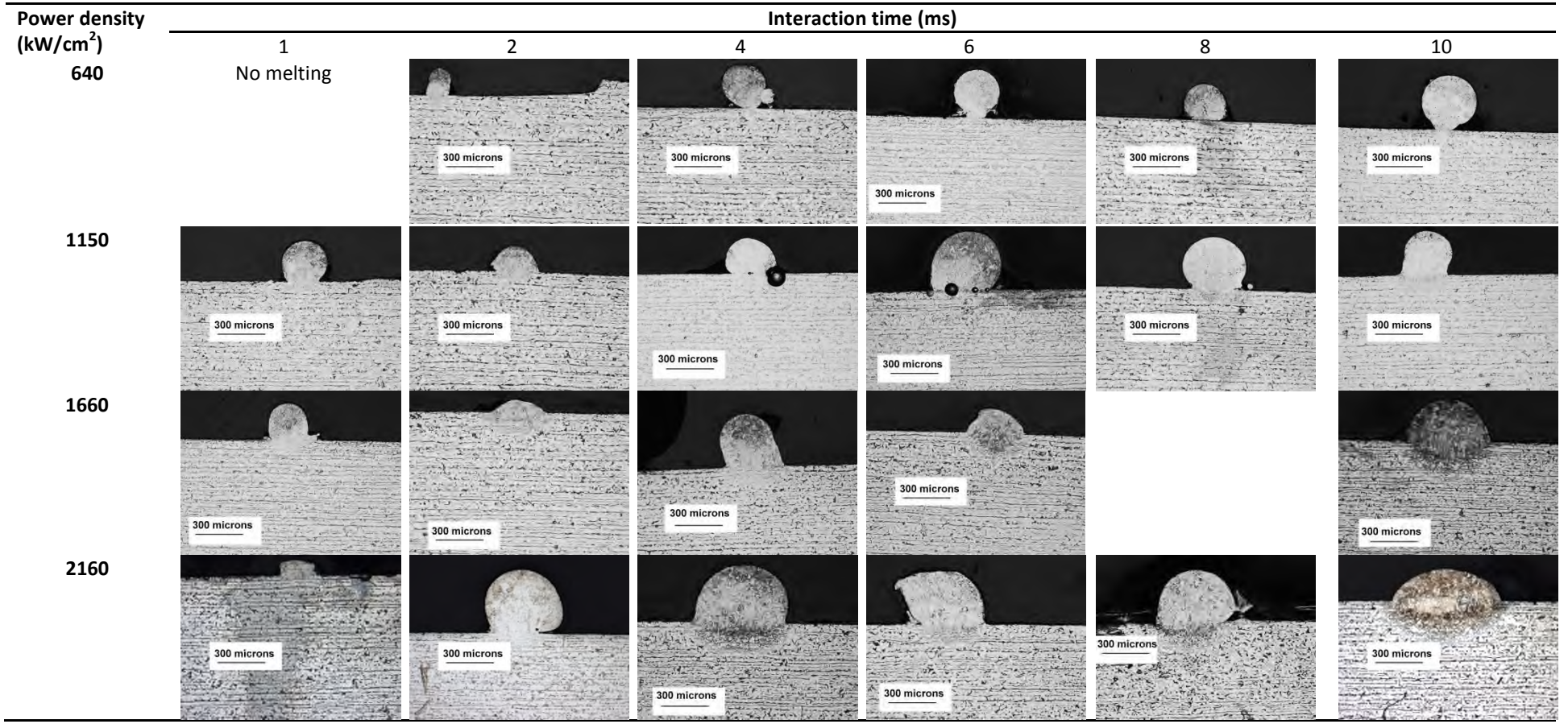

Figure 8-12: Macrographs of built layers produced with layer thickness of 200 μm and different combination of interaction parameters

Power density (kW/cm^2)	Interaction time (ms)					
	1	2	4	6	8	10
2670		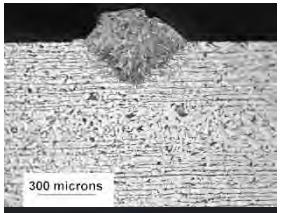			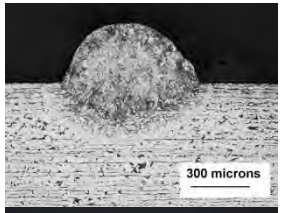	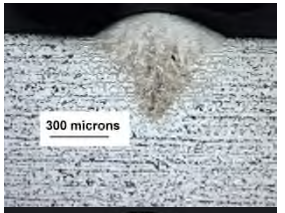
3570		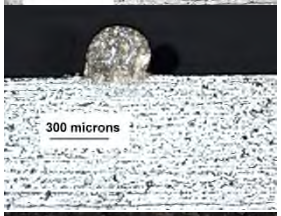	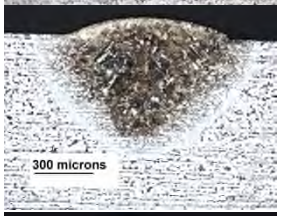	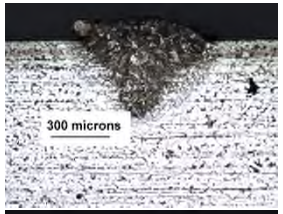	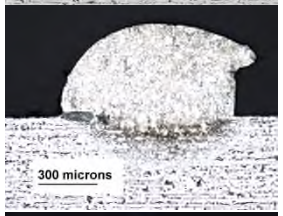	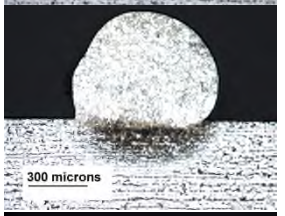
5350	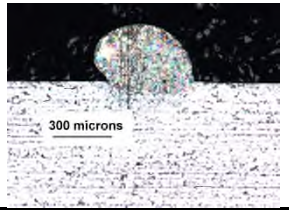	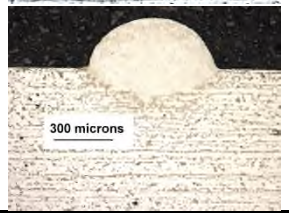	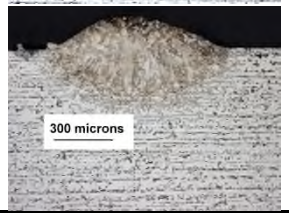		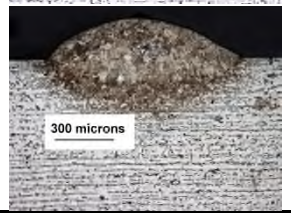	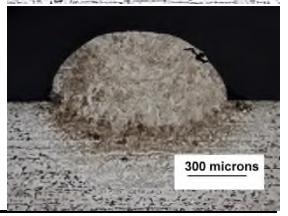

Figure 8-13: Macrographs of built layers produced with layer thickness of 200 μm and different combination of interaction parameters

Table 8-3: Process map of the built layer (powder melting) produced with different combinations of interaction parameters (based on data from Figure 9-13). Key - N: No melting (white colour), B: balling formation (sky blue colour), x: balling and discontinuity (red colour) and +: smooth bead and melting (yellow colour)

Power density (kW/cm^2)	Interaction time (ms)					
	1	2	4	6	8	10
640	N	B	B	B	B	B
1150	x	x	x	x	x	x
1660	x	x	x	x	x	+
2160	x	x	x	+	+	+
2670	+	+	+	+	+	+
3570	+	+	+	+	+	+
5350	+	+	+	+	+	+

Figures 8-14 and 8-15 show the macrographs of the bead-on-plate welds (solid melting) produced with a beam diameter of 0.10 mm and interaction parameters shown in Table 8-2. The welds exhibit conduction profiles when the power density applied was equal to or less than 2.67 MW/cm^2 with interaction time less than 8 ms. The depth of penetration is shallow and weld width becomes wider with increasing interaction time, as shown in Figures 8-14 and 8-15. However, at higher power density, the weld of transition (mixed) and keyhole regimes were obtained. There is a significant increase in the aspect ratio (depth/width) of the welds beyond power density of 2.67 MW/cm^2 and interaction time 8 ms, as shown in Figure 8-16. The welds produced with power density of 5350 kW/cm^2 show characteristics of keyhole regime with an aspect ratio greater than 0.6. Table 8-4 shows the summary of solid melting. The range

of interaction parameters that enabled achievement of good fusion of powder with the substrate spread across the conduction, transition (mixed) and keyhole regimes, as shown in Table 8-3 and Table 8-4 (coloured yellow).

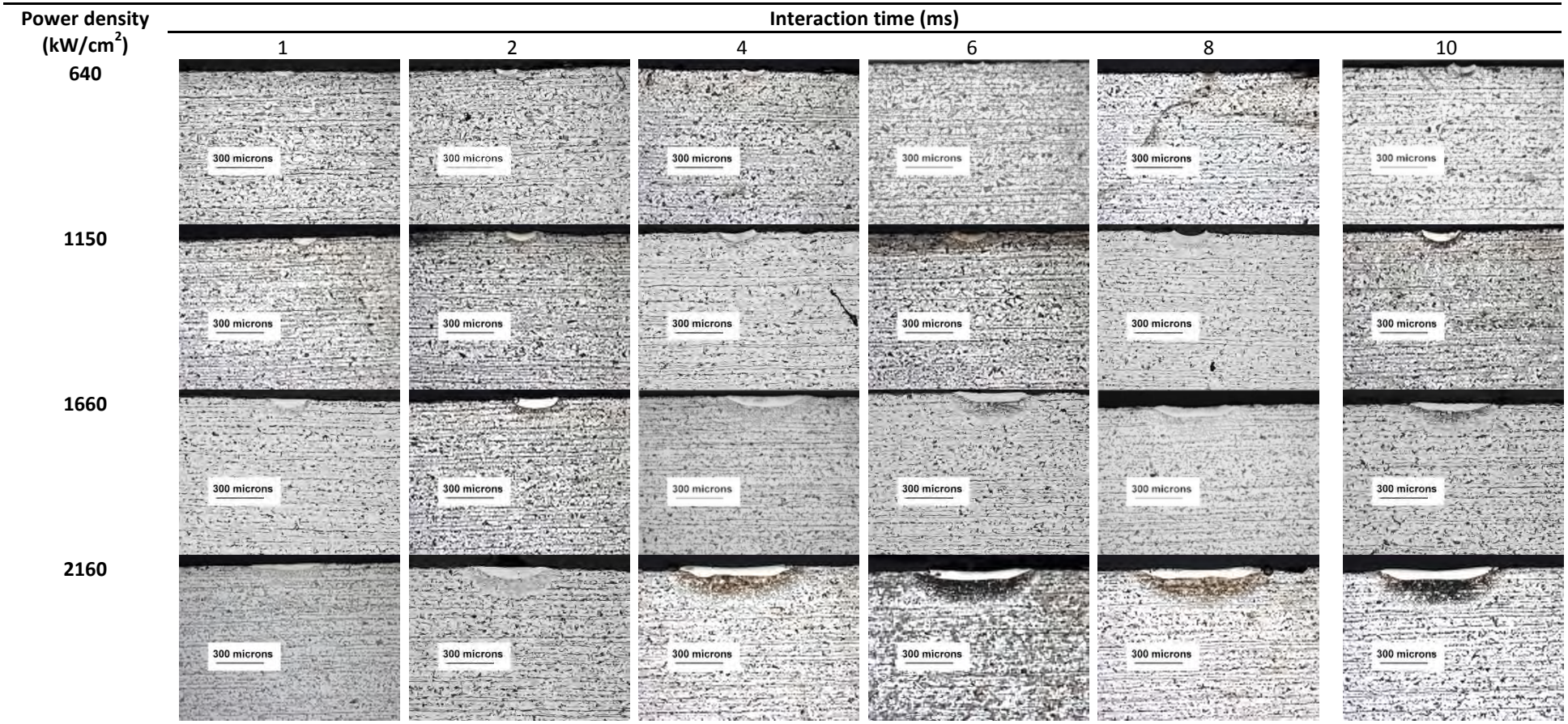

Figure 8-14: Macrographs of the bead-on-plate welds in solid steel produced with different combination of interaction parameters (the same macrographs is on page 93)

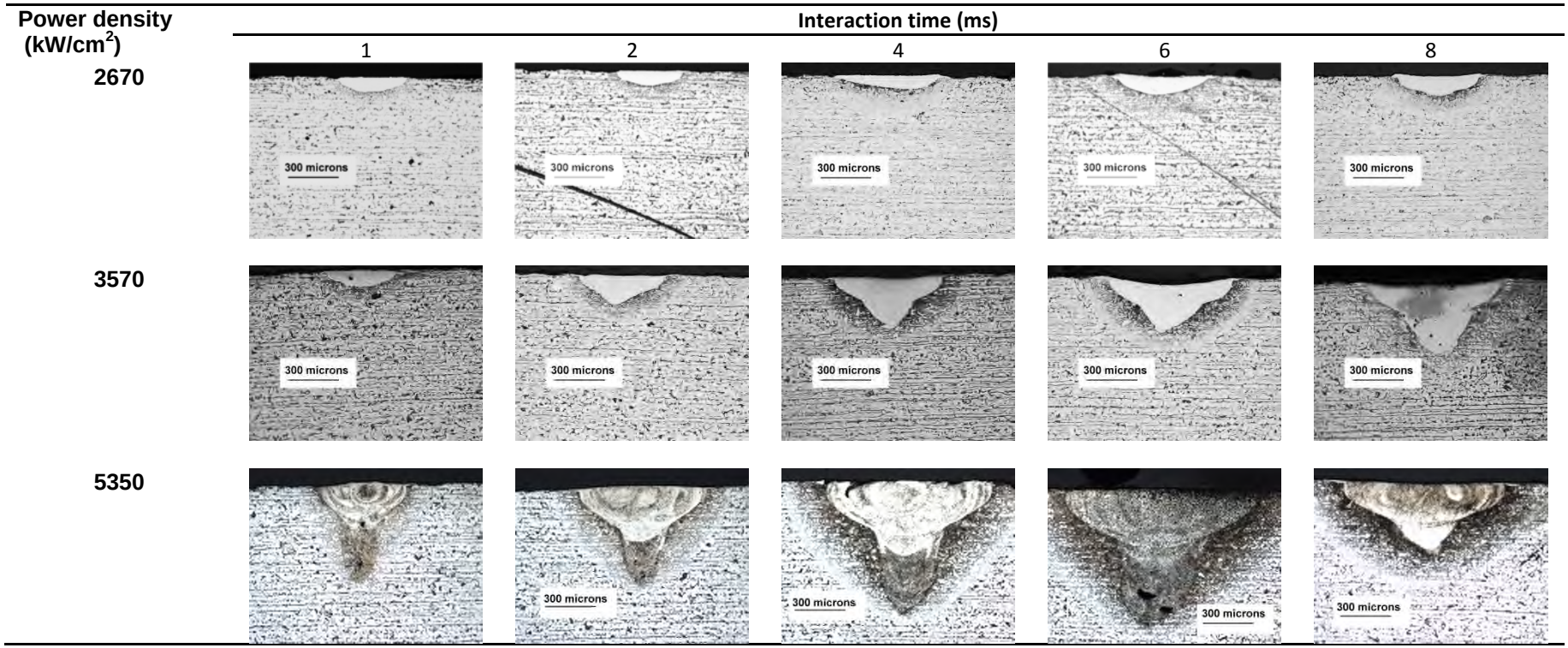

Figure 8-15: Macrographs of the bead-on-plate welds in solid steel produced with different combination of interaction parameters (the same macrographs is on page 94)

Table 8-4: Process map of the bead-on-plate welds (solid melting) produced with different combinations of interaction parameters (based on data from Figures 8-14 and Figure 8-15). Key C: conduction weld (royal blue or yellow), T: transition and keyhole welds (yellow)

Power density (kW/cm^2)	Interaction time (ms)					
	1	2	4	6	8	10
640	C	C	C	C	C	C
1150	C	C	C	C	C	C
1660	C	C	C	C	C	C
2160	C	C	C	C	C	C
2670	C	C	C	C	C	C
3570	C	C	T	T	T	K
5350	K	K	K	K	K	K

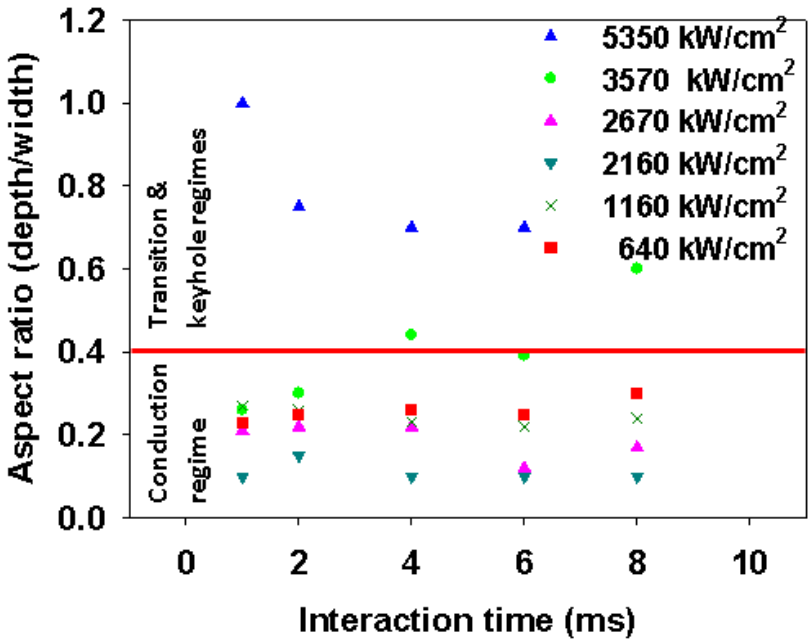

Figure 8-16: Dependence of aspect ratio of solid material on power density and interaction time

Figure 8-17 to Figure 8-32 show comparison of selected bead-on-plate welds and powder built layers. Some build layers in powder exhibit lack of fusion between the layers and the substrate. Note that the powder layer thickness in every case was much greater than the penetration depth in conduction welding of the solid material. It can also be seen in the single layer deposited tracks that the profile exhibits lacks of continuity and balling (Figure 8-18 and Figure 8-20) due to insufficient energy for this thickness of powder layer. The macrographs of the build layers with complete fusion are presented in Figure 8-23, Figure 8-25, Figure 8-27, Figure 8-29 and Figure 8-31. The corresponding single track of layers are presented in Figure 8-24, Figure 8-26, Figure 8-28, Figure 8-30 and Figure 8-32. These figures indicate that the build layers are relatively smooth and stable, because of greater energy input. Furthermore, the build height of powder melting is significantly higher than the depth of penetration of conduction welding of solid melting. The comparison of the build width and weld width, on the other hand indicates that the profiles are equal only when the

process is in steady state. Thus, the melt volume of the powder is higher than the melt area of the substrate, which indicates better utilisation of laser energy in powder melting than in conduction welding. Figure 8-29 and Figure 8-31 show beads of keyhole profile for solid melting and conduction profile for powder melting. This indicates that build profile formed is largely dependent on the interaction parameters and powder properties.

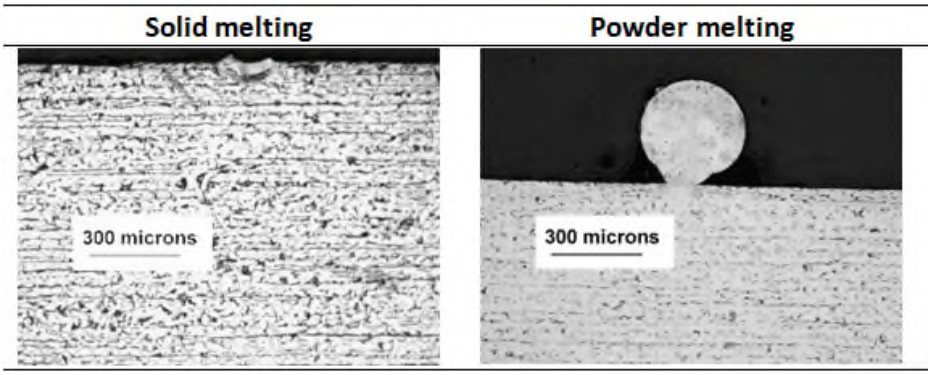

Figure 8-17: Comparison of bead-on-plate weld with a single layer powder deposition at constant power density of 640 kW/cm^2, interaction time of 10 ms and layer thickness of 200 µm

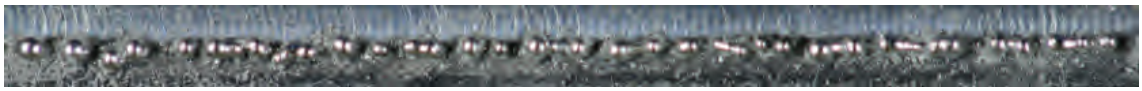

Figure 8-18: Top view of deposited track for 200 µm powder layer thickness, power density of 640 kW/cm^2 and interaction time of 10 ms

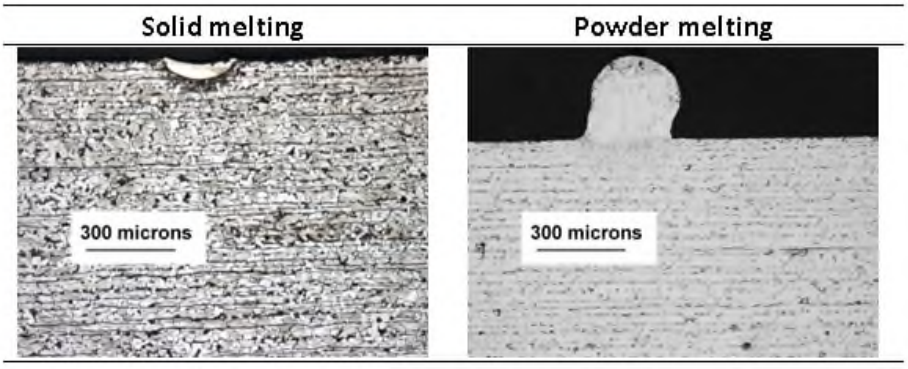

Figure 8-19: Comparison of bead-on-plate weld with a single layer powder deposition at constant power density of 1150 kW/cm^2, interaction time of 10 ms and layer thickness of 200 µm

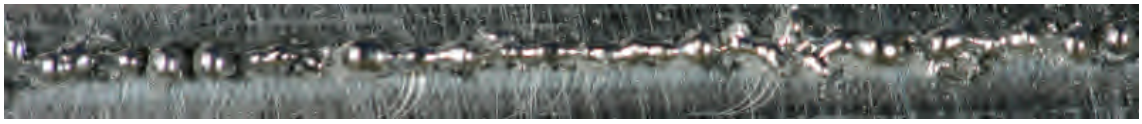

Figure 8-20: Top view of deposited track for 200 µm powder layer thickness, power density of 1150 kW/cm^2 and interaction time of 10 ms

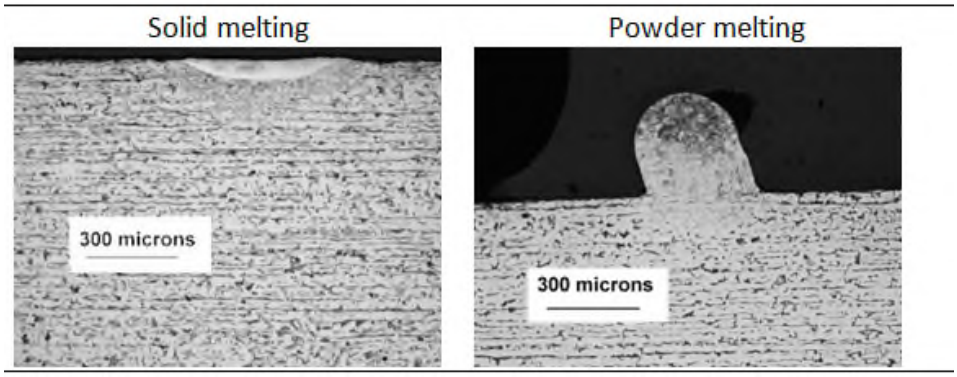

Figure 8-21: Comparison of bead-on-plate weld with a single layer powder deposition at constant power density of 1660 kW/cm^2, interaction time of 4 ms and layer thickness 200 µm

Figure 8-22: Top view of deposited track for 200 µm powder layer thickness, power density of 1660 kW/cm^2 and interaction time of 4 ms

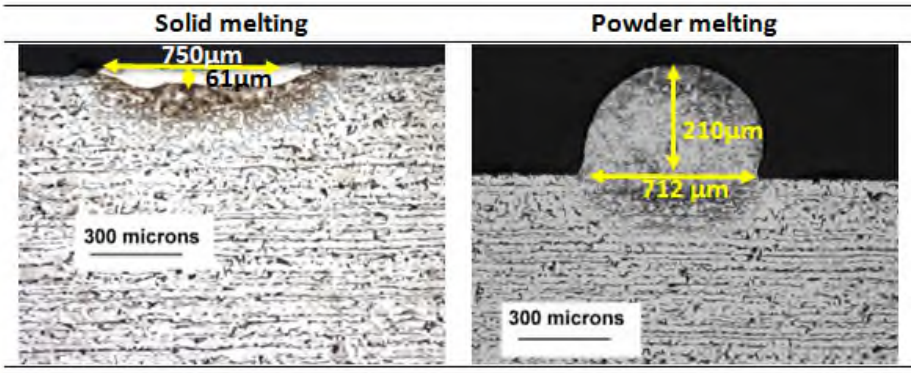

Figure 8-23: Comparison of bead-on-plate weld with a single layer powder deposition at constant power density of 2160 kW/cm^2, interaction time of 4 ms and layer thickness of 200 µm

Figure 8-24: Top view of deposited tracks for 200 µm powder layer thickness, power density of 2160 kW/cm^2 and interaction time of 4 ms

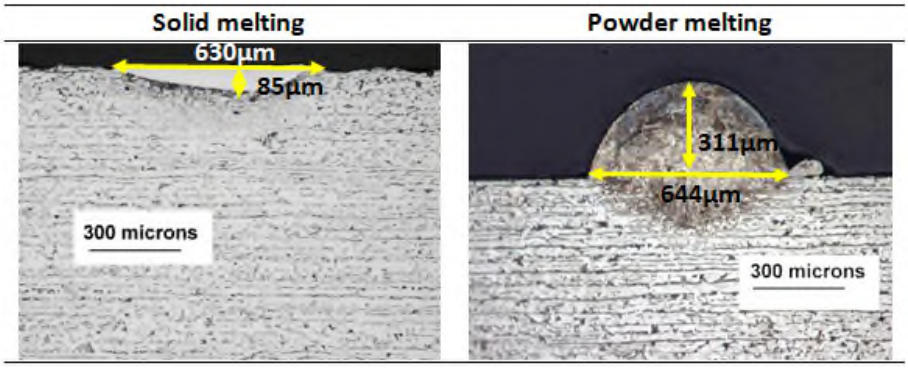

Figure 8-25: Comparison of bead-on-plate weld with a single layer powder deposition at constant power density of 2670 kW/cm^2, interaction time of 4 ms and layer thickness of 200 µm

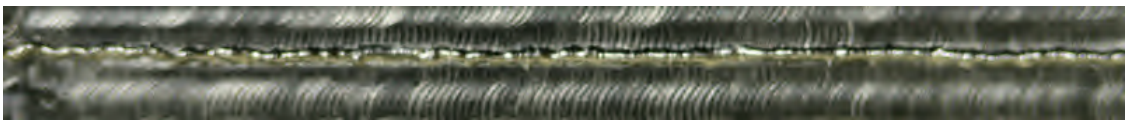

Figure 8-26: Top view of deposited tracks for 200 µm powder layer thickness, power density of 2670 kW/cm^2 and interaction time of 4 ms

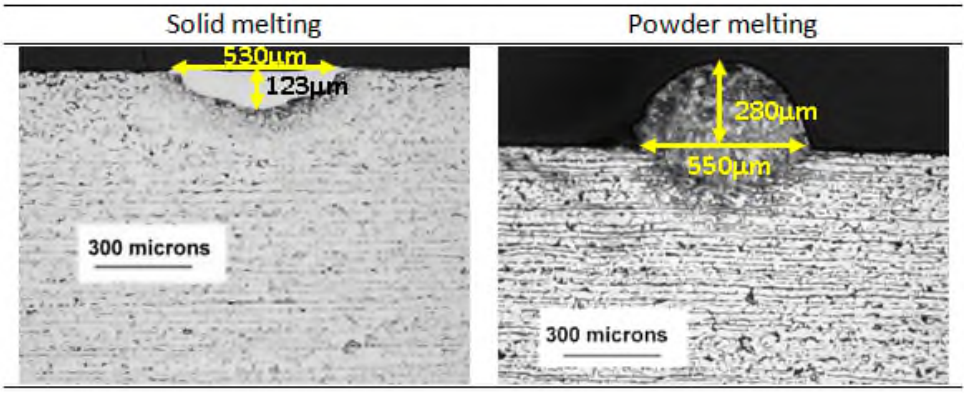

Figure 8-27: Comparison of bead-on-plate weld with a single layer powder deposition at constant power density of 2670 kW/cm^2, interaction time of 8 ms and layer thickness of 200 µm

Figure 8-28: Top view of deposited tracks for 200 µm powder layer thickness, power density of 2670 kW/cm^2 and interaction time of 8 ms

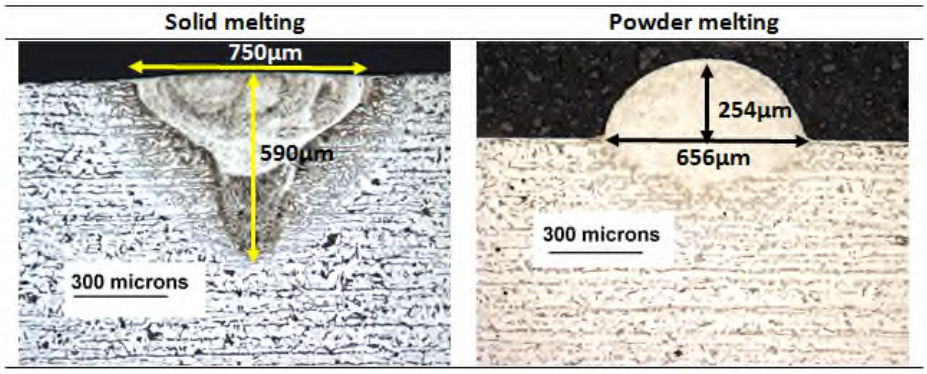

Figure 8-29: Comparison of bead-on-plate weld with a single layer powder deposition at constant power density of 5350 kW/cm^2, interaction time of 2 ms and layer thickness of 200 µm

Figure 8-30: Top view of deposited tracks for 200 µm powder layer thickness, power density of 5350 kW/cm^2 and interaction time of 2 ms

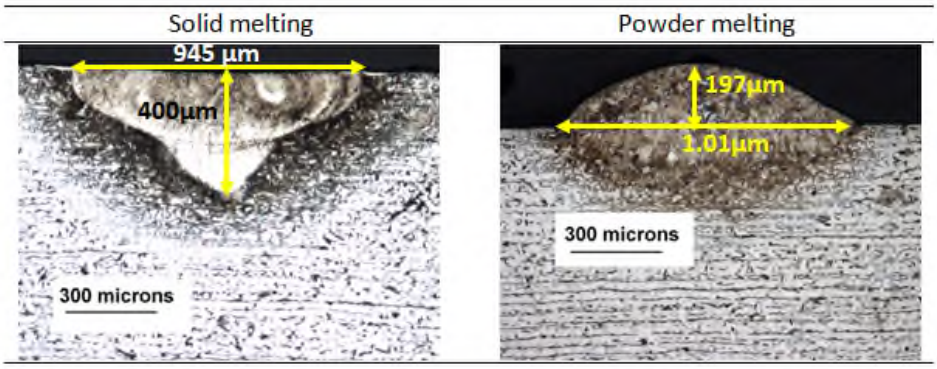

Figure 8-31: Comparison of bead-on-plate weld with a single layer powder deposition at constant power density of 5350 kW/cm^2, interaction time of 8 ms and layer thickness of 200 µm

Figure 8-32: Top view of fused 200 µm powder layer to the substrate at constant power density of 5350 kW/cm^2 and interaction time of 8 ms

Figure 8-33 shows the relationship between the aspect ratio (ratio build height to build width) and energy density. The figure shows how build profiles can be compared to the weld bead profile presented in Figure 6-9 (page 97). A good build profile should exhibit an aspect ratio of 0.5. Figure 8-33 indicate that some of build layers were partially formed with aspect ratio more than 0.6 due to insufficient energy for the layer thickness of 0.20 mm. The build width was measured at the substrate as shown in Figure 4-7 (page 55). Therefore, in some cases, the aspect ratio was very high due to insufficient energy i.e. balling effect. The stable beads of conduction and transition profiles correspond to aspect ratio between 0.2 and 0.6 are also shown. When the energy is high for the layer thickness, the build height significantly reduced with increasing build width. Thus, the aspect ratio reduces as shown in Figure 8-33.

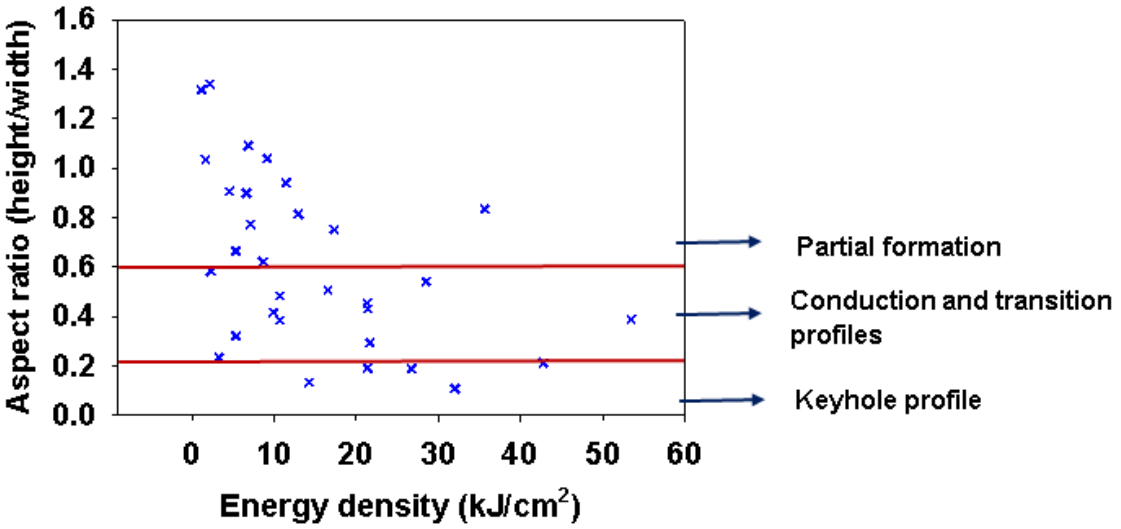

Figure 8-33: Aspect ratio of powder melting as a function of energy density with a beam diameter of 0.10 mm

Figure 8-34 and Figure 8-35 show the comparison between the solid and powder melting bead areas. Figure 8-34 shows the dependence of bead areas on the interaction time for constant power density. Figure 8-35 shows the dependence of bead area on the power density at constant interaction time. The build area of powder melting is quite higher than weld area of solid melting at the same interaction parameters with conduction profile. However, for a typical keyhole profile, the build area is less than weld area. In addition, power density has higher effect on the bead profile than the interaction time.

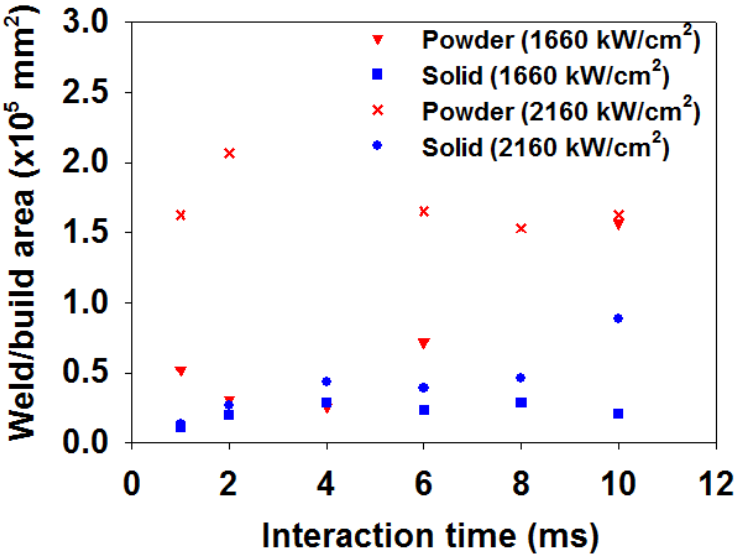

Figure 8-34: Comparison of weld area of solid melting with a build area of powder melting at constant power density of 1660 and 2160 kW/cm^2 and layer thickness of 200 µm

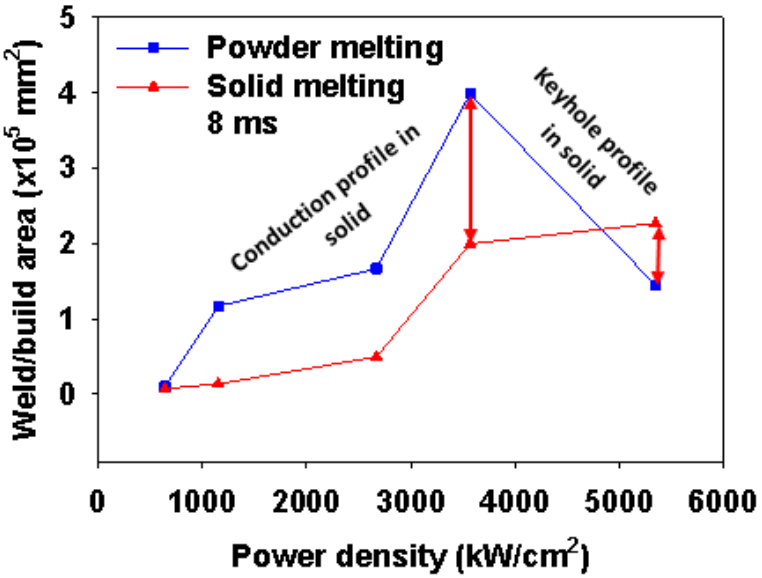

Figure 8-35: Comparison of weld area of solid melting with a build area of powder deposition at constant interaction time of 8 ms and layer thickness of 200 µm

8.4 Discussion

In Sections 5.3 and 5.4 of Chapter 5, it was shown that in solid melting, power density and interaction time (product is energy density) control the depth of penetration and interaction time and beam diameter controls the weld width. In powder melting, the melting behaviour is different from that of solid melting in some ways. The main parameter that controls the build height in powder melting is the layer thickness. As expected, when the layer thickness doubled, the build height also increased by a factor of two for the same energy applied, when the energy was sufficient. A certain threshold energy density is required to fuse a particular thickness of powder. Therefore, increasing the energy density from 1.0 kJ/cm^2 to 12.0 kJ/cm^2 caused no significant difference in build height, as shown in Figure 8-1, Figure 8-3 and Figure 8-4. When the thickness of powder layer is greater than the energy required to fuse it completely to the substrate, the molten pool solidifies rapidly and there is not enough time for bonding with the substrate. Then build height formed is higher than layer thickness because the surface tension pulls the liquid pool. The low temperature of liquid in this regime results in strong surface tension, which forces the liquid metal to reduce its surface energy by attaining circular shape (Gusarov et al., 2009; Tolochko et al., 2004). Poor wetting and strong surface tension due to the low temperature of the liquid is also responsible for the lack of fusion between the powder particles and the substrate (Figure 8-35). This behaviour depends on the powder size and layer thickness. Lack of fusion occurs when the energy absorbed is not sufficient for wetting between the powder particles and the substrate. At a higher energy density, the dilution between melted powder and the substrate will reduce the layer height. In solid melting, power density and interaction time together control the depth of penetration whilst the layer thickness controls build height in powder melting. In solid melting within the conduction regime, the effect of beam diameter on the depth of penetration was less significant (see Figure 5-6 page 73). Similar behaviour was noticed on build height in powder melting when the beam diameter was increased at constant power density and interaction time. There is

no significant influence of beam diameter on the build height, as shown in Figure 8-7.

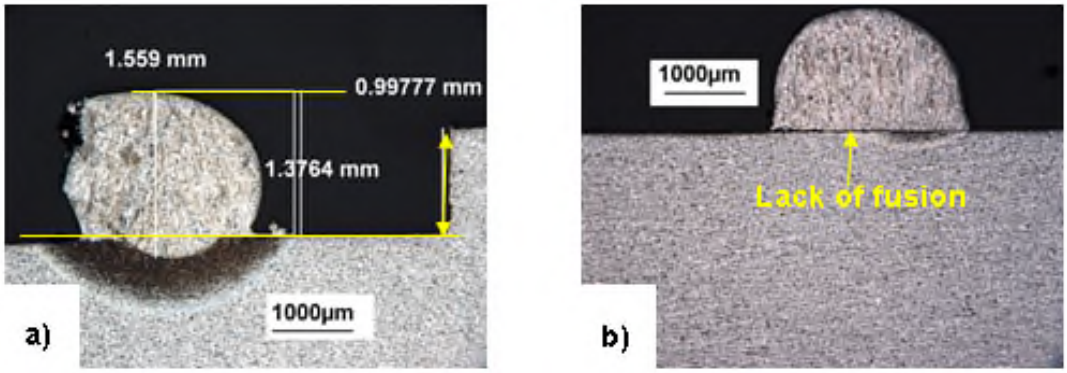

Figure 8-36: Examples of defects in powder melting a) humping formation b) lack of fusion below minimum energy for fusion

Interaction time and beam diameter control the weld width profile in conduction welding (see Figure 5-11 page 77) for solid melting with large beams. In powder melting, the same parameters control the build width, as shown in Figure 8-2, Figure 8-3 and Figure 8-7 for large beam diameters. Both the weld and build widths reach saturation at the point where they approach the size of the beam on the workpiece. In solid melting, depth of penetration is similar with different beam diameters but the weld width varied by adjusting parameters in such a way to maintain energy density constant. Powder melting behaves in a similar way with large beams due to their welding regimes. In conduction regime, the depth is similar but weld width varied for different beam diameters and constant energy density (the product of power density and interaction time). This can also be due to the energy required to fuse a given layer. Greater energy, which is required to achieve melting with larger beam diameters, leads to a bigger melt pool and longer solidification time. In that case, the melt flow has a significant influence on bead profile. Therefore, when the applied energy density is sufficient to fuse a given layer thickness, the build height is not sensitive to

the beam diameter because of the effect of surface tension acting on the deposited tracks.

Powder melting seems to be more efficient than solid melting when the same interaction parameters are applied. Shown in Figure 8-8 and Figure 8-9 is the comparison between depths of penetration in solid melting and build heights in powder melting for large beams. The build height is slightly higher than the depth of penetration. Furthermore, the comparison of weld width with build width was shown in Figure 8-10 and Figure 8-11 for a large beam. These figures showed that the widths of both solid and powder are similar. These suggest that melt area in powder is higher than weld area. The melt behaviour with small beams was different from that of large beams. The build height in powder was significantly higher than the depth of penetration in solids. The weld and build widths were significantly wider than the beam diameter for both solid and powders. The result shows that powder exhibited higher melt area than solid material. This is evident in Figure 8-33 and Figure 8-34. This shows that in conduction regime, powder melting is more efficient than solid melting. The difference in melt area between solid material and powder material becomes more significant for smaller beam diameters. Within the region of conduction weld profiles in solid melting, powder melting is more efficient. However, in keyhole or transition regime, solid melting exhibited a similar or higher melt area (see Figure 8-34). Note however that the weld profiles for powder melting are very variable due to surface tension effects, so the difference as shown in this figure (especially the point at 3570 kW/cm^2) may not be this large in reality.

The higher build area obtained in powder melting compared to the weld area in solid melting is likely to be due to the difference in the energy utilised for melting (i.e. as opposed to that lost due to reflection from the surface and that is lost to heating the surrounding material). Both powder and solid substrate absorbed energy whilst exposed to the laser beam. However, the extent of the energy utilised for melting depends on the material properties: thermal diffusivity, surface roughness, oxidation state etc. In powder melting, due to the higher surface roughness of the powder, there are multiple reflections, which enhance

the laser absorption in the powder. In addition, powder materials are characterised with lower thermal diffusivity because of the presences of voids. The large spaces between the powder particles lead to a very low effective thermal conductivity. This means that the lateral thermal losses would be much lower leading to higher energy utilisation and therefore melt area.

Furthermore, it is expected that there might be significant shrinkage of the build profile due to the voids between the particles and their random arrangement. The build height results obtained indicate that the build height is higher or the same as the layer thickness for build layer of proper deposition when applied energy is sufficient. However, molten metal shrinkage does not seem to affect the build profile. The fact is that the low conduction losses in powder melting are compensated for the low thermal diffusivity.

Within the interaction parameters investigated for the small beams, three regimes of conduction, transition (mixed) and keyhole were observed in solid melting. In the first regime, the welds exhibited less or semi-circle profile and the second region consisted of welds of transition and keyhole profiles of deeper penetration, as shown in Table 8-4. Powder melting consisted of four regions. In the first region no melting but heating of the powder by the laser energy occurs. In this region, there are no physical changes or bonding between the adjacent powder particles. In the second region, there is a significant melting. The agglomerated powder particles spheroidise because of high surface tension. The size and shape formed depend on the applied energy density. The third region consists of significant melting and clustering of the powder particles. Smooth build achieved in the fourth region. Full melting of powder particles occurred due to the interaction between the laser beam and powder. In this case, the melt pool was similar to conduction welding in solid material, which formed stable beads with some of deep penetration. The balling effect was completely absent in this region. This implies that a certain threshold energy density is required to melt and fuse a particular layer of powder. The energy has to overcome losses into the substrate (melting into the substrate beneath) and melting of the powder. Therefore, the solidification time needs to

be long enough to provide good wetting between powder particles and the substrate. By comparing the bead profiles of solid melting to the powder melting, the region with no melting and balling corresponded to the conduction welding regime in solid melting. This is can be seen in Figure 8-33 (powder melting) where the aspect ratio was significantly higher than 0.6. This implies that the applied interaction time and power density (low energy density) is too low for build layer formation but sufficient for surface melting. The powder layer serves as screening surface. Thus, little energy could reach the substrate and no bonding in this low energy regime occurs. On further increase of the energy density (power density or interaction time), the surface free energy increases (lower surface tension) causing the powder particle to agglomerate into the melt pool and resulting in further transfer of heat and melting. The semi-circular build profile achieved in powder melting corresponded to conduction, transition and keyhole regimes in solid melting. The regions of stable layers and weld bead were coloured as yellow in Tables 8-3 and 8-4. This implies that interaction parameters for conduction, transition or keyhole welding in solids all correspond to stable build layers. In addition, at a very high energy density therefore there is a deep penetration of powder into substrate, which cause low aspect ratio in the build profile (see Figure 8-33).

Similar to solids, three welding regimes are possible in powder melting, conduction, transition and keyhole. All the welds shown with the large beam diameters are in conduction mode. Those with longer interaction times or higher power densities show significant penetration into the substrate but would still be considered as conduction welds. For the small (0.10 mm) beam diameter, profiles shown in Figures 8-12 and 8-13 for the builds that are fully fused to the substrate, the profiles are mainly those of conduction regime with some showing keyhole behaviour. However, it should be noted that the keyhole profiles appear to be randomly distributed with some being at lower energy density then other conduction profiles. It is believed that this is due to the large powder particle size that was used. The particle size was similar to that of the layer height with laser beam diameter being smaller. It seems likely that the

keyhole profiles appeared when the laser beam passed through a gap between the powder particles and interacted directly with the substrate.

More importantly, it is clear from the comparison between solid and powder melting that although when solid melting is in transition or keyhole mode powder melting is still in conduction mode. A clear example of this is shown in Figure 8-29 and Figure 8-31. This means that the welding regime in powders is different to that of solid materials under the same conditions when the laser beam diameter is of the order of the powder particle size. Given that, this is the case in most powder bed systems this is a very important observation. Camera observation of the powder bed process gives the impression that the process is operating in the keyhole welding regime with evidence of high spatter levels. Furthermore, in Chapter 6, from Figure 6.10 and Figure 6-11 it is clear that if a solid material is put directly in a powder bed system then transition and keyhole welds are the results. However, here it is shown here that in powder melting under these conditions the conduction welding regime results. It seems that it may be difficult to form a keyhole in powder materials, especially when the beam size is comparable to that of the powder particles. The large spatter that is observed in powder bed systems may be the result of individual particles being ejected due to local vapourisation.

9 **Critical discussion**

The main challenge associated with powder bed additive manufacturing (AM) systems is the selection of parameters to control the build profile. The current approach is difficult and transferring the data between machines is complex. The complexity arises from the fact that each of the machines is characterised with a different optical set-up (leading to variations in beam diameter). Therefore, selection of building parameters (laser power and travel speed) is based on an engineering approach that is, on an individual basis. Furthermore, powder bed AM is highly complex process due to inhomogeneous properties of powders and small beam diameters often used. This suggests that the quality of build profiles in powder melting depends on the powder type, size and distributions of powder particles, and beam diameter. To improve processing rate, whilst keeping a high resolution, it is a common practice to use galvo-scanners to achieve fast movement across the working envelope with smaller beams. However, one of the downsides of the galvo-scanner is the distortion of the projected beam, which is continuously changing depending on the magnitude of inclination of the beam and welding direction. Therefore, the spatial distribution of the laser energy and build profile will change with a position of the laser spot in the powder bed. In addition, the deposition rates are relatively low with small beam diameters.

In laser welding, it was shown that fundamental laser material interaction parameters (FLMIP) of power density, interaction and specific point energy can be used to characterise uniquely the build profile, independently of a laser system. This is because the fusion characteristic is controlled by the spatial and temporal distribution of laser energy, which controls thermal cycle and the resulting microstructure and bead profile, as shown in Figure 9-1. In keyhole welding, a combination of interaction parameters that control weld profile was identified and tested on different machines. The approach enabled transfer of welding parameters among various machines with different optical set-ups.

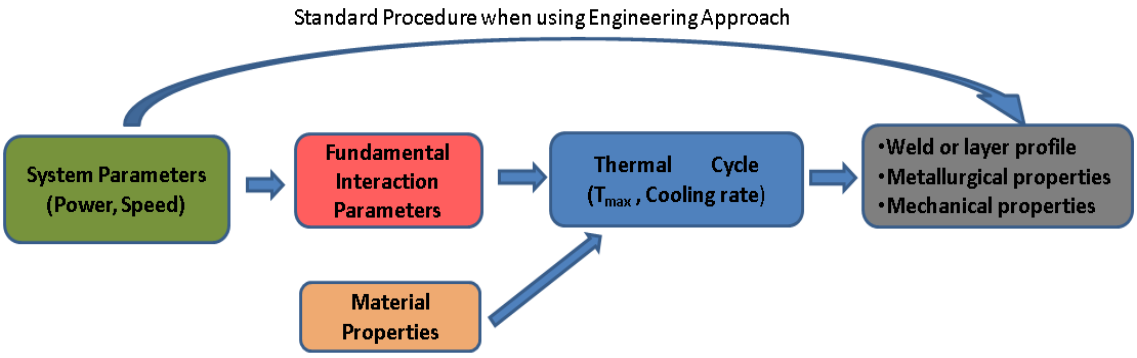

Figure 9-1: Relationship between system parameters and material responses (Suder, 2012)

The current study proposed the use of similar interaction parameters to control the spatial and temporal energy distribution of a laser beam and bead profile in conduction welding and powder melting. This would enable the characterisation of the build profile independent of the optical set-up and beam diameter of powder bed machines. The aim is to understand the effect of beam diameter and spatial distribution of energy on bead profile in powder melting and to develop a phenomenological model for control of deposited powder beads with variable beam diameters. It is assumed that to maximise the quality of deposited powder tracks vaporisation should be avoided. Therefore, conduction regime was of the main interest in this work. Due to the inhomogeneous properties and complex melting behaviour of powders, which depends on the powder type, particle sizes and distribution, the initial experiments were conducted in solid materials of known and homogenous properties. In addition, to simplify the investigation of melting behaviour and maximise reliability of the process, relatively big beam diameters were used, as compared to commercial powder beds. Subsequently, the melting of solid material was compared with powder material for the same material types but different form. A difference in absorptivity and thermal conductivity was expected. The experiments were later expanded to a wider range of beam diameters, comparable to those used in a

standard powder bed AM. In addition, some additional tests were carried out on a commercial powder bed.

In the studies conducted with big beam diameters, it was found that the material response to laser energy in conduction welding is very different from keyhole. The depth of penetration is controlled by power density and interaction time (whose product is energy density). The weld width depends on the beam diameter and interaction time.

Additional phenomena were discovered when using small beam diameters. In this case, the depth of penetration did not only depend on the energy density but also on the applied energy due to high conduction losses (see Figure 9-2). Therefore, for beam diameters below 3.0 mm the depth of penetration decreased with decreasing beam size at constant energy density until no melting was eventually observed. Theoretical analysis, based on the analytical solution of heat equation, showed that the ratio of conduction losses to the energy utilised for melting increases with decreasing beam diameters. The data suggest that it may be difficult to achieve conduction regime with beam diameters typically used in powder bed additive manufacturing, unless the conduction losses are adequately minimised. It was only possible to achieve such welds when the interaction time was reduced significantly, but then the low rate of energy input had to be compensated by increasing power density. This means that with small beam diameters, the optimum processing window for conduction welding is relatively narrow, and the transition between conduction and keyhole is rapid. Processing in this operating regime is difficult because the process oscillates on the borderline between no melting and vaporisation. Thus, to develop a processing model for conduction welding and powder fusion, similar to the power factor in keyhole welding, these conduction losses have to be included in the model. A correction factor should be added to compensate for the increase of conduction losses for small beam diameters.

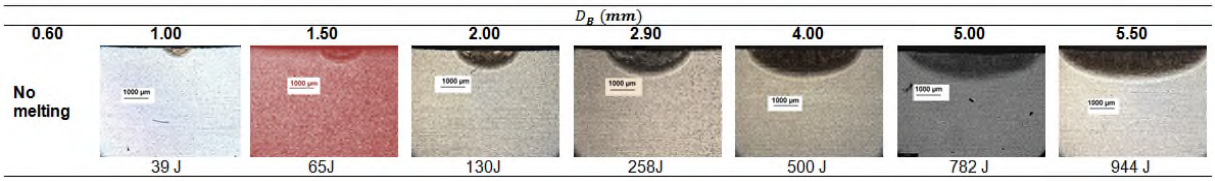

Figure 9-2: Bead on plate welds produced at constant energy density of 4.0 kJ/cm^2 (33.1 kW/cm^2 and 120 ms) when beam diameter is changing

The main parameters controlling melting efficiency are interaction time and beam diameter. Melting efficiency increases with decreasing interaction time and increasing beam diameters. The optimum melting efficiency (32%) was achieved at an interaction time of 25 ms. Melting efficiency increased with increasing beam diameter and then reached a plateau at a beam diameter of 3.00 mm. This corresponds to the region where depth of penetrated started to be dependent only on the energy density (Figure 9.2)

A profile of the weld bead formed during melting of solid or powder depends on the beam diameter and welding regimes. Comparison of solid melting to powder melting with bigger beams and the same processing conditions showed similar bead profiles. This is because both processes were in conduction regime for similar conditions. Also with a big beam the ratio of beam diameter to the particle sizes of powder was relatively high, ensuring uniform melting. The welding regime of powder material is different from the solid material when beam diameter is reduced. In this case, a rapid change of processing regime conduction to transition or keyhole was observed depending on a powder type, particle sizes and distributions and the beam diameter.

For all beam diameters, powder melting resulted in more spatter than conduction welding (see Figure 9-3). In addition, the efficiency for powder melting was higher than the solid melting. The powder fusion is highly dependent on the ratio of beam diameter to the powder particle size. It was also found that when the beam diameter was smaller than the powder particle sizes, the deposited beads were inhomogeneous. Some regions of the same tracks

were in keyhole regime and others in conduction. Furthermore, it was found that it is more difficult to generate keyhole for small beam diameters in powder and underlying substrate than in processing of solid material (see Figure 9-4). In this case, the conditions providing keyhole weld beads in solid melting did not guarantee the keyhole profiles in powder, despite an existence of vaporisation.

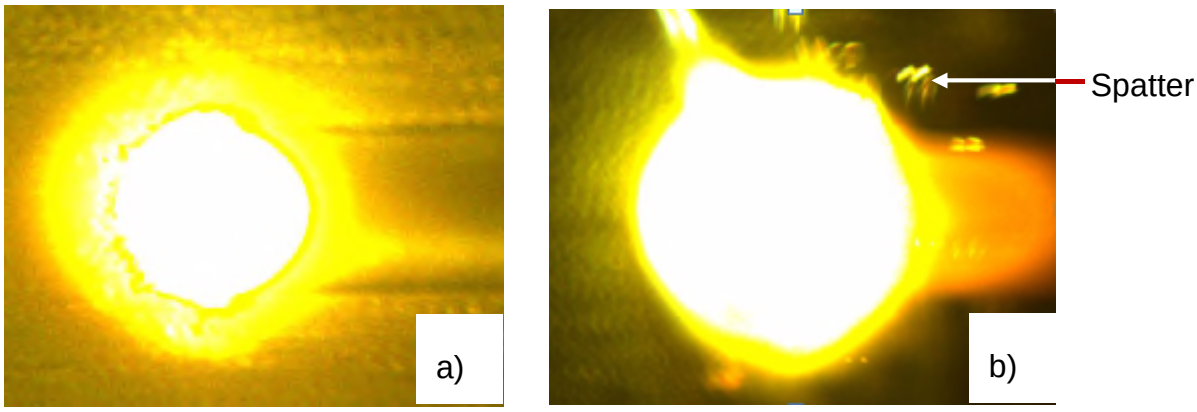

Figure 9-3: Melting characteristics in two different materials for the same processing conditions (a) solid melting (b) powder melting

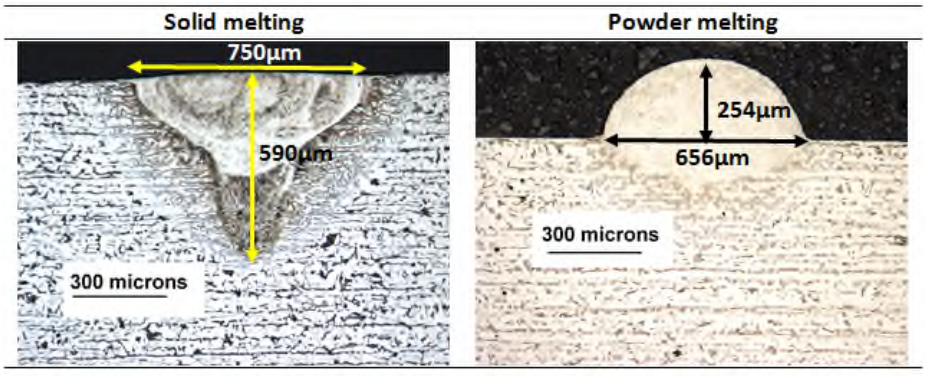

Figure 9-4: Comparison of bead profiles between solid melting and single layer powder melting for the same welding conditions: power density of 5350 kW/cm^2, interaction time of 2 ms, beam diameter of 0.10 mm and layer thickness of 0.20 mm

In addition, it has been found that the bead profile is affected by the power density distribution of a laser beam. Two different cases with the same nominal beam diameters but one with a top-hat beam and another with a pseudo-Gaussian beam showed a deeper penetration and less homogenous weld profile with the pseudo-Gaussian beam. This is due to the higher peak power density. The results indicate that varying the beam diameter by processing in an out-of-focus configuration leads to a change of energy distribution and hence bead profile.

The distortion aspect of the projected laser spot on the workpiece by the galvo-scanner was simulated by applying a tilting angle to a laser head. It was found that the weld profile depends on the elongation direction of the laser spot. A change of the shape of the projected beam affects the power density and interaction time, which leads to a change in weld profile. Although this effect was investigated on a much bigger beam than used in commercial powder beds, for small beams, the relative change of the interaction parameters and weld profile should be similar. This means that to maintain constant fusion characteristics and bead profile, the processing parameters should be continuously adjusted to compensate for the changes in the laser spot profile when using galvo-scanners. The power density and interaction time could serve as such a correction procedure. This would require adjustment of the laser power to give the same power density. The travel speed would need to be increased in the direction of the elongation. It is believed that the effect will be magnified in the case of using bigger powder beds with much greater processing volumes due to the higher angles encountered.

10 Conclusions and recommendations

10.1 Conclusions

The use of laser material interaction parameters to understand the melting behaviour and characterise of the bead profiles in solid and powder materials have led to the following findings:

- The same parameters do not control the weld profile in the conduction regime as in the keyhole regime. In conduction regime, both the interaction time and the power density control the weld depth. The product of these is the energy density but this alone is not sufficient to determine the weld depth across the whole range of beam diameters. In addition, power density plays a critical role in the transition between the welding regimes.
    - For large and medium beam diameters, the rate of increase of depth of penetration with interaction time is greater than with increasing power density. The depth of penetration is also independent of the beam diameter when below the vaporisation threshold.
    - For small beam diameters, power density is more critical, since it helps to compensate for high thermal losses from the bulk material. Therefore, at this operating regime, the response of penetration depth to power density is high. For small beam diameters, the ratio between conduction losses and energy utilised for melting increases rapidly. Therefore, below a particular beam diameter, power density is (rate of energy supplied) required to overcome these losses. In this range, the depth of penetration is not only controlled by the energy density but also depends on applied energy and hence on beam diameter.
    - So as the beam diameter varies from large to small the penetration depth is controlled more and more by power density.

This is because the change in geometry of the weld means that the thermal conduction losses become much more significant as a proportion of the applied energy as the weld becomes smaller. Therefore, the applied energy has to be applied more quickly (i.e. with a higher power density) in order to balance the thermal losses.

- As the beam diameter is reduced, the required power density for melting becomes much higher. This means that gap between this and the threshold power density for vaporisation becomes smaller. Therefore, the operational window for conduction welds with small beams typical of those uses in powder systems becomes very narrow.
- The weld width in conduction welds is mainly dependent on the beam diameter, when the interaction time is long enough to allow the heat to conduct to the material. Therefore, when the interaction time is increased for this range of beam diameters, the weld width approached a plateau at a level proportional to the size of the laser spot.
- The effect of galvo-scanner on the beam shape was experimentally simulated. Elongation of the laser beam in the welding direction causes an increase in beam length. However, there was no change in the weld profile. This is because although the power density was decreased the interaction time was simultaneously increased. However, when travelling in the direction perpendicular to the elongation direction the weld width was increased and penetration depth decreased. This is because the power density was decreased whilst the interaction time remained the same. The weld width was also wider because of the wider beam size orthogonal to the travel direction.
- The power density distribution of a laser beam has a major influence on the weld profiles in conduction welding. Defocused beams with a pseudo-Gaussian power density profile resulted in deeper welds than focused beams with a top-hat profile for the same nominal beam diameter, which is attributed to a higher peak power density. This means

that using lasers of different beam shapes may introduce additional aspects to the profiles of resulting welds.

The conclusions from the study of the melting behaviour of solid and powder materials are shown below.

- The build profiles in powder melting were different to weld profiles of conduction welds. The parameters that control build heights in powder melting are the thickness of powder layer and energy density (power density and interaction time). The energy density has to be sufficient to fuse the powder thickness. The height of deposited tracks changes with energy density due to change in dilution and wetting of liquid metal. The parameters that control the depth of penetration in solid melting are of power density and interaction time.
- Similar to solid melting, the build width depends on the beam diameter and interaction time.
- Greater melting efficiency was found in powder as compared to solid, especially for small beam diameters. In addition, powder melting exhibited more spatter and expulsion than solid material, for the same processing parameters.
- The welding regime of powder melting was investigated by comparing the weld profile in solids to the build profile in powders when the same interaction parameters are applied. It has been found that most of the build profiles indicated conduction welding only. The particle size used in these experiments was quite large compared to laser beam diameter. So, it is believed that any keyholes that were observed were where there were gaps between the particles which the laser beam passed through and interacted to the (solid) substrate. So, it seems that despite using parameters that would generate a keyhole in solid material this does not happen in powder melting. This area needs further study including

looking at the effect of the laser beam diameter powder particle size ratio.

The research question that was asked was can a phenomenological mode similar to the power factor be developed for the welding regimes used in laser powder bed systems. This will enhance transfer of data between machines. Currently, the question has not been answered in case of small beam diameter in powder melting. Controlling fundamental material interaction parameters in conduction welding have been established for a wide range of beam diameters. However, the dependence of these parameters varies with beam diameter so similar approach is difficult. Furthermore, it has been shown that even though the parameters used in typical powder bed systems would generate a keyhole in solid and powder they do not appear to do so in a powder. Therefore, there is not a direct correlation between solid and powder melting for small beam sizes. Further studies of the powder melting regime are required.

10.2 Contribution to knowledge

A detailed examination of the fundamental material interaction parameters in laser conduction welding has been carried out. Furthermore, this has been done over a wide range of beam diameters identifying that the behaviour seen is not beam diameter independent as in keyhole welding. A direct comparison of solid and powder melting using identical processing conditions has been made leading to a much better of understanding of powder melting effects seen powder bed systems. The effect of processing using angled beams has been investigated and identified what compensation strategies are needed to avoid this effect in powder bed systems.

10.3 Future work recommendation

- Much more detailed studies of powder melting with small beams are required including
    - High speed imaging of the melting process of powders
    - Studies of the effect of the powder size/beam size ratio
- A study of the effect of constant energy density on the build profile (for powder melting) is required. This would enable identification of conduction losses as a function of beam diameter and help identify optimum conditions for maximum melting efficiency.
- Investigation of the relative importance of power density and interaction time for powder melting for different beam diameters
- Investigate the effect of powder density on melting behaviour
- Investigation to gain an understanding of the effect of change in beam shapes (top hat, Gaussian distribution, distortion of beam shapes) on the build profile at constant beam diameter, laser power and travel speed is required. It can also include how the laser power and travel speed can be adjusted to compensate for the change in beam shape to achieve similar build profile.

REFERENCES

Aidun, D.K., Martin, S.A., 1997. Effect of Sulfur and Oxygen on Weld Penetration of High-Purity Austenitic Stainless Steels. JMEPEG 6, 496–502.

Alkahari, M.R., Furumoto, T., Ueda, T., Hosokawa, A., Tanaka, R., Abdul Aziz, M.S., 2012. Thermal Conductivity of Metal Powder and Consolidated Material Fabricated via Selective Laser Melting. Key Eng. Mater. 523-524, 244–249. doi:10.4028/www.scientific.net/KEM.523-524.244

Anawa, E.M., Olabi, A.G., 2008. Using Taguchi method to optimize welding pool of dissimilar laser-welded components. Opt. Laser Technol. 40, 379–388. doi:10.1016/j.optlastec.2007.07.001

Ashby, M.F., Easterling, K.E., 1984. The transformation hardening of steel surfaces by laser beams—I. Hypo-eutectoid steels. Acta Metall. 32, 1935–1948. doi:10.1016/0001-6160(84)90175-5

Assuncao E., 2012. Investigation of conduction to keyhole mode transition.

Assuncao, E., Williams, S., Yapp, D., 2012. Interaction time and beam diameter effects on the conduction mode limit. Opt. Lasers Eng. 50, 823–828. doi:10.1016/j.optlaseng.2012.02.001

Assuncao, E., Ganguly, S., Yapp D. and Williams, S., 2010. Conduction mode-Broadeningthe range of applications for laser welding, in: 63th Annual Assembly and International Conference of the International Institute of Welding. pp. 705–709.

Averyanova, M., Cicala, E., Bertrand, P., Grevey D., 2012. Experimental design approach to optimize selective laser melting of martensitic 17-4 PH powder: part I – single laser tracks and first layer. Rapid Prototyp. J. 18, 28–37. doi:10.1108/13552541211193476

Badrossamay, M., Childs, T.H.C., 2007. Further studies in selective laser melting of stainless and tool steel powders. Int. J. Mach. Tools Manuf. 47, 779–784. doi:10.1016/j.ijmachtools.2006.09.013

Bardin, F., Morgan, S., Williams, S., McBride, R., Moore, A.J., Jones, J.D.C., Hand, D.P., 2005. Process control of laser conduction welding by thermal imaging measurement with a color camera. Appl. Opt. 44, 6841–6848. doi:10.1364/AO.44.006841

Benyounis, K.Y., Olabi, A.G., Hashmi M.S.J., 2005. Effect of laser welding parameters on the heat input and weld-bead profile. J. Mater. Process. Technol. 164-165, 978–985. doi:10.1016/j.jmatprotec.2005.02.060

Bertrand, P., Bayle, F., Combe, C., Goeuriot, P., Smurov, I., 2007. Ceramic components manufacturing by selective laser sintering. Appl. Surf. Sci.

254, 989–992. doi:10.1016/j.apsusc.2007.08.085

Buchbinder, D., Schleifenbaum, H., Heidrich, S., Meiners, W., Bültmann, J., 2011. High Power Selective Laser Melting (HP SLM) of Aluminum Parts. Phys. Procedia 12, 271–278. doi:10.1016/j.phpro.2011.03.035

Burgardt, P., Heiple, C.R., Vegas, L., 1986. Interaction between Impurities and Welding Variables in Determining GTA Weld Shape. Weld. Res. Suppl. Suppl 150–155.

Casalino, G., Campanelli, S.L., Contuzzi, N., Ludovico, A.D., 2015. Experimental investigation and statistical optimisation of the selective laser melting process of a maraging steel. Opt. Laser Technol. 65, 151–158. doi:10.1016/j.optlastec.2014.07.021

Chelladurai, A.M., Gopal, A.G., Murugan, S., Venugopal, S., Jayakumar, T., 2014. Energy Transfer Modes in Pulsed Laser Seam Welding. Mater. Manuf. Process. 30, 162–168. doi:10.1080/10426914.2014.965829

Childs, T.H.C., Hauser, C., Badrossamay, M., 2005. Selective laser sintering (melting) of stainless and tool steel powders: experiments and modelling. Proc. Inst. Mech. Eng. Part B J. Eng. Manuf. 219, 339–357. doi:10.1243/095440505X8109

Cottam, R., Brandt, M., 2011. Laser Cladding of Ti-6Al-4V Powder on Ti-6Al-4V Substrate: Effect of Laser Cladding Parameters on Microstructure. Phys. Procedia 12, 323–329. doi:10.1016/j.phpro.2011.03.041

Desmond, K.W., Weeks, E.R., 2013. Influence of Particle Size Distribution on Random Close Packing of shapes. arXiv.org cond-mat 022204, 1–6. doi:10.1103/PhysRevE.90.022204

Duley, W.W., 1999. Laser welding. John Wiley and Sons, Canada.

Eagar, T.W., Tsai, N.S., 1983. Temperature fields produced by traveling distributed heat sources. Weld. J. 62, 346–355.

El Cheikh, H., Courant, B., Branchu, S., Hascoët, J.-Y., Guillén, R., 2012. Analysis and prediction of single laser tracks geometrical characteristics in coaxial laser cladding process. Opt. Lasers Eng. 50, 413–422. doi:10.1016/j.optlaseng.2011.10.014

El-Batahgy, A.-M., 1997. Effect of laser welding parameters on fusion zone shape and solidification structure of austenitic stainless steels. Mater. Lett. 32, 155–163.

Elsen M.V., Al-Bender F., Kruth, J.P., 2008. Application of dimensional analysis to selective laser melting. Rapid Prototyp. J. 14, 15–22. doi:10.1108/13552540810841526

Eriksson I, Powell J, K.A.F.., 2014. Surface tension generated defects in full

penetration laser keyhole welding. J. Laser Appl. 26.

Fuerschbach P.W., Eisler G.R., 2002. Effect of laser spot weld energy and duration on melting and absorption. Sci. Technol. Weld. Join. 7, 241–246. doi:10.1179/136217102225004293

Fuerschbach, P.W., 1996. Measurement and Prediction of Energy Transfer Efficiency in Laser beam Welding. Weld. Journal. 75, 24–278.

Fuerschbach, P.W., Eisler, G.R., 1999. Effect of Very High Travel Speeds on Melting Efficiency in Laser Beam Welding. J. Mater. Manuf. 108, 1–7.

Gao, M., Zeng, X., Qianwu, H., 2007. Effect of gas shielding parameters on weld penetration of CO2 laser-TIG yhbrid welding. J. Mater. Process. Technol. 84, 177 – 183.

Greses, J., Barlow, C, Y., Hilton, P.A., Steen, W, M., 2003. Effect of Different Gas Environments on CO2 and Nd:YAG Laser Welding Process Efficiencies. Proc. SPIE 4831, 257–262.

Guan, K., Wang, Z., Gao, M., Li, X., Zeng, X., 2013. Effects of processing parameters on tensile properties of selective laser melted 304 stainless steel. Mater. Des. 50, 581–586. doi:10.1016/j.matdes.2013.03.056

Gusarov, A. V., Yadroitsev, I., Bertrand, P., Smurov, I., 2009. Model of Radiation and Heat Transfer in Laser-Powder Interaction Zone at Selective Laser Melting. J. Heat Transfer 131, 072101. doi:10.1115/1.3109245

Gusarov, A. V, Yadroitsev, I., Bertrand, P., Smurov, I., 2007. Heat transfer modelling and stability analysis of selective laser melting. Appl. Surf. Sci. 254, 975–979. doi:10.1016/j.apsusc.2007.08.074

Hanzl, P., Zetek, M., Bakša, T., Kroupa, T., 2015. The Influence of Processing Parameters on the Mechanical Properties of SLM Parts. Procedia Eng. 100, 1405–1413. doi:10.1016/j.proeng.2015.01.510

Hauser, C., 2003. Selective Laser sintering of a stainless steel powder.

Heiple, C.R., Roper, J. R., 1981. Effect of Selenium on GTAW Fusion Zone Geometry. Weld. Res. Suppl. 143–145.

Hess, A., Schuster, R., Heider, A., Weber, R., Graf, T., 2011. Continuous wave laser welding of copper with combined beams at wavelengths of 1030 nm and of 515 nm. Phys. Procedia 12, 88–94. doi:10.1016/j.phpro.2011.03.012

Hu, Y., He, X., Yu, G., Ge, Z., Zheng, C., Ning, W., 2012. Heat and mass transfer in laser dissimilar welding of stainless steel and nickel. Appl. Surf. Sci. 258, 5914–5922. doi:10.1016/j.apsusc.2012.02.143

Huang, Y., Zeng, X., 2010. Investigation on cracking behavior of Ni-based coating by laser-induction hybrid cladding. Appl. Surf. Sci. 256, 5985–5992. doi:10.1016/j.apsusc.2010.03.106

Ion, J.C., 2005. Laser Processing of Engineering Materials, First. ed. Elsevier, Oxford.

Jia, Q., Gu, D., 2014. Selective laser melting additive manufacturing of Inconel 718 superalloy parts: Densification, microstructure and properties. J. Alloys Compd. 585, 713–721. doi:10.1016/j.jallcom.2013.09.171

Kaplan, A.F.H., 2011. Modelling the primary impact of an Yb:Fibre laser beam profile on the keyhole front. Phys. Procedia 12, 627–637. doi:10.1016/j.phpro.2011.03.079

Kaplan, A.F.H., Matti, R.S., 2015. Absorption peaks depending on topology of the keyhole front and wavelength. J. Laser Appl. 27, S29012. doi:10.2351/1.4906469

Khan, M., Dickens, P., 2012. Selective laser melting (SLM) of gold (Au). Rapid Prototyp. J. 18, 81–94. doi:10.1108/13552541211193520

King, W.E., Barth, H.D., Castillo, V.M., Gallegos, G.F., Gibbs, J.W., Hahn, D.E., Kamath, C., Rubenchik, A.M., 2014. Observation of keyhole-mode laser melting in laser powder-bed fusion additive manufacturing. J. Mater. Process. Technol. doi:10.1016/j.jmatprotec.2014.06.005

Knupfer, S.M., Moore, A.J., 2010. The effects of laser forming on the mechanical and metallurgical properties of low carbon steel and aluminium alloy samples. Mater. Sci. Eng. A 527, 4347–4359. doi:10.1016/j.msea.2010.03.069

Kobryn, P.A., Moore, E.H., Semiatin, S.L., 2000. The Effect of Laser Power and Traverse Speed on Microstructure, Porosity, and Build height in Laser-Deposited Ti-6Al-4V 43, 299–305.

Kong, C.Y., Scudamore, R.J., Allen, J., 2010. High-rate laser metal deposition of Inconel 718 component using low heat-input approach. Phys. Procedia 5, 379–386. doi:10.1016/j.phpro.2010.08.159

Kruth, J. P., Wang, X., Laoui, T., Froyen, L., 2006. Lasers and materials in selective laser sintering. Emerald Insight 23, 357–371.

Kruth, J., Levy, G., Klocke, F., Childs, T.H.C., 2007. Consolidation phenomena in laser and powder-bed based layered manufacturing. Ann. CIRP 56, 730–759. doi:10.1016/j.cirp.2007.10.004

Kruth, J.P., Froyen, L., Van Vaerenbergh, J., Mercelis, P., Rombouts, M., Lauwers, B., 2004. Selective laser melting of iron-based powder. J. Mater. Process. Technol. 149, 616–622. doi:10.1016/j.jmatprotec.2003.11.051

Lautrup B., 2011. Surface tension, in: Physics of Contuous Matter. CRC Press, pp. 70 – 94.

Lewis, G.K., Schlienger, E., 2000. Practical considerations and capabilities for

laser assisted direct metal deposition. Mater. Des. 21, 417–423. doi:10.1016/S0261-3069(99)00078-3

Li, J., Chen, C., Wang, D., 2012. Surface modification of titanium alloy with laser cladding RE oxides reinforced Ti3Al–matrix composites. Compos. Part B Eng. 43, 1207–1212. doi:10.1016/j.compositesb.2011.08.040

Liu, H., Xu, Q., Wang, C., Zhang, X., 2015. Corrosion and wear behavior of Ni60CuMoW coatings fabricated by combination of laser cladding and mechanical vibration processing. J. Alloys Compd. 621, 357–363. doi:10.1016/j.jallcom.2014.10.030

Liu, Z.H., Chua, C.K., Leong, K.F., Kempen, K., Thijs, L., Yasa, E., Kruth, J.P., 2011. A Preliminary Investigation on Selective Laser Melting of M2 High Speed Steel, in: Innovative Developments in Virtual and Physical Prototyping. Taylor and Francis Group, Leiria Portugal, pp. 339–346.

Louvis, E., Fox, P., Sutcliffe, C.J., 2011. Selective laser melting of aluminium components. J. Mater. Process. Technol. 211, 275–284. doi:10.1016/j.jmatprotec.2010.09.019

Maji, P.K., Banerjee, A.J., Banerjee, P.S., Karmakar, S., 2014. Additive manufacturing in prosthesis development – a case study. Rapid Prototyp. J. 20, 480–489. doi:10.1108/RPJ-07-2012-0066

Majumdar, P., Xia, H., 2007. A Green's function model for the analysis of laser heating of materials. Appl. Math. Model. 31, 1186–1200. doi:10.1016/j.apm.2006.04.007

McVey, R. W., Todd, J.A., Martukannitz, R.P., 2007. Absorption of laser irradiation in a porous powder layer. J. Laser Appl. 19, 214–224.

Meco, S., Pardal, G., Ganguly, S., Miranda,S., 2012. Overlap conduction laser welding of aluminium to steel. Int. J. Adv. Manuf. Technol. doi:10.1007/s00170-012-4512-6

Ming, G., Xiaoyan, Z., Qianwu, H., 2007. Effects of gas shielding parameters on weld penetration of CO2 laser-TIG hybrid welding. J. Mater. Process. Technol. 184, 177–183. doi:10.1016/j.jmatprotec.2006.11.019

Moradi, M., Ghoreishi, M., 2010. Influences of laser welding parameters on the geometric profile of NI-base superalloy Rene 80 weld-bead. Int. J. Adv. Manuf. Technol. 55, 205–215. doi:10.1007/s00170-010-3036-1

Mullen, L., Stamp, R.C., Fox, P., Jones, E., Ngo, C., Sutcliffe, C.J., 2010. Selective laser melting: A unit cell approach for the manufacture of porous, titanium, bone in-growth constructs, suitable for orthopedic applications. II. Randomized structures. J. Biomed. Mater. Res. - Part B Appl. Biomater. 92, 178–188. doi:10.1002/jbm.b.31504

Nagaoka, T., Kimoto, Y., Watanabe, H., Fukusumi, M., Morisada, Y., 2015.

Friction stir processing of a D2 tool steel layer fabricated by laser cladding 83, 224–229.

Olakanmi, E.O., 2013. Selective laser sintering/melting (SLS/SLM) of pure Al, Al–Mg, and Al–Si powders: Effect of processing conditions and powder properties. J. Mater. Process. Technol. 213, 1387–1405. doi:10.1016/j.jmatprotec.2013.03.009

Osakada, K., Shiomi, M., 2006. Flexible manufacturing of metallic products by selective laser melting of powder. Int. J. Mach. Tools Manuf. 46, 1188–1193. doi:10.1016/j.ijmachtools.2006.01.024

Pantsar, H., Kujanpa, V., Zhu, P., 2004. Diode laser beam absorption in laser transformation hardening of low alloy steel. J. Laser Appl. 16.

Patschger A., Bliedtner J.P, Bergmann P.B, 2013a. Approaches to increase process efficiency in laser micro welding. Phys. Procedia 41, 592–602. doi:10.1016/j.phpro.2013.03.121

Patschger A., Güpner, M., Bliedtner, J., Bergmann, J., 2013b. Remote Micro Welding With Multi-Mode and Single-Mode Fiber Lasers – A comparison, in: International Congress on Applications of Lasers and Electro-Optics. Miami Fi, USA, pp. 805–815.

Paydas, H., Mertens, A., Carrus, R., Lecomte-Beckers, J., Tchoufang Tchuindjang, J., 2015. Laser cladding as repair technology for Ti–6Al–4V alloy: Influence of building strategy on microstructure and hardness. Mater. Des. 85, 497–510. doi:10.1016/j.matdes.2015.07.035

Pinkerton, A.J., Li, L., 2004. The development of temperature elds and powder ow during laser direct metal deposition wall growth 218, 531–541.

Qi, H., Mazumder, J., Ki, H., 2006. Numerical simulation of heat transfer and fluid flow in coaxial laser cladding process for direct metal deposition. J. Appl. Phys. 100, 024903. doi:10.1063/1.2209807

Qu, C.C., Li, J., Bai, L.L., Shao, J.Z., Song, R., Chen, J.L., 2015. Effects of the thickness of the pre-placed layer on microstructural evolution and mechanical properties of the laser-clad coatings 644, 450–463.

Quintino, L., Miranda, R.M., Williams, S., Kong, C.J., 2011. Gas shielding in fibre laser welding of high strength pipeline steel. Sci. Technol. Weld. Join. 16, 399–404. doi:10.1179/1362171810Y.0000000002

Rombouts, M., Froyen, L., Mercelis, P., Leuven, K., 2006. Fundamentals of Selective Laser Melting of alloyed steel powders. CIRP Ann. - Manuf. Technol. 55, 187–192.

Romero, P., Otero, N., González, A., García, G., Scano, A., 2011. Additive Generation of Surface Microstructures for Fluid-Dynamic Applications by using Single-Mode Fibre Laser Assisted Microcladding 12, 268–277.

doi:10.1016/j.phpro.2011.03.133

Roper, J.R., Stagner, R.T., Aden, R.J., 1983. Surface Active Element Effects on the Shape of GTA , Laser , and Electron Beam Welds 72–77.

Sánchez-Amaya, J.M., Delgado T., González-Rovira L., Botana F.J., 2009. Laser welding of aluminium alloys 5083 and 6082 under conduction regime. Appl. Surf. Sci. 255, 9512–9521. doi:10.1016/j.apsusc.2009.07.081

Sayegh, G., 1998. Welding, in: Schuocker, D. (Ed.), Handbook of the Eurolaser. Chapman and Hall, London, pp. 256–311.

Schleifenbaum, H., Meiners, W., Wissenbach, K., Hinke, C., 2010. Individualized production by means of high power Selective Laser Melting. CIRP J. Manuf. Sci. Technol. 2, 161–169. doi:10.1016/j.cirpj.2010.03.005

Semak, V., Matsunawa, A., 1999. The role of recoil pressure in energy balance during laser materials processing. J. Phys. D. Appl. Phys. 30, 2541–2552. doi:10.1088/0022-3727/30/18/008

Shepeleva, L., Medres, B., Kaplan, W.D., Bamberger, M., Weisheit, a., 2000. Laser cladding of turbine blades. Surf. Coatings Technol. 125, 45–48. doi:10.1016/S0257-8972(99)00603-9

Shon, Y., Joshi, S.S., Katakam, S., Shanker Rajamure, R., Dahotre, N.B., 2015. Laser additive synthesis of high entropy alloy coating on aluminum: Corrosion behavior. Mater. Lett. 142, 122–125. doi:10.1016/j.matlet.2014.11.161

Simchi, A., 2004. The role of particle size on the laser sintering of iron powder. Metall. Mater. Trans. B 35B, 937–948.

Simonelli, M., Tse, Y.Y., Tuck, C., 2014. Effect of the build orientation on the mechanical properties and fracture modes of SLM Ti–6Al–4V. Mater. Sci. Eng. A 616, 1–11. doi:10.1016/j.msea.2014.07.086

Song, B., Dong, S., Deng, S., Liao, H., Coddet, C., 2014. Microstructure and tensile properties of iron parts fabricated by selective laser melting. Opt. Laser Technol. 56, 451–460. doi:http://dx.doi.org/10.1016/j.optlastec.2013.09.017

Song, B., Dong, S., Zhang, B., Liao, H., Coddet, C., 2012. Effects of processing parameters on microstructure and mechanical property of selective laser melted Ti6Al4V. Mater. Des. 35, 120–125. doi:10.1016/j.matdes.2011.09.051

Stanciu, E.M., Dumitru, G., Pavalache, A., Iacobescu, G., 2012. Laser welding parameters influence on the geometrical aspect ratio of the melted zone in stainless steel. U.P.B Sci. Bull., 74, 179 – 186.

Steen, W.M., 2010. Laser Material Processing, 4th ed, Laser Material

Processing. Springer-Verlag London Limited, London. doi:10.100/978-1-84996-062-5

Steen, W.., Mazumder J, 1999. Laser Material Processing, Fourth. ed. Springer-Verlag London Limited, London. doi:DOI 10.1007/978-1-84996-062-5

Suder, W.J., Williams, S., 2014. Power factor model for selection of welding parameters in CW laser welding. Opt. Laser Technol. 56, 223–229. doi:10.1016/j.optlastec.2013.08.016

Suder, W.J., Williams, S.W., 2012. Investigation of the effects of basic laser material interaction parameters in laser welding. J. Laser Appl. 24, 032009–1–10. doi:10.2351/1.4728136

Suder, W.J., 2012. Study of fundamental parameters in hybrid laser welding.

Sun, Y., Hao, M., 2012. Statistical analysis and optimization of process parameters in Ti6Al4V laser cladding using Nd:YAG laser. Opt. Lasers Eng. 50, 985–995. doi:10.1016/j.optlaseng.2012.01.018

Tang, Y., Loh, H.T., Fuh, J.Y.H., Wong, Y.S., Lu, L., Ning, Y., Wang, X., 2004. Accuracy analysis and improvement for direct laser sintering. Innov. Manuf. Syst. Technol. 119260.

Tolochko, N.K., Khlopk,Y.V., Mozzharov, S.E., Sobolenko, N.V., Yadroitsev, I.A., 1997. Measurement of the absorption coefficient of freely poured one-component metallic powders and its change during laser sinterin. Powder Metall. Met. Ceram. 36, 433–437.

Tolochko, N.K., Arshinov, M.K., Gusarov, A. V., Titov, V.I., Laoui, T., Froyen, L., 2003. Mechanisms of selective laser sintering and heat transfer in Ti powder. Rapid Prototyp. J. 9, 314–326. doi:10.1108/13552540310502211

Tolochko, N.K., Laoui, T., Khlopkov, Y. V, Mozzharov, S.E., Titov, V.I., Ignatiev, M.B., 2000. Absorptance of powder materials suitable for laser sintering. Rapid Prototyp. J. 6, 155–160. doi:Doi 10.1108/13552540010337029

Tolochko, N.K., Mozzharov, S.E., Yadroitsev, I.A.., Laoui, T., Froyen, L., Titov, V.I., Ignatiev, M. B., 2004. Balling processes during selective laser treatment of powders. Rapid Prototyp. J. 10, 78–87. doi:10.1108/13552540410526953

Toyserkani, E., Khajepour, A., Corbin, S., 2005. Laser Cladding. CRC Press, Washington.

Tsao K.C., Wu, C.S., 1988. Fluid Flow and Heat Transfer in GMA Weld Pools Determination of the Electromagnetic. Weld. Res. Suppl.

Tsopanos, S., Mines, R.A.W., McKown, S., Shen, Y., Cantwell, W.J., Brooks, W., Sutcliffe, C.J., 2010. The Influence of Processing Parameters on the Mechanical Properties of Selectively Laser Melted Stainless Steel

Microlattice Structures. J. Manuf. Sci. Eng. 132, 041011. doi:10.1115/1.4001743

Turner, J.S., 1973. Buoyancy effects in fluids, 1st ed. Press Syndicate of University of Cambridge, Cambridge.

Valiente Bermejo, M.A., Karlsson, L., Svensson, L.-E., Hurtig, K., Rasmuson, H., Frodigh, M., Bengtsson, P., 2014. Effect of shielding gas on welding performance and properties of duplex and superduplex stainless steel welds. Weld. World 59, 239–249. doi:10.1007/s40194-014-0199-7

Verhaeghe, G., Hilton, P., 2005. The effect of spot sizeand laser beam quality on welding perfoemance when using high power continuos wave solid-state lasers, in: International Congress on Applications of Lasers and Electro-Optics. Florida.

Verwimp, J., Rombouts, M., Geerinckx, E., Motmans, F., 2011. Applications of Laser Cladded WC-Based Wear Resistant Coatings. Phys. Procedia 12, 330–337. doi:10.1016/j.phpro.2011.03.042

Volpp, J., 2012. Investigation on the Influence of Different Laser Beam Intensity Distributions on Keyhole Geometry During Laser Welding. Phys. Procedia 39, 17–26. doi:10.1016/j.phpro.2012.10.009

Wang, H., Shi, Y., Gong, S., Duan, A., 2007. Effect of assist gas flow on the gas shielding during laser deep penetration welding. J. Mater. Process. Technol. 184, 379–385. doi:10.1016/j.jmatprotec.2006.12.014

Yadroitsev, I., Gusarov, A., Yadroitsava, I., Smurov, I., 2010. Single track formation in selective laser melting of metal powders. J. Mater. Process. Technol. 210, 1624–1631. doi:10.1016/j.jmatprotec.2010.05.010

Yang, H.-J., Hwang, P.-J., Lee, S.-H., 2002. A study on shrinkage compensation of the SLS process by using the Taguchi method. Int. J. Mach. Tools Manuf. 42, 1203–1212. doi:10.1016/S0890-6955(02)00070-6

Yasa, E., Deckers, J., Kruth, J.-P., 2011. The investigation of the influence of laser re-melting on density, surface quality and microstructure of selective laser melting parts. Rapid Prototyp. J. 17, 312–327. doi:10.1108/13552541111156450

Ye, X., Ma, M., Cao, Y., Liu, W., Ye, X., Gu, Y., 2011. The Property Research on High-entropy Alloy AlxFeCoNiCuCr Coating by Laser Cladding. Phys. Procedia 12, 303–312. doi:10.1016/j.phpro.2011.03.039

Zhang, B., Dembinski, L., Coddet, C., 2013. The study of the laser parameters and environment variables effect on mechanical properties of high compact parts elaborated by selective laser melting 316L powder. Mater. Sci. Eng. A 584, 21–31. doi:10.1016/j.msea.2013.06.055

Zhang, B., Liao, H., Coddet, C., 2012. Effects of processing parameters on

properties of selective laser melting Mg–9%Al powder mixture. Mater. Des. 34, 753–758. doi:10.1016/j.matdes.2011.06.061

Zhao, C.X., Kwakernaak, C., Pan, Y., Richardson, I.M., Saldi, Z., Kenjeres, S., Kleijn, C.R., 2010. The effect of oxygen on transitional Marangoni flow in laser spot welding. Acta Mater. 58, 6345–6357. doi:10.1016/j.actamat.2010.07.056

Zhao, H., Debroy, T., 2001. Weld Metal Composition Change during Conduction Mode Laser Welding of Aluminum Alloy 5182. Metall. Mater. Trans. B 32, 163–172.